

**UCSF**

**UC San Francisco Electronic Theses and Dissertations**

**Title**

Targeting Solute Carrier Transporters for Drug Delivery to the Central Nervous System

**Permalink**

<https://escholarship.org/uc/item/4qd5p455>

**Author**

Geier, Ethan George

**Publication Date**

2013

Peer reviewed|Thesis/dissertation

TARGETING SOLUTE CARRIER TRANSPORTERS FOR DRUG  
DELIVERY TO THE CENTRAL NERVOUS SYSTEM

by

Ethan George Geier

DISSERTATION

Submitted in partial satisfaction of the requirements for the degree of

DOCTOR OF PHILOSOPHY

in

Pharmaceutical Sciences and Pharmacogenomics

in the

GRADUATE DIVISION

of the

UNIVERSITY OF CALIFORNIA, SAN FRANCISCO



## **ACKNOWLEDGEMENTS**

My successful pursuit of a Ph.D. is the direct result of the invaluable interactions with the exceptional faculty, graduate students, postdoctoral fellows, and administrators across many different departments at UCSF, but especially the department of Bioengineering and Therapeutic Sciences. Outside of UCSF, my wonderful family and fiancé played an equally integral role in achieving this goal. Both the work presented in my dissertation research, and the even more extensive portion that is not presented here would have been impossible without the support and effort of countless people over the past 5 years.

First, Dr. Kathleen M. Giacomini has been an outstanding mentor throughout my graduate school career, and I cannot thank her enough for her endless support and guidance. From the long hours of helping me to prepare for my oral qualifying exam, to writing grants and reviewing manuscripts with her, she has taught me a tremendous amount about what it takes to succeed as a research scientist. Without a doubt, the vital knowledge I have gained from these experiences will continue to help shape and develop my scientific career for years to come.

I would also like to thank my oral qualification committee, consisting of Drs. Andrej Sali, Deanna Kroetz, Mitchell Berger, and Roland Bainton, for taking the time to review and give critical feedback on my dissertation proposal. In addition to Dr. Giacomini, I also want to thank Drs. Kroetz and Bainton for their efforts on my dissertation committee. Both took the time to meet with me on numerous occasions to guide me through my dissertation research, and I could not have completed this work without the helpful discussions and advice that I received from them.



All members of the Giacomini laboratory over the past 5 years deserve a special thank you for their constant support, advice, and mentorship. I am particularly grateful for the mentorship of Drs. Sook Wah Yee, Swati More, and Avner Schlessinger of the Sali lab, who provided helpful discussions and taught me valuable technical skills that allowed me to perform most of the studies presented here. Fellow Giacomini lab graduate students, Kari Morrissey, Eugene Chen, and Lawrence Lin also provided particularly helpful discussions and technical support during my time in the lab. Finally, I am grateful for having the opportunity to work with and learn from Tsuyoshi Minematsu, Par Matsson, Ligong Chen, Matthias Wittwer, Arik Zur, Shuanglian Li, Jim Shima, Amber Dahlin, Sophie Stocker, Youcai Zhang, Chris Wen, Srijib Goswami, Adrian Stecula, and Xiaomin Liang. Daily interactions with all of these previous and current lab members provided valuable experiences that helped me develop as a scientist, and made the Giacomini lab an enjoyable workplace everyday.

Successfully completing graduate school and earning a Ph.D. is an extremely arduous process that inevitably affects the people closest to you. For this reason, I am tremendously grateful for the unwavering support of my mother, father, and the rest of my family over the past 5 years. Achieving this goal would have been impossible without them.

Finally, I owe a very special thank you to my fiancé, Danielle Hammond, for her patience, support, and unconditional love throughout this process. She has always been there to help me through the low points of graduate school life, and made sure we took the time to celebrate the high points. This accomplishment is as much hers as it is mine, and there is nobody else I would have rather had by my side during this journey.

## **ABSTRACT**

### **Targeting Solute Carrier Transporters for Drug Delivery to the Central Nervous System**

Ethan George Geier

The blood-brain barrier (BBB) is a major reason that approximately 95% of small molecule drugs developed to target the central nervous system (CNS) fail. Thus, new approaches for delivering drugs across the BBB should be explored. The goal of this research was to identify solute carrier (SLC) influx transporters expressed at the BBB, and determine how SLCs can be exploited to deliver low CNS permeability platinum drugs across the BBB.

My first goal was to identify SLC transporters expressed at the human BBB. In human brain microvessels isolated from cerebral cortex, expression profiling of 359 SLC transporters, comparative expression with human kidney and liver samples, and immunoassays confirmed and identified BBB drug transporters, including *SLC7A5*, *SLC22A3*, *SLC47A1*, and *SLC19A1*. Furthermore, pharmacokinetic studies in mice with small molecule inhibitors of the reduced folate carrier (Rfc), established Rfc-mediated uptake of methotrexate across the BBB.

The large neutral amino acid transporter 1, LAT1 is one of several SLC transporters that mediate drug uptake across the BBB. The role of LAT1 in CNS drug delivery was characterized by (a) using LAT1 expressing cell lines to determine whether LAT1 can be targeted to deliver synthetic anti-cancer platinum analogs to the CNS; (b) creating and characterizing a mouse model with reduced function Lat1 as a tool for

assessing LAT1 targeted drugs *in vivo*; and (c) using virtual screening of ~19,000 compounds against a comparative structural model of LAT1. One out of seven LAT1-targeted synthetic platinum analogs was a cytotoxic substrate of the transporter. Although Lat1 deletion appears to be embryonic lethal, Lat1 heterozygous mice have decreased Lat1 mRNA expression, and gabapentin and levodopa brain accumulation. Four novel LAT1 ligands were identified by comparative modeling, virtual screening, and experimental validation. These results provided a rationale for the enhanced brain permeability of two drugs. Two hits also inhibited proliferation of a cancer cell line by different mechanisms, providing useful chemical tools to characterize the role of LAT1 in cancer. The research presented here has important implications for LAT1-targeted CNS drug delivery and cancer therapy, and provide important tools to continue to address these implications in future studies.

## TABLE OF CONTENTS

<b>Title Page</b>	<b>i</b>
<b>Acknowledgements</b>	<b>iii</b>
<b>Abstract</b>	<b>v</b>
<b>Table of Contents</b>	<b>vii</b>
<b>List of Tables</b>	<b>x</b>
<b>List of Figures</b>	<b>xii</b>
 <b>Chapter 1</b>	
<b>Membrane transporters at the blood-brain barrier and regulation of drug permeability to the central nervous system</b>	<b>1</b>
Introduction	1
ABC Efflux Transporters	2
Multidrug Resistance Protein 1	3
Breast Cancer Resistance Protein	4
Multidrug Resistance-associated Proteins	6
SLC Influx Transporters	7
Large-neutral Amino Acid Transporter 1	7
Equilibrative Nucleoside Transporter 1	9
Monocarboxylate Transporter 1	9
Organic Anion Transporting Polypeptides	10
Future Directions	14

Summary of Dissertation Chapters	15
Chapter 2	15
Chapter 3	16
Chapter 4	16
References	17

## **Chapter 2**

### **Expression Profiling and Characterization of**

#### **Solute Carrier Transporters in the Human Blood-Brain Barrier**

Introduction	27
Materials and Methods	29
Results	35
Discussion	56
References	61

## **Chapter 3**

### **Development of LAT1-targeted Cisplatin Analogs and a Lat1 Null Mouse**

Introduction	68
Materials and Methods	70
Results	77
Discussion	90
References	94

## **Chapter 4**

### **Structure-based Ligand Discovery for the**

#### **Large-neutral Amino Acid Transporter 1, LAT1** 100

Introduction 100

Materials and Methods 102

Results 113

Discussion 131

References 135

## **Chapter 5**

### **Summary and Conclusions** 151

Chapter 2 152

Chapter 3 153

Chapter 4 154

Challenges and Future Directions 155

References 156

## List of Tables

### Chapter 1

Table 1.1. Membrane transporters mediating drug uptake into the CNS	12
---	----

### Chapter 2

Table 2.1. Tissue donor information	29
Table 2.2. Genes expressed in human BMVs in comparison to housekeeping genes and paired cerebral cortex samples	44
Table 2.3. Pharmacokinetic parameters and kidney accumulation of [ <sup>3</sup> H]-methotrexate	53

### Chapter 3

Table 3.1. Cytotoxic potency of LAT1-targeted platinum compounds and cisplatin against HEK-LAT1 cells	81
Table 3.2. Observed versus expected genotypes of pups from heterozygous breeding pairs	82
Table 3.3. Body and organ weights of heterozygous and wild type mice	86
Table 3.4. Pharmacokinetic parameters after intravascular administration of a 300 ng/kg bolus dose of [ <sup>3</sup> H]-gabapentin to heterozygous and wild type mice	86

### Chapter 4

Table 4.1. Anti-LAT1 shRNA sequences	109
--------------------------------------	-----

Table 4.2. Assessment of the LAT-1 models	114
Table 4.3. Small molecules tested in uptake kinetic assays	121



## List of Figures

### Chapter 1

Figure 1.1. ABC and SLC drug transporters expressed at the human BBB	13
--	----

### Chapter 2

Figure 2.1. Validation of BMV enrichment from cerebral cortex samples	37
Figure 2.2. Transporter mRNA expression levels in BMVs	38
Figure 2.3. Validation of OpenArray gene expression results	39
Figure 2.4. Comparative expression analysis of drug transporters in BMV, kidney and liver samples	40
Figure 2.5. Protein expression of SLC transporters in BMVs	42
Figure 2.6. Confirmation of SLC transporter protein expression in BMVs and antibody specificity	43
Figure 2.7. The role of the reduced folate carrier Rfc in methotrexate uptake into the mouse brain	54

### Chapter 3

Figure 3.1. Chemical structures of LAT1-targeted platinum compounds	76
Figure 3.2. Characterization of HEK-LAT1 cells	78
Figure 3.3. Rate of platinum accumulation in HEK-LAT1 cells	79
Figure 3.4. Strategy for targeted deletion of Lat1 in C57BL/6NTac ES cells	83
Figure 3.5. Lat1 mRNA and protein expression in heterozygous and wild type littermate mice	87

Figure 3.6. Pharmacokinetic and tissue distribution of Lat1 drug substrates	89
---	----

## Chapter 4

Figure 4.1. LAT1-AdiC alignment	106
Figure 4.2. Conservation and hydrophobicity profiles for the LAT1 model and AdiC structure	107
Figure 4.3. Predicted LAT1 structure and ligand binding mode	116
Figure 4.4. Binding sites of LAT1 and AdiC	118
Figure 4.5. Predicted binding modes for LAT1 ligands	123
Figure 4.6. Validation of LAT1 function in HEK-LAT1 cells	124
Figure 4.7. Experimental validation of predicted LAT1 ligands	126
Figure 4.8. Substrate determination and cytotoxicity characterization of predicted ligands	129
Figure 4.9. Validation of LAT1 knock-down in T98G glioblastoma cells	130

## **CHAPTER 1**

### **Membrane transporters at the blood-brain barrier and regulation of drug permeability to the central nervous system**

#### **Introduction**

Membrane transporters are of significant pharmacological and physiological importance due to their roles as major determinants of the absorption, distribution and elimination of numerous exogenous and endogenous substances. To date, two major superfamilies of transporters have been identified in the human genome. These are the solute carrier superfamily (SLC), consisting of 55 families and at least 362 transporter genes coding for proteins that function primarily as facilitated influx pumps [1], and the ATP binding cassette superfamily (ABC), which includes seven families and 48 members, most of which are active efflux pumps relying on ATP hydrolysis for energy [2, 3]. Given the importance of transporters as permeability barriers and enhancers for nutrients, xenobiotics and clinically relevant drugs, a number of studies have explored their expression levels and cellular localization in tissues involved in drug absorption, distribution, metabolism and elimination (ADME) [2, 4-11]. These studies have contributed greatly to our understanding of the molecular processes that govern drug distribution across tissue barriers.

The blood-brain barrier (BBB) regulates exchange between the blood and the brain through the unique properties of the endothelial cells forming the CNS vasculature to maintain the neural microenvironment [12, 13]. However, these properties, such as the presence of several ABC efflux transporters and drug metabolizing enzymes, simultaneously prevent most drugs from permeating the CNS [14, 15]. The two primary

routes by which small molecules pass through the BBB are transcellular passive diffusion and carrier-mediated transport. Low molecular weight (< 450 Da), lipophilic molecules tend to passively diffuse across the BBB, whereas more hydrophilic molecules require carrier-mediated processes to reach the CNS [16, 17]. These carriers are primarily SLC transporters that mediate the CNS uptake of essential nutrients such as carbohydrates, amino acids and vitamins from the blood. Moreover, many of these transporters are also involved in influx of drugs into the CNS, suggesting that they can be targeted to facilitate drug penetration across the BBB.

The remainder of this introductory chapter will focus on the different drug transporters that regulate drug penetration across the BBB. These transporters will be discussed in two groups: SLC influx transporters that facilitate, and ABC efflux transporters that restrict the entry of drugs into the CNS. Only transporters with evidence of protein expression at the human BBB will be discussed. However, the functional evidence for transporter contributions to CNS drug permeability will primarily be derived from non-human experimental models, such as knockout (KO) mice, due to the obvious ethical considerations and technical limitations with sampling from the human CNS.

### **ABC Efflux Transporters**

ABC transporters expressed at the BBB primarily function to prevent circulating small molecules such as toxins and drugs from reaching the CNS by coupling the hydrolysis of ATP with transport of these substrates against their concentration gradient back into the blood [18, 19]. While the goal of this research focuses on characterizing

and targeting SLC influx transporters to deliver drugs across the BBB, it is important to note the integral role that ABC transporters play in supporting BBB function. Moreover, the majority of previous studies investigating membrane transporter function at the BBB have focused on ABC efflux transporters, particularly *ABCB1* (MDR1). Even though mRNA expression of ABC transporter genes from all identified subfamilies have been detected at the human BBB [20], only members of the *ABCB*, *ABCC*, and *ABCG* subfamilies have been functionally characterized in the context of drug delivery to the CNS. Furthermore, the results of these studies have led to the proposed strategy of targeting ABC transporters with selective inhibitors to enhance the CNS permeability of their drug substrates. However, this leaves the CNS more vulnerable to insult from circulating toxins, and has not yet proven to be clinically efficacious [21]. The ABC transporters that support BBB function are discussed by subfamily below.

### **Multidrug Resistance Protein 1 (MDR1; P-glycoprotein; *ABCB1*)**

MDR1 is the most extensively studied transporter at the BBB, and its ability to greatly reduce the CNS permeability of many different drug classes, including anticancer, antiviral, and antiepileptic drugs is well established [18, 22]. Aside from being expressed in organs such as the small intestine, liver, and kidney, it is highly expressed on the blood-facing membrane of the brain endothelial cells of many different species [23], where it transports lipophilic, uncharged and cationic compounds into the blood [21, 24] (Table 1.1). This function at the BBB was first established by demonstrating that *Mdr1a* KO mice were much more sensitive to the antiparasitic drug ivermectin relative to wild type mice [25]. The authors of this study determined that this

was caused by increased brain accumulation of ivermectin in the Abcb1a KO mice relative to wild type mice, and went on to demonstrate that other MDR1 substrates behaved in a similar manner in these mice. Since this seminal study, numerous others have employed a similar approach to investigate the impact of MDR1 on CNS drug penetration [26, 27]. More recently, positron emission tomography (PET) has been used to investigate MDR1 function at the human BBB. This noninvasive technique for determining transporter activity at the BBB measures the brain accumulation of  $^{11}\text{C}$ -labeled MDR1 substrate, such as verapamil or loperamide, when given with and without an MDR1 inhibitor [28, 29]. However, nearly all studies using this technique have only observed modest (two-fold or less) increases in brain accumulation of the labeled probe substrate when administered with an inhibitor versus without [21]. Thus, at the BBB, MDR1 clearly functions to restrict drug penetration into the CNS in both preclinical animal models of drug disposition and humans.

### **Breast Cancer Resistance Protein (BCRP; MXR; ABCG2)**

BCRP is the next most extensively characterized efflux transporter at the BBB after MDR1. It has a broader tissue expression pattern than MDR1 [23], but is similar to MDR1 in that it is expressed in the blood-facing membrane of the BBB [30, 31] (Table 1.1). Furthermore, BCRP appears to be expressed at levels comparable to MDR1 in the human BBB [15]. BCRP was initially discovered through its interactions with various anticancer drugs, such as mitoxantrone and topotecan, and since then has been shown to transport antivirals and cholesterol lowering statins [18, 23]. At the BBB, BCRP extrudes its substrates from brain endothelial cells back into the blood, preventing them

from reaching the CNS. This function has primarily been established through the observed increase in brain accumulation of BCRP substrates, such as daidzein and genistein in BCRP KO mice relative to wild type mice [32]. Although these compounds are not considered drugs, they clearly establish BCRP-mediated efflux at the BBB to prevent xenobiotic penetration into the brain.

Since BCRP and MDR1 have overlapping substrate profiles, some studies have used dual Bcrp/Mdr1a/1b KO mice to distinguish between the contributions of each transporter to limiting drug penetration across the BBB [27, 32, 33]. These studies have found that the brain accumulation of certain dual Mdr1 and Bcrp drug substrates, such as flavopiridol and elacridar, increase disproportionately in Bcrp/Mdr1a/1b KO mice relative to what would be expected from the individual knockout mice. In other words, the increased brain uptake in the dual knockout is greater than the sum of the increased brain uptake observed in the individual knockout mice. This phenomenon may be due to the nonlinear function relating brain drug distribution to the fraction excreted ( $f_e$ ) by efflux transport pathways ( $\text{fold change in CNS distribution} = 1/(1-f_e)$ ), such that CNS exposure increases exponentially as a greater fraction of excretory transport pathways, whether it be one or multiple transporters, is inhibited [34]. However, this is likely to only be observed in preclinical genetic knockout models of drug transport where complete inhibition of each transporter is achieved, and not observed in clinical situations where chemical inhibition of MDR1, BCRP, and other BBB efflux transporters is generally about 50% or less [21]. Differences in the brain accumulation of PET probes such as  $^{11}\text{C}$ -tarividar in these three strains of knockout mice have also been used to demonstrate this phenomenon [35], but unlike PET studies interrogating MDR1 function

at the human BBB, these studies have been limited to preclinical animal models. Nevertheless, it is clear that BCRP and MDR1 prevent many drugs from crossing the BBB, and provide a formidable barrier to delivering drugs into the CNS.

### **Multidrug Resistance-associated Proteins (MRPs; *ABCCs*)**

MRPs transport a wide variety of neutral and/or anionic drugs and drug conjugates, and are expressed in most human tissues, including the brain endothelial cells of several different species [20] (Table 1.1). However, only Mrp1, Mrp4 and Mrp5 proteins have been detected and localized to the blood-facing membrane at the human BBB, where they are presumed to restrict drug entry into the brain [36]. Despite these findings, only MRP4 protein was detected at the human BBB by mass spectrometry [15]. Furthermore, studies in Mrp1 KO mice have demonstrated virtually no measurable function at the rodent BBB [37, 38], while MRP5 function at the BBB has not been characterized. MRP4, however, appears to play a minor role in limiting brain exposure to certain drugs, as demonstrated by increased brain accumulation of adefovir and topotecan in Mrp4 KO mice relative to wild type mice [39, 40]. It should be noted that while these changes were reported to be statistically significant, they are less than two-fold in magnitude, and far smaller than the ~100-fold increase in brain accumulation of some drugs in Mdr1a KO relative to wild type mice. Therefore, the contribution of MRPs to limiting drug penetration across the BBB into the CNS appears to be minimal.



## **SLC Influx Transporters**

Unlike ABC efflux transporters, SLC influx transporters primarily function to transport small molecules into the CNS from the systemic circulation either on their own or in combination with another SLC transporter. Also unlike ABC transporters, far less is known about the full complement of SLCs expressed at the human BBB, let alone how they contribute to drug transport here. This has led some to believe that the contribution of carrier-mediated processes to drug uptake into the CNS may be greater than is currently presumed [19]. Nevertheless, several SLC drug transporters have been identified at the human BBB and functionally characterized in animal models. These transporters fall into two major categories: nutrient and established drug transporters. Established drug transporters found at the BBB have primarily been characterized to interact with drug substrates in organs outside of the CNS, such as the organic anion transporting polypeptides (OATPs) in the liver and intestine. Nutrient transporters have been characterized through their interactions with endogenous substrates such as amino acids, and were later found to transport nutrient mimetic drugs at the BBB. The SLC transporters contributing to drug uptake across the BBB are considered below.

### **Large-neutral Amino Acid Transporter 1 (LAT1; *SLC7A5*)**

LAT1 is a sodium-independent exchanger highly expressed in the brain, testis, placenta, and many types of cancer where it mediates transport of large-neutral amino acids (e.g., tyrosine) across the cell membrane [41]. More specifically, LAT1 is expressed at the human BBB, and is presumed to have the same localization pattern as

the rodent and bovine BBBs, where it is present in both the blood- and brain-facing membranes [15, 42, 43] (Table 1.1). LAT1 also transports several prescription drugs used to treat different CNS diseases, such as the antiparkinsonian drug L-DOPA and the anticonvulsant gabapentin [44-47]. Furthermore, LAT1 is the only SLC influx transporter that has been shown to contribute to drug uptake across the human BBB. This was demonstrated indirectly in Parkinsonian patients by observing a decreased response to L-DOPA when administered with the LAT1 competitive inhibitors L-leucine and L-phenylalanine, despite no changes in L-DOPA plasma concentrations [48]. These results are supported by PET studies that demonstrated a decrease in  $^{18}\text{F}$ -L-6-fluorodopa brain accumulation in cynomolgus monkeys when the PET tracer is dosed after an intraperitoneal injection of L-phenylalanine versus alone [49]. These studies provide clear evidence for LAT1-mediated uptake of several drugs across the BBB into the human brain and suggest that LAT1 may be targeted to enhance drug delivery to the CNS.

Studies of targeting LAT1 to enhance CNS drug delivery are a major focus of this dissertation research, and are aimed at addressing the following questions. Are there chemically novel LAT1 ligands that can be identified through comparative modeling and *in vitro* cell-based assays? Can a genetically deficient Lat1 knockout mouse model be created and used to evaluate the contribution of Lat1 to drug uptake across the BBB into the CNS? Can low CNS permeable platinum chemotherapeutics be targeted to LAT1, and if so do these LAT1-targeted platinum drugs have enhanced penetration across the BBB?

### **Equilibrative Nucleoside Transporter 1 (ENT1; *SLC29A1*)**

ENT1 mediates the facilitated transport of purine and pyrimidine nucleosides, and is ubiquitously expressed in human tissues. Aside from endogenous nucleosides, ENT1 also transports numerous nucleoside analog drugs, including the anticancer drugs cytarabine and gemcitabine [50]. Even though ENT1 protein is expressed at the human BBB [15], its localization here is yet to be determined (Table 1.1). Nevertheless, ENT1-mediated uptake of several nucleoside analogs at the rodent BBB has been observed. The brain uptake of the PET probe, 3'-deoxy-3'-fluorothymidine was reduced by approximately 30% in Ent1 KO mice and wild type mice treated with the Ent1 inhibitor, nitrobenzylmercaptapurine ribonucleoside (NBMPR), relative to untreated wild type mice [51]. In another study, brain exposure to the A1 adenosine receptor agonist, tecadenoson, was reduced three-fold in NBMPR treated mice relative to untreated controls [52]. Although ENT1-mediated drug uptake at the BBB is evident from these studies, it is not clear whether ENT1 acts alone or in concert with another BBB transporter to transport drugs into the brain.

### **Monocarboxylate Transporter 1 (MCT1; *SLC16A1*)**

MCT1 transports small, aliphatic monocarboxylates such as lactate and acetate by either co-transport with a proton or in exchange for another monocarboxylate, and is ubiquitously expressed in human tissues [14, 53]. At the BBB, Mct1 has a similar expression pattern to Lat1 in that it is expressed in both the blood- and brain-facing membranes of the rat BBB [42] (Table 1.1). Furthermore, MCT1 transports the general anesthetic, gamma-hydroxybutyric acid (GHB) [54], and may also transport other drugs,

including valproic and salicylic acids [55]. MCT1 function at the BBB has been characterized in rats, where GHB uptake into the brain was reduced two-fold by concomitant treatment with the Mct1 competitive inhibitor, lactate, as compared to untreated controls [56, 57]. The authors concluded that this uptake was due to Mct1 since it is the only MCT present at the rat BBB. However, this does not exclude the presence of an unidentified transporter at the BBB that may also interact with lactate and GHB. Even though there is some evidence for MCT1-mediated drug uptake across the BBB, this function cannot be definitively attributed to MCT1 without using animal models with altered MCT1 function at the BBB.

### **Organic Anion Transporting Polypeptides (OATPs; *SLCOs*)**

OATPs are sodium-independent anion exchangers, and range in tissue distribution from single tissues to ubiquitous expression [58]. There is some disagreement over which OATP proteins are expressed at the human BBB, with OATP1A2 (*SLCO1A2*) and OATP2B1 (*SLCO2B1*) having been detected by immunohistochemistry (IHC) but not by mass spectrometry [15, 59, 60]. In these same IHC studies, human OATP2B1 was localized to the blood-facing membrane of the BBB, with the localization of OATP1A2 not determined. To further complicate matters, there appear to be species differences in the localization of both proteins. IHC studies in rats localized Oatp2b1 to either the brain-facing membrane of the BBB or pericytes that surround the brain microvessels [42]. The OATP1A2 rodent homolog Oatp1a4 localizes to the brain-facing membrane of the rat BBB [42], while in mice, Oatp1a4 localizes to both membranes [61] (see Table 1.1 for summary). Despite the differences in

expression pattern, both OATPs transport a wide range of drug substrates, including cholesterol-lowering statins and the antihistamine fexofenadine [62-65]. However, only the function of Oatp1a4 at the BBB has been investigated. Studies in mice using the in situ brain perfusion technique demonstrated large (up to seven-fold) reductions in the brain uptake of pitavastatin, rosuvastatin, taurocholate and ochratoxin A in Oatp1a4 KO mice relative to wild type mice [61]. However, the authors of this study went on to demonstrate that there were no differences in the brain accumulation of pitavastatin, rosuvastatin and taurocholate after systemic infusions of each drug in Oatp1a4 KO and wild type mice. Even though this study provides evidence for OATP function at the BBB under the artificial in situ brain perfusion conditions, the contribution of these transporters to drug uptake into the CNS appears to be minimal under physiological conditions, perhaps suggesting low expression levels on the endothelial plasma membrane.

**Table 1.1.** Membrane transporters mediating drug uptake into the CNS.

Gene	Protein	Transport Mechanism	BBB Probe Substrates	Human Localization	Rodent Localization
<i>ABCB1</i>	MDR1; P-gp	Active	Loperamide, Verapamil, Ivermectin, Vinblastine, Paclitaxel, Domperidone, Ondansetron, Cyclosporin A	Blood	Blood (mouse; rat)
<i>ABCG2</i>	BCRP; MXR	Active	Daidzein, Genistein	Blood	Blood (mouse; rat)
<i>ABCC1</i>	MRP1	Active	Unknown	Blood	Brain (mouse; rat)
<i>ABCC4</i>	MRP4	Active	Adefovir; Topotecan	Blood	Blood (rat)
<i>ABCC5</i>	MRP5	Active	Unknown	Blood	Brain (rat); Blood (mouse)
<i>SLC7A5</i>	LAT1	Facilitative	Levodopa	Blood/Brain	Blood/Brain (rat)
<i>SLC29A1</i>	ENT1	Facilitative	Tecadonson	Unknown	Unknown
<i>SLC16A1</i>	MCT1	H <sup>+</sup> -coupled, Facilitative	gamma-Hydroxybutyrate	Unknown	Blood/Brain (rat)
<i>SLCO1A2</i> <i>S/co1a4</i>	OATP1A2 Oatp1a4	Facilitative	Pitavastatin, Rosuvastatin, Taurocholate, Ochratoxin A, Digoxin	Unknown	Brain (rat); Blood/Brain (mouse)
<i>SLCO2B1</i>	OATP2B1	Facilitative	Unknown	Blood	Pericyte/Brain (rat)

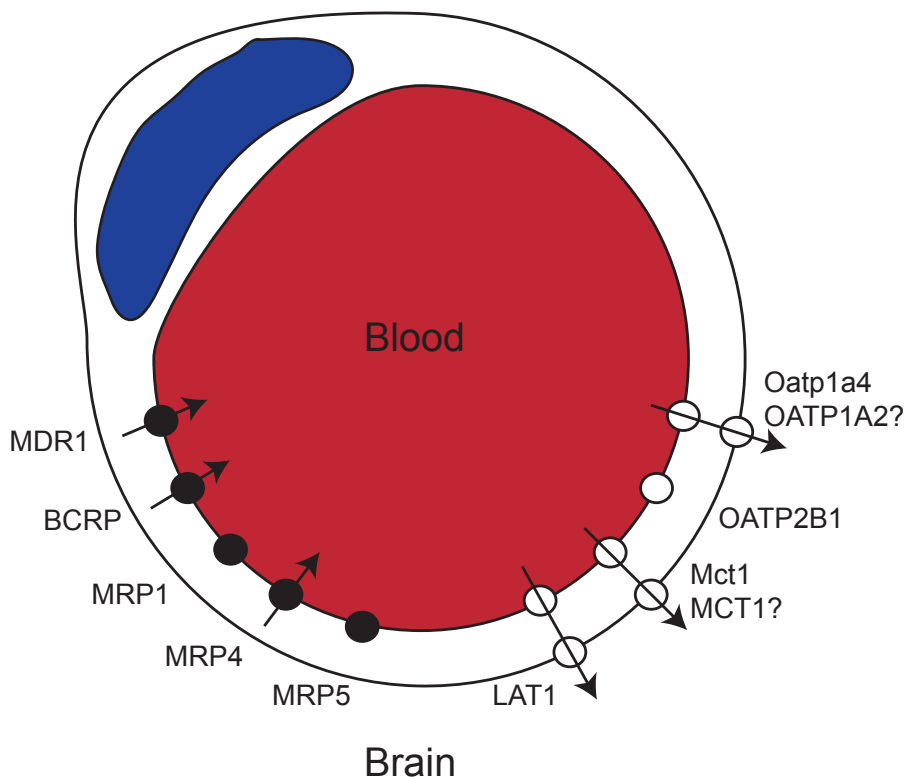


**Figure 1.1.** ABC and SLC drug transporters expressed at the human BBB. Black and white circles represent ABC and SLC transporters, respectively, that have been localized at the human BBB, with the exception of OATP1A2 and MCT1, for which localization at the rodent BBB is shown. Transporters that mediate drug penetration across the BBB have arrows that indicate the experimentally determined direction of transport. Red represents the blood and blue represents the endothelial cell nucleus. The brain parenchyma is also labeled as the space surrounding the outer endothelial cell membrane.

## **Future Directions**

Membrane transporters clearly play an important role in how the BBB regulates CNS drug uptake. While the contribution of ABC efflux transporters, such as MDR1 and BCRP to regulating drug penetration across the BBB has been studied extensively, the contribution of SLC influx transporters to this process is not well understood. Our poor understanding of how SLC transporters function at the BBB originates with not knowing which SLCs are expressed, let alone their localization at the human BBB. Even for SLCs with evidence of function at the BBB, such as ENT1, the localization is unknown (Table 1.1). Clearly, further studies identifying and localizing SLC transporters expressed at the human BBB will help elucidate their contributions not just to drug, but also to overall small molecule uptake across the BBB.

The few studies investigating SLC function at the BBB suggest that transporters such as LAT1 facilitate drug uptake into the CNS, and may provide a novel strategy for delivering drugs across the BBB. Indeed, this idea has been explored in several studies that have demonstrated drugs modified to become LAT1 substrates have enhanced brain accumulation relative to the unmodified drugs [66, 67]. However, these proof of concept studies used small molecule inhibitors that do not specifically target LAT1, and measured drug uptake into the brain under non-physiological conditions. Further studies exploring how transporters such as LAT1 may be targeted to enhance drug uptake across the BBB are needed to help validate this approach as a viable strategy for delivering drugs to the CNS.



## **Summary of Dissertation Chapters**

SLC transporters are important mediators of drug disposition, and help regulate the distribution of nutrients, xenobiotics, and drugs in all tissues throughout the body. This is particularly true of the CNS, where the BBB prevents free exchange between the blood and the brain. The goal of this research is to test the hypothesis that SLC influx transporters can be exploited to deliver drugs across the BBB into the CNS. This hypothesis is addressed in the following chapters.

### **Chapter 2. Profiling and Characterization of Solute Carrier Transporters in the Human Blood-Brain Barrier**

The neuroprotective function of the BBB presents a major challenge for CNS drug delivery. Critical to this function, BBB membrane transporters include ABC transporters that limit drug penetration across the BBB, and the less well characterized SLC influx transporters. The goal of this chapter was to identify drug transporters expressed at the human BBB, and determine their functionality at the BBB using mice. The expression of 359 SLC and 49 ABC transporters in human cerebral cortex and isolated brain microvessels (BMV) was characterized. *ABCB1* and *ABCG2* were the most highly enriched ABC transporters in BMVs. Analysis of SLC transporters identified uncharacterized BBB transporters (e.g. *SLC19A3* and *SLC47A2*), and found xenobiotic transporters expressed at similar or higher mRNA levels in BMVs relative to human liver or kidney samples. Immunohistochemistry identified the reduced folate carrier (RFC), MATE1 and OCT3 protein in BMVs. In mice, methotrexate uptake into the brain was sensitive to two Rfc inhibitors, indicating Rfc-mediated CNS permeability of

methotrexate. These findings highlight contributions of SLC transporters to BBB function.

### **Chapter 3. Targeting LAT1 with Chemically Modified Cisplatin Analogs**

LAT1 is a sodium-independent exchanger of amino acids that also mediates drug uptake across the BBB. Cisplatin is an effective anticancer drug that has low CNS permeability, and is amenable to chemical modifications. Furthermore, some modified cisplatin derivatives inadvertently have enhanced transporter interactions (e.g. oxaliplatin with organic cation transporters). There are two goals for the studies in this chapter: demonstrate that LAT1-targeted cisplatin analogs are LAT1 substrates *in vitro*, and generate a mouse model with reduced Lat1 function to investigate LAT1-specific drug uptake across the BBB. Cell-based assays identified one out of seven LAT1-targeted platinum compounds to be a weak LAT1 substrate with similar cytotoxic potency as cisplatin. Although homozygous deletion of Lat1 in mice is embryonic lethal, Lat1 heterozygous mice had reduced brain accumulation of two Lat1 drug substrates. These results indicate that LAT1 is capable of transporting cytotoxic platinum-based compounds, and that Lat1 heterozygous mice serve as a model for determining Lat1-mediated brain uptake of drugs and other small molecule substrates.

### **Chapter 4. Structure-based Ligand Discovery for the Large-neutral Amino Acid Transporter 1, LAT1**

LAT1 was first discovered for its ability to transport branched-chain and aromatic amino acids such as leucine and phenylalanine. Even though the amino acid substrate

profile of LAT1 is well established, the endogenous, xenobiotic, and drug ligand profile of LAT1 is unknown. Identifying such ligands will aid in the design of new LAT1-targeted drug analogs. Thus, the goal of this chapter was to identify and characterize novel LAT1 ligands that could be used to design novel LAT1-targeted platinum compounds. Four ligands, including one chemically novel substrate, were identified by comparative modeling, virtual screening, and experimental validation. These results may rationalize the enhanced brain permeability of two drugs, including the anticancer agent acivicin. Aside from the BBB, LAT1 also plays an important role in cancer development. In this context, two hits were found to inhibit proliferation of a cancer cell line by different LAT1-specific mechanisms. Taken together, these results provide new chemical tools for characterizing the role of LAT1 in cancer metabolism and drug uptake across the BBB.

## References

1. Hediger MA, Romero MF, Peng JB, Rolfs A, Takanaga H, Bruford EA. The ABCs of solute carriers: physiological, pathological and therapeutic implications of human membrane transport proteinsIntroduction. *Pflugers Arch*. 2004;447(5):465-8.
2. Holland IB. ABC transporters, mechanisms and biology: an overview. *Essays Biochem*. 2011;50(1):1-17.
3. Borst P, Elferink RO. Mammalian ABC transporters in health and disease. *Annu Rev Biochem*. 2002;71:537-92.
4. Hagenbuch B. Molecular properties of hepatic uptake systems for bile acids and organic anions. *J Membr Biol*. 1997;160(1):1-8.

5. Hagenbuch B, Gao B, Meier PJ. Transport of xenobiotics across the blood-brain barrier. *News Physiol Sci.* 2002;17:231-4.
6. Hagenbuch B. Drug uptake systems in liver and kidney: a historic perspective. *Clin Pharmacol Ther.* 2010;87(1):39-47. PMCID: 2819296.
7. Koepsell H. Organic cation transporters in intestine, kidney, liver, and brain. *Annu Rev Physiol.* 1998;60:243-66.
8. Nigam SK, Bush KT, Bhatnagar V. Drug and toxicant handling by the OAT organic anion transporters in the kidney and other tissues. *Nat Clin Pract Nephrol.* 2007;3(8):443-8.
9. Schinkel AH, Jonker JW. Mammalian drug efflux transporters of the ATP binding cassette (ABC) family: an overview. *Adv Drug Deliv Rev.* 2003;55(1):3-29.
10. Sweet DH, Bush KT, Nigam SK. The organic anion transporter family: from physiology to ontogeny and the clinic. *Am J Physiol Renal Physiol.* 2001;281(2):F197-205.
11. You G. The role of organic ion transporters in drug disposition: an update. *Curr Drug Metab.* 2004;5(1):55-62.
12. Abbott NJ, Patabendige AA, Dolman DE, Yusof SR, Begley DJ. Structure and function of the blood-brain barrier. *Neurobiology of disease.* 2010;37(1):13-25.
13. Hurko O, Ryan JL. Translational research in central nervous system drug discovery. *NeuroRx.* 2005;2(4):671-82.
14. Shawahna R, Uchida Y, Decleves X, Ohtsuki S, Yousif S, Dauchy S, et al. Transcriptomic and quantitative proteomic analysis of transporters and drug

metabolizing enzymes in freshly isolated human brain microvessels. *Mol Pharm.* 2011;8(4):1332-41.

15. Uchida Y, Ohtsuki S, Katsukura Y, Ikeda C, Suzuki T, Kamiie J, et al. Quantitative targeted absolute proteomics of human blood-brain barrier transporters and receptors. *J Neurochem.* 2011;117(2):333-45.

16. Clark DE. In silico prediction of blood-brain barrier permeation. *Drug Discov Today.* 2003;8(20):927-33.

17. Begley DJ. ABC transporters and the blood-brain barrier. *Curr Pharm Des.* 2004;10(12):1295-312.

18. Loscher W, Potschka H. Drug resistance in brain diseases and the role of drug efflux transporters. *Nat Rev Neurosci.* 2005;6(8):591-602.

19. Mensch J, Oyarzabal J, Mackie C, Augustijns P. In vivo, in vitro and in silico methods for small molecule transfer across the BBB. *J Pharm Sci.* 2009;98(12):4429-68.

20. Warren MS, Zerangue N, Woodford K, Roberts LM, Tate EH, Feng B, et al. Comparative gene expression profiles of ABC transporters in brain microvessel endothelial cells and brain in five species including human. *Pharmacol Res.* 2009;59(6):404-13.

21. Kalvass JC, Polli JW, Bourdet DL, Feng B, Huang SM, Liu X, et al. Why Clinical Modulation of Efflux Transport at the Human Blood-Brain Barrier Is Unlikely: The ITC Evidence-Based Position. *Clin Pharmacol Ther.* 2013;94(1):80-94.

22. Schinkel AH. The physiological function of drug-transporting P-glycoproteins. *Semin Cancer Biol.* 1997;8(3):161-70.

23. International Transporter C, Giacomini KM, Huang SM, Tweedie DJ, Benet LZ, Brouwer KL, et al. Membrane transporters in drug development. *Nat Rev Drug Discov.* 2010;9(3):215-36.
24. Thiebaut F, Tsuruo T, Hamada H, Gottesman MM, Pastan I, Willingham MC. Immunohistochemical localization in normal tissues of different epitopes in the multidrug transport protein P170: evidence for localization in brain capillaries and crossreactivity of one antibody with a muscle protein. *J Histochem Cytochem.* 1989;37(2):159-64.
25. Schinkel AH, Smit JJ, van Tellingen O, Beijnen JH, Wagenaar E, van Deemter L, et al. Disruption of the mouse *mdr1a* P-glycoprotein gene leads to a deficiency in the blood-brain barrier and to increased sensitivity to drugs. *Cell.* 1994;77(4):491-502.
26. Doran A, Obach RS, Smith BJ, Hosea NA, Becker S, Callegari E, et al. The impact of P-glycoprotein on the disposition of drugs targeted for indications of the central nervous system: evaluation using the MDR1A/1B knockout mouse model. *Drug Metab Dispos.* 2005;33(1):165-74.
27. Liu X, Ding X, Deshmukh G, Liederer BM, Hop CE. Use of the cassette-dosing approach to assess brain penetration in drug discovery. *Drug Metab Dispos.* 2012;40(5):963-9.
28. Sasongko L, Link JM, Muzi M, Mankoff DA, Yang X, Collier AC, et al. Imaging P-glycoprotein transport activity at the human blood-brain barrier with positron emission tomography. *Clin Pharmacol Ther.* 2005;77(6):503-14.
29. Kreisl WC, Liow JS, Kimura N, Seneca N, Zoghbi SS, Morse CL, et al. P-glycoprotein function at the blood-brain barrier in humans can be quantified with the substrate radiotracer <sup>11</sup>C-N-desmethyl-loperamide. *J Nucl Med.* 2010;51(4):559-66.

30. Sisodiya SM, Martinian L, Scheffer GL, van der Valk P, Scheper RJ, Harding BN, et al. Vascular colocalization of P-glycoprotein, multidrug-resistance associated protein 1, breast cancer resistance protein and major vault protein in human epileptogenic pathologies. *Neuropathol Appl Neurobiol.* 2006;32(1):51-63.
31. Agarwal S, Hartz AM, Elmquist WF, Bauer B. Breast cancer resistance protein and P-glycoprotein in brain cancer: two gatekeepers team up. *Curr Pharm Des.* 2011;17(26):2793-802.
32. Kodaira H, Kusuhara H, Fujita T, Ushiki J, Fuse E, Sugiyama Y. Quantitative evaluation of the impact of active efflux by p-glycoprotein and breast cancer resistance protein at the blood-brain barrier on the predictability of the unbound concentrations of drugs in the brain using cerebrospinal fluid concentration as a surrogate. *J Pharmacol Exp Ther.* 2011;339(3):935-44.
33. Kodaira H, Kusuhara H, Ushiki J, Fuse E, Sugiyama Y. Kinetic analysis of the cooperation of P-glycoprotein (P-gp/Abcb1) and breast cancer resistance protein (Bcrp/Abcg2) in limiting the brain and testis penetration of erlotinib, flavopiridol, and mitoxantrone. *J Pharmacol Exp Ther.* 2010;333(3):788-96.
34. Zamek-Gliszczyński MJ, Kalvass JC, Pollack GM, Brouwer KL. Relationship between drug/metabolite exposure and impairment of excretory transport function. *Drug Metab Dispos.* 2009;37(2):386-90.
35. Wanek T, Kuntner C, Bankstahl JP, Bankstahl M, Stanek J, Sauberer M, et al. A comparative small-animal PET evaluation of [11C]tariquidar, [11C]elacridar and (R)-[11C]verapamil for detection of P-glycoprotein-expressing murine breast cancer. *Eur J Nucl Med Mol Imaging.* 2012;39(1):149-59.

36. Nies AT, Jedlitschky G, König J, Herold-Mende C, Steiner HH, Schmitt HP, et al. Expression and immunolocalization of the multidrug resistance proteins, MRP1-MRP6 (ABCC1-ABCC6), in human brain. *Neuroscience*. 2004;129(2):349-60.
37. Cisternino S, Rousselle C, Lorico A, Rappa G, Scherrmann JM. Apparent lack of Mrp1-mediated efflux at the luminal side of mouse blood-brain barrier endothelial cells. *Pharm Res*. 2003;20(6):904-9.
38. Wang F, Zhou F, Kruh GD, Gallo JM. Influence of blood-brain barrier efflux pumps on the distribution of vincristine in brain and brain tumors. *Neuro Oncol*. 2010;12(10):1043-9.
39. Leggas M, Adachi M, Scheffer GL, Sun D, Wielinga P, Du G, et al. Mrp4 confers resistance to topotecan and protects the brain from chemotherapy. *Mol Cell Biol*. 2004;24(17):7612-21.
40. Belinsky MG, Guo P, Lee K, Zhou F, Kotova E, Grinberg A, et al. Multidrug resistance protein 4 protects bone marrow, thymus, spleen, and intestine from nucleotide analogue-induced damage. *Cancer Res*. 2007;67(1):262-8.
41. Kanai Y, Segawa H, Miyamoto K, Uchino H, Takeda E, Endou H. Expression cloning and characterization of a transporter for large neutral amino acids activated by the heavy chain of 4F2 antigen (CD98). *The Journal of biological chemistry*. 1998;273(37):23629-32.
42. Roberts LM, Black DS, Raman C, Woodford K, Zhou M, Haggerty JE, et al. Subcellular localization of transporters along the rat blood-brain barrier and blood-cerebral-spinal fluid barrier by in vivo biotinylation. *Neuroscience*. 2008;155(2):423-38.



43. Sanchez del Pino MM, Peterson DR, Hawkins RA. Neutral amino acid transport characterization of isolated luminal and abluminal membranes of the blood-brain barrier. *J Biol Chem.* 1995;270(25):14913-8.
44. Uchino H, Kanai Y, Kim DK, Wempe MF, Chairoungdua A, Morimoto E, et al. Transport of amino acid-related compounds mediated by L-type amino acid transporter 1 (LAT1): insights into the mechanisms of substrate recognition. *Mol Pharmacol.* 2002;61(4):729-37.
45. del Amo EM, Urtti A, Yliperttula M. Pharmacokinetic role of L-type amino acid transporters LAT1 and LAT2. *Eur J Pharm Sci.* 2008;35(3):161-74.
46. Geier EG, Schlessinger, A., Fan, H., Gable, J. E., Irwin, J. J., Sali, A., Giacomini, K. M. Structure-based ligand discovery for the Large-neutral Amino Acid Transporter 1, LAT-1. *PNAS.* 2013.
47. Dickens D, Webb SD, Antonyuk S, Giannoudis A, Owen A, Radisch S, et al. Transport of gabapentin by LAT1 (SLC7A5). *Biochem Pharmacol.* 2013;85(11):1672-83.
48. Nutt JG, Woodward WR, Hammerstad JP, Carter JH, Anderson JL. The "on-off" phenomenon in Parkinson's disease. Relation to levodopa absorption and transport. *N Engl J Med.* 1984;310(8):483-8.
49. Hammerstad JP, Pate BD, Hewitt KA, Chan GL, Ruth TJ, Calne DB. The transport of L-6-fluorodopa and its metabolites from blood to cerebrospinal fluid and brain. *Ann Neurol.* 1993;34(4):603-8.
50. Baldwin SA, Beal PR, Yao SY, King AE, Cass CE, Young JD. The equilibrative nucleoside transporter family, SLC29. *Pflugers Arch.* 2004;447(5):735-43.

51. Paproski RJ, Wuest M, Jans HS, Graham K, Gati WP, McQuarrie S, et al. Biodistribution and uptake of 3'-deoxy-3'-fluorothymidine in ENT1-knockout mice and in an ENT1-knockdown tumor model. *J Nucl Med*. 2010;51(9):1447-55.
52. Lepist EI, Damaraju VL, Zhang J, Gati WP, Yao SY, Smith KM, et al. Transport of A1 adenosine receptor agonist tecadenoson by human and mouse nucleoside transporters: evidence for blood-brain barrier transport by murine equilibrative nucleoside transporter 1 mENT1. *Drug Metab Dispos*. 2013;41(4):916-22.
53. Halestrap AP, Wilson MC. The monocarboxylate transporter family--role and regulation. *IUBMB Life*. 2012;64(2):109-19.
54. Wang Q, Lu Y, Morris ME. Monocarboxylate transporter (MCT) mediates the transport of gamma-hydroxybutyrate in human kidney HK-2 cells. *Pharm Res*. 2007;24(6):1067-78.
55. Hosoya K, Kondo T, Tomi M, Takanaga H, Ohtsuki S, Terasaki T. MCT1-mediated transport of L-lactic acid at the inner blood-retinal barrier: a possible route for delivery of monocarboxylic acid drugs to the retina. *Pharm Res*. 2001;18(12):1669-76.
56. Roiko SA, Vijay N, Felmler MA, Morris ME. Brain extracellular gamma-hydroxybutyrate concentrations are decreased by L-lactate in rats: role in the treatment of overdoses. *Pharm Res*. 2013;30(5):1338-48.
57. Roiko SA, Felmler MA, Morris ME. Brain uptake of the drug of abuse gamma-hydroxybutyric acid in rats. *Drug Metab Dispos*. 2012;40(1):212-8.
58. Klaassen CD, Aleksunes LM. Xenobiotic, bile acid, and cholesterol transporters: function and regulation. *Pharmacol Rev*. 2010;62(1):1-96.

59. Gao B, Hagenbuch B, Kullak-Ublick GA, Benke D, Aguzzi A, Meier PJ. Organic anion-transporting polypeptides mediate transport of opioid peptides across blood-brain barrier. *J Pharmacol Exp Ther*. 2000;294(1):73-9.
60. Bronger H, König J, Kopplow K, Steiner HH, Ahmadi R, Herold-Mende C, et al. ABC drug efflux pumps and organic anion uptake transporters in human gliomas and the blood-tumor barrier. *Cancer Res*. 2005;65(24):11419-28.
61. Ose A, Kusuhara H, Endo C, Tohyama K, Miyajima M, Kitamura S, et al. Functional characterization of mouse organic anion transporting peptide 1a4 in the uptake and efflux of drugs across the blood-brain barrier. *Drug Metab Dispos*. 2010;38(1):168-76.
62. Cvetkovic M, Leake B, Fromm MF, Wilkinson GR, Kim RB. OATP and P-glycoprotein transporters mediate the cellular uptake and excretion of fexofenadine. *Drug Metab Dispos*. 1999;27(8):866-71.
63. Fujino H, Saito T, Ogawa S, Kojima J. Transporter-mediated influx and efflux mechanisms of pitavastatin, a new inhibitor of HMG-CoA reductase. *J Pharm Pharmacol*. 2005;57(10):1305-11.
64. Nozawa T, Imai K, Nezu J, Tsuji A, Tamai I. Functional characterization of pH-sensitive organic anion transporting polypeptide OATP-B in human. *J Pharmacol Exp Ther*. 2004;308(2):438-45.
65. Kitamura S, Maeda K, Wang Y, Sugiyama Y. Involvement of multiple transporters in the hepatobiliary transport of rosuvastatin. *Drug Metab Dispos*. 2008;36(10):2014-23.

66. Killian DM, Hermeling S, Chikhale PJ. Targeting the cerebrovascular large neutral amino acid transporter (LAT1) isoform using a novel disulfide-based brain drug delivery system. *Drug delivery*. 2007;14(1):25-31.
67. Gynther M, Jalkanen A, Lehtonen M, Forsberg M, Laine K, Ropponen J, et al. Brain uptake of ketoprofen-lysine prodrug in rats. *International journal of pharmaceutics*. 2010;399(1-2):121-8.

## **CHAPTER 2**

### **Expression Profiling and Characterization of Solute Carrier Transporters in the Human Blood-Brain Barrier**

#### **Introduction**

The blood-brain barrier (BBB) regulates exchange between the blood and the central nervous system (CNS) through unique properties of the endothelial cells forming the CNS vasculature [1, 2]. This function helps maintain the neural microenvironment while simultaneously preventing most drugs from permeating the CNS, thereby limiting treatment options for many diseases. It is estimated that around 95% of small molecule drugs developed to target the CNS fail, and this is in large part due to their inability to efficiently penetrate the BBB [2]. Clearly there is a need to better understand the properties of the BBB that regulate drug entry into the CNS.

The two primary routes by which most small molecules pass through the BBB to the CNS are transcellular passive diffusion and carrier-mediated transport. Low molecular weight (< 450 Da), lipophilic molecules tend to passively diffuse across the BBB, whereas more hydrophilic molecules require carrier-mediated processes to reach the CNS [3, 4]. Furthermore, both paths require overcoming the ATP-binding cassette (ABC) transporters and metabolic enzymes expressed in CNS endothelial cells [5, 6]. For example, ABC transporters such as MDR1 have well-established roles in preventing small molecule drugs from crossing the BBB [7, 8]. Accordingly, most BBB transporter expression profiling and functional studies have focused on ABCs, whereas the solute carrier (SLC) transporters as a group have been largely overlooked.

SLC transporters play major roles in the delivery of nutrients to the CNS [9], and are also capable of transporting small molecule drugs across the BBB. For example, the large-neutral amino acid transporter 1, LAT1, is expressed at the BBB and has previously been thought to mediate the transport of a few drugs with amino acid-like structures across the BBB, e.g., the anti-parkinsonian drug L-DOPA [6, 10]. However, recent structure-function studies from our laboratory suggest that the transporter may facilitate the uptake of a wider range of chemical structures beyond amino acid analogs [11]. There is also evidence for nucleoside analog uptake into the CNS via the equilibrative nucleoside transporter 1 expressed at the BBB [12, 13]. Despite these examples, the full complement of SLC transporters expressed at the human BBB remains unclear, and the extent to which SLC transporters may contribute to small molecule drug penetration across the BBB is unknown.

In this study, we isolated human brain microvessels (BMV) to identify SLC transporters expressed at the human BBB. The transporter expression profile was determined using a real-time PCR (RT-PCR) OpenArray containing probes for 359 SLC and 46 ABC transporters [14]. Unlike most previous BBB expression profiling studies, transcriptomic studies were followed up with immunoassays to determine the presence of transporter protein in BMVs. Finally, transporter expression results were translated to functional studies investigating the contribution of the reduced folate carrier (RFC) to methotrexate uptake into the CNS of mice. These studies suggest that the BBB is rich in expression of SLC transporters and imply an important role for this superfamily in CNS homeostasis and drug delivery.

## Materials and Methods

**Tissue acquisition.** Four partial human cerebral cortex samples were procured from the National Disease Research Interchange (Philadelphia, PA). Donor demographics and medical history are provided in Table 2.1. For comparative expression profiling of non-ocular tissue, normal human liver and kidney tissue were commercially obtained (Asterand, Detroit, MI). All tissues were acquired in accordance with UCSF Institutional Review Board and ethics committee guidelines (IRB number 11-06153).

**Table 2.1.** Tissue donor information.

Brain Region	Analysis	Age	Sex	Race	Cause of Death	Comorbidities
Cortex	OpenArray, TaqMan IHC, WB	62	M	C	Respiratory arrest	COPD, cardiomyopathy, high blood pressure
Cortex	OpenArray, TaqMan	63	M	C	Cardio-pulmonary arrest	COPD, hypertension, heart disease, hypothyroidism
Cortex	TaqMan	68	F	C	Intracranial hemorrhage	Hypertension
Cortex	IHC	65	M	C	Cardiac arrest	Heart disease, hypertension, bladder cancer, anemia, gout, type II diabetes

IHC, immunohistochemistry; WB, western blot; M, Male; F, Female; C, Caucasian; COPD, chronic obstructive pulmonary disease.

**BMV isolation.** BMVs were isolated using a previously established protocol [15]. Approximately one gram of tissue was homogenized in ice cold Hanks' balanced salt

solution (HBSS; Invitrogen, Carlsbad, CA) with a Potter–Elvehjem homogenizer (Thomas Scientific, Swedesboro, NJ). The homogenate was centrifuged for 5 min at 1000 *g* at 4°C, and the supernatant was aspirated. The pellet was resuspended in an autoclaved 17% dextran solution (Sigma-Aldrich, St Louis, MO) and centrifuged for 15 min at 4250 *g* at 4°C. The myelin-enriched supernatant was aspirated and the resulting BMV-enriched pellet was resuspended in ice cold HBSS. This solution was applied to a 40 µm nylon mesh filter, and BMVs retained on the filter were washed with 40 ml of ice cold HBSS. BMVs were recovered from the filter, and centrifuged for 5 min at 4250 *g* at 4°C. The resulting pellet was then used immediately for RNA extraction or immunohistochemistry (IHC).

***RNA extraction and reverse transcriptase PCR.*** Total RNA was extracted from the BMV-enriched samples (n=3), cerebral cortex (n=3), liver (n=59), and kidney (n=60) tissue homogenates using TRIzol Reagent and RNeasy Plus Micro Kit (Qiagen, Valencia, CA), according to the kit instructions. After separation of the organic and aqueous phases by centrifugation, total RNA was isolated from the aqueous phase using an RNeasy Plus Micro Kit. After isolation, RNA samples were stored at -80°C. Total RNA (up to 1 µg) was reverse transcribed using the SuperScript VILO cDNA Synthesis Kit (Life Technologies, Grand Island, NY) according to the manufacturer's instructions. The resulting cDNA samples were stored at -80°C.

***Real Time-PCR.*** High-throughput, RT-PCR was performed using a customized OpenArray® system (Life Technologies) as previously described [14]. cDNA at a concentration of 108 ng/µL and SYBR Green qPCR reagent (Fast Start DNA SYBR Green kit, Roche, CA) were dispensed into custom plates containing 448 pre-validated



real-time SYBR Green PCR assays. RT-PCR occurred in a computer-controlled imaging thermal cycler where 9216 PCR amplifications and dissociation curves were implemented in less than four hours. The transporter genes analyzed and the PCR primers used are described in a previous study [14]. Post-acquisition data processing generated fluorescence amplification and melt curves for each through-hole in the array, from which cycle threshold ( $C_T$ ) and melt temperature ( $T_m$ ) were computed and used for further data analysis.

The relative expression of each gene in the different tissues was calculated by the  $\Delta\Delta C_T$  comparative expression method [16]. The  $\Delta C_T$  values for all the genes in each sample were calculated by subtracting the mean  $C_T$  values for three housekeeping genes (GAPDH,  $\beta$ -Actin, and  $\beta 2$  microglobulin) from the  $C_T$  for each target gene. The relative quantity of each gene was then determined by calculating the  $2^{-\Delta C_T}$  value. To determine the fold change in gene expression relative to a reference tissue, the log2-transformed relative quantity values from each tissue were compared to each other.

Microplate-based SYBR green RT-PCR was used to measure cell type marker gene expression. Two ng of BMV or cerebral cortex cDNA was used as a template, and PCR primers for either platelet endothelial cell adhesion molecule (*PECAM1*), vascular endothelial cadherin (*VEC*), glucose transporter 1 (*GLUT1*), synaptophysin (*SYP*), or glial fibrillary acidic protein (*GFAP*). RT-PCR reactions were carried out in 96-well reaction plates in a volume of 10  $\mu$ L using the Fast SYBR green Universal Master Mix (Life Technologies). Reaction plates were run on the Applied Biosystems 7900HT Fast Real-Time PCR System with the following profile: 95°C for 20 seconds followed by 40

cycles of 95°C for 3 seconds and 60°C for 30 seconds. The relative expression of each mRNA was calculated by the comparative  $\Delta\Delta C_t$  method described above.

Microplate-based TaqMan RT-PCR was done using BMV cDNA as a template and TaqMan Gene Expression Assays for human GAPDH (Hs99999905\_m1), ACTB (Hs01060665\_m1), PGK1 (Hs99999906\_m1), ABCB1 (Hs00184491\_m1), ABCG2 (Hs01053790\_m1), SLC2A1 (Hs00892681\_m1), SLC5A6 (Hs00221573\_m1), SLC7A5 (Assay ID: Hs01001190\_m1), SLC19A2 (Hs00949696\_m1), SLC22A3 (Hs01009568), SLC47A1 (Hs00217320), SLC47A2 (Hs00398719\_m1), SLCO1A2 (Hs00366488\_m1), SLCO2B1 (Hs\_00200670), and SLCO3A1 (Hs00203184\_m1). RT-PCR reactions were carried out in 96-well reaction plates in a volume of 10  $\mu$ L using the TaqMan Fast Universal Master Mix (Life Technologies). Reactions were run on the Applied Biosystems 7500 Fast Real-Time PCR System with the following profile: 95°C for 20 seconds followed by 40 cycles of 95°C for 3 seconds and 60°C for 30 seconds. The relative expression of each mRNA was calculated by the comparative  $\Delta\Delta C_t$  method.

**Western blot analysis.** Western blotting of human BMV and human embryonic kidney (HEK) transfected cell lysates was performed as previously described [17]. Protein was extracted from BMVs and HEK cells by incubating with prechilled CellLytic Mcell lysis buffer (Sigma-Aldrich, St Louis, MO) containing a protease inhibitor cocktail for 20 min at 4°C. Homogenates were centrifuged for 10 min at 15,000 rpm at 4°C, and the protein concentration of the supernatant determined by BCA protein assay (Thermo Fisher Scientific, Rockford, IL) using the manufacturer's protocol. Up to 50  $\mu$ g of total protein was subjected to SDS-PAGE using a tris-glycine 4-15% polyacrylamide gel (Bio-Rad, Hercules, CA), and then transferred onto a polyvinylidene difluoride membrane

(Bio-Rad, Hercules, CA). Membranes were blocked in Protein-free T20 Blocking Buffer (Thermo Fisher Scientific, Rockford, IL) for 1 hr at room temperature, and then incubated with primary antibodies diluted in blocking buffer overnight at 4°C (see Materials and Methods section for antibody information). Membranes were then washed with tris-buffered saline containing 0.1% tween 20 (TBST) at pH 7.4 6 times for 5 min prior to incubating with HRP-conjugated goat anti-rabbit IgG diluted in TBST for 1 hr at room temperature. Membranes were then washed 6 times for 5 min in TBST again, and developed with SuperSignal West Femto Kit (Thermo Fisher Scientific, Rockford, IL) using the manufacturer's protocol. All scanned membrane images were processed using ImageJ.

***Immunohistochemistry.*** IHC analysis of isolated BMVs was performed as previously described [18]. BMV-enriched pellets were resuspended in ice cold HBSS and seeded onto positively charged glass slides, and fixed with 4% paraformaldehyde for 15 min at 4°C. Slides were then washed and stored in HBSS at 4°C until use (within one week of fixing). Fixed BMVs were permeabilized and nonspecific antibody binding blocked by treatment with 30% normal goat serum in phosphate-buffered saline (PBS) containing 0.1% tween 20 (PBST) at pH 7.4 for 1 hr at room temperature, and incubated overnight at 4°C in PBS containing 3% normal goat serum and primary antibodies against the following target proteins: LAT1 (Epitomics, Burlingame, CA), OCT3 (Genway, San Diego, CA), RFC (Sigma-Aldrich), MATE1 (Sigma-Aldrich, St Louis, MO), OATP1B3 (Sigma-Aldrich) and Rfc (LifeSpan Biosciences, Seattle, WA). Negative control sections were stained without primary antibody at this step. Slides were then washed with PBS 6 times for 5 min and incubated with an Alexa 488 conjugated

secondary antibody (Life Technologies) for 1 hr at room temperature. Slides were washed with PBS 6 times for 5 min again, and mounted in VECTASHIELD Mounting Medium with DAPI (Vector Labs, Burlingame, CA). Fluorescent imaging was done on a Zeiss AxioImager M1 microscope with AxioCam Mrm camera (Carl Zeiss Microscopy, Thornwood, NY), and bright field imaging was done on a Leica DM IL LED microscope with DFC400 camera (Leica Microsystems, Buffalo Grove, IL). Image files were processed with ImageJ [19].

***Animals.*** C57BL/6J mice were housed under a 12-hour light/dark cycle with free access to water and folate deficient food (Harlan Laboratories, Indianapolis, IN). All animals used in experiments were between 8 to 10 weeks of age. mice were obtained from the Jackson Laboratory (Bar Harbor, ME). Mice were maintained on a folate deficient diet for 2 weeks prior to experiments. All experiments in mice were approved by the Institutional Animal Care and Use Committee of University of California at San Francisco (protocol # AN089117-01B).

***Pharmacokinetic and tissue accumulation studies.*** Male C57BL/6J mice were dosed with 15 µg/kg <sup>3</sup>H-methotrexate in saline alone, with 1.5 mg/kg bromosulfophthalein (Sigma-Aldrich), or with 1.5 mg/kg folinic acid (Sigma-Aldrich) via tail vein injection. Blood samples were collected at 5, 10, 15, 30, and 60 min by tail bleeding into heparinized microhematocrit capillary tubes (Fisher Scientific, Pittsburgh, PA). Mice were sacrificed 60 min after injection, perfused with 10 mL of ice cold PBS, and brain, liver, and kidney tissues were collected immediately. Blood was centrifuged to obtain plasma, and tissues were homogenized in Solvable (PerkinElmer, Waltham, MA). The amount of <sup>3</sup>H-MTX in plasma and tissue samples was quantified by liquid

scintillation counting using a Beckman LS 6500 scintillation counter (Brea, CA).

Pharmacokinetic parameters were obtained by non-compartmental analysis using WinNonlin 6.3 (Pharsight Corporation, Mountain view, CA).

**Statistical analysis.** Data were compared by one-way ANOVA followed by Dunnett's multiple comparison test. All statistics were done with GraphPad Software (La Jolla, CA), and probability values lower than 0.05 were considered statistically significant.

## Results

**Validation of BMV enrichment.** Human cerebral cortex samples (Table S1) from three donors were used to prepare BMV enriched fractions for human BBB transporter identification by mRNA expression profiling. BMV enrichment was determined by visual inspection (Figure 2.1A) and measuring expression of pan-endothelial (*PECAM1* and *VEC*), brain endothelial (*GLUT1*), neuronal (*SYP*), and astrocytic (*GFAP*) cell markers (Figure 2.1B). Visual inspection indicated that the majority of blood vessels in BMV fractions were  $\leq 10\ \mu\text{m}$  diameter. Furthermore, cell marker analysis revealed that all measured endothelial cell genes increased from 3 to 45-fold, while *SYP* and *GFAP* were both reduced approximately 2-fold in BMV enriched fractions relative to paired whole cerebral cortex samples. These results indicate that the BMV fraction was successfully enriched with the blood vessels comprising the BBB.

**Transporter mRNA expression profile in BMVs.** A custom RT-PCR OpenArray platform was used to profile expression of 359 SLC and 46 ABC transporter genes in validated BMV enriched and paired whole cerebral cortex samples from two donors

(Table 2.1). We detected expression of 244 and 248 SLC genes in both BMV and cerebral cortex samples, respectively, while 42 ABC genes were expressed across all BMV and cerebral cortex samples. Out of all transporter genes detected, 225 SLC and 39 ABC genes were detected in both paired BMV-cerebral cortex samples, with 46 SLC and 13 ABC genes expressed at least two-fold higher on average in BMVs relative to cerebral cortex. Table 2.2 contains a complete list of genes detected in BMVs and their relative expression levels. The 25 most highly expressed transporter genes relative to cerebral cortex are shown in Figure 2.2A. Nineteen SLC and 3 ABC genes were uniquely detected in both BMV samples, and not detected in both cerebral cortex samples (Figure 2.2B). Importantly, this analysis identified many transporters previously unknown to have enriched expression in human BMVs, including *SLC6A13*, *SLC19A3*, all *SLC26s* and *SLC47A2* (Figure 2.2; Table 2.2).

Several transporters previously identified in the human BBB, such as *SLC7A5*, *SLCO2B1*, *ABCB1*, and *ABCG2*, were also enriched in our BMV samples (Figure 2.2B). Enrichment of these and several other genes (*SLC22A3*, *SLC47A1*, *SLC47A2* and *SLC5A6*) was confirmed by TaqMan gene expression analysis of three BMV and paired cerebral cortex samples (Figure 2.3). OpenArray results indicated that *SLC19A2*, *SLCO1A2*, and *SLCO3A1* were not enriched in BMV samples, and were included as negative controls. Furthermore, linear regression analysis on the OpenArray and TaqMan enrichment values yielded an  $r^2 = 0.60$  (Figure 2.3), indicating good agreement between the two RT-PCR technologies, and confirming the array-based expression profiling results.

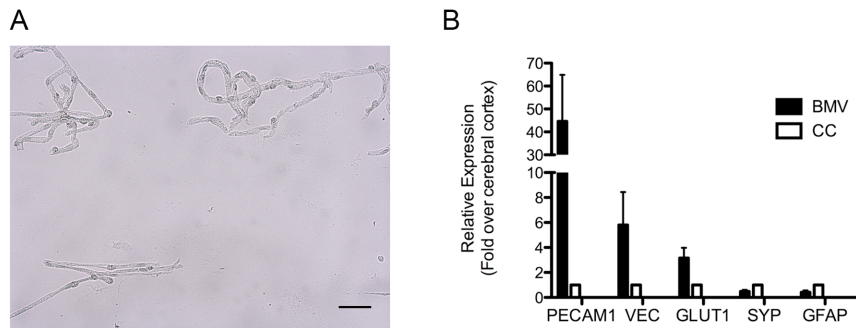


**Figure 2.1.** Validation of BMV enrichment from cerebral cortex samples. (A) Representative image of an aliquot from a BMV enriched sample. The scale bar is set to 50  $\mu$ m. (B) Expression of cell-type marker genes in BMV and paired cerebral cortex samples. Messenger RNA expression levels of BMV samples are normalized to paired cerebral cortex. Platelet endothelial cell adhesion molecule (*PECAM1*) and vascular endothelial cadherin (*VEC*) are pan-endothelial cell markers, while glucose transporter 1 (*GLUT1*) is a brain endothelial cell marker. Synaptophysin (*SYP*) is a neuronal cell marker and glial fibrillary acidic protein (*GFAP*) is an astrocytic cell marker. Values represent the mean  $\pm$  SEM (n=3).

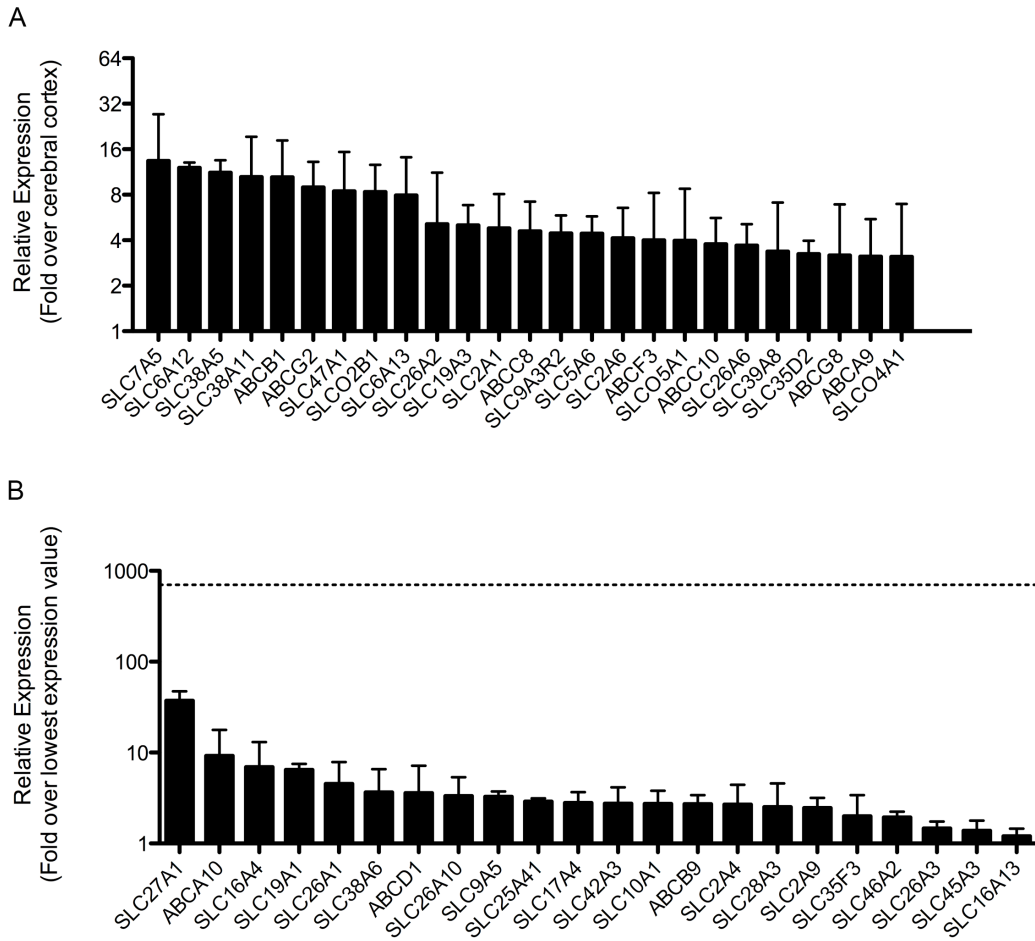


**Figure 2.2.** Transporter gene mRNA expression levels in BMVs. Relative expression of SLC and ABC genes was determined by OpenArray-based RT-PCR. (A) The top 25 genes with the most enriched mRNA expression in BMVs relative to paired cerebral cortex are depicted (see Table 2.2 for complete list). Only genes detected across both BMV and both cerebral cortex samples were included. (B) Genes detected in both BMV samples but not in both cerebral cortex samples. Expression levels were normalized to the lowest average expression value detected in BMV samples, and the dotted line represents the highest average expression level detected. All values represent the mean  $\pm$  SD (n=2).



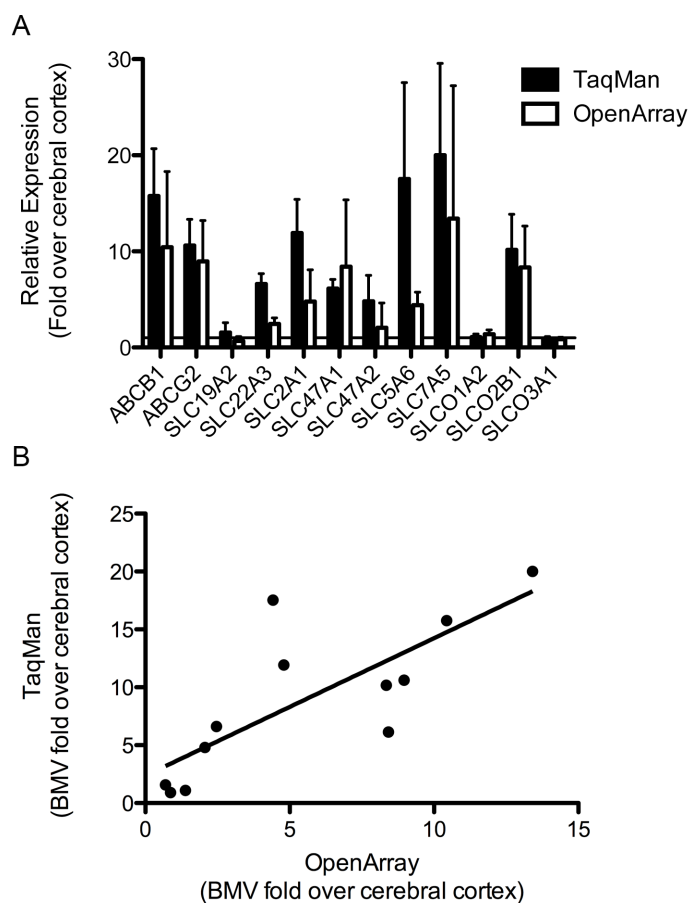


**Figure 2.3.** Validation of OpenArray gene expression results. (A) The mRNA expression levels of 12 genes in BMV and cerebral cortex samples (n=3) were determined by TaqMan RT-PCR and compared to OpenArray results. (B) Linear regression of the relative mRNA expression in BMV samples determined by TaqMan RT-PCR versus those determined by OpenArray RT-PCR ( $r^2=0.60$ ). All values represent the mean  $\pm$  SD. Linear regression was done using Prism 5 GraphPad software.

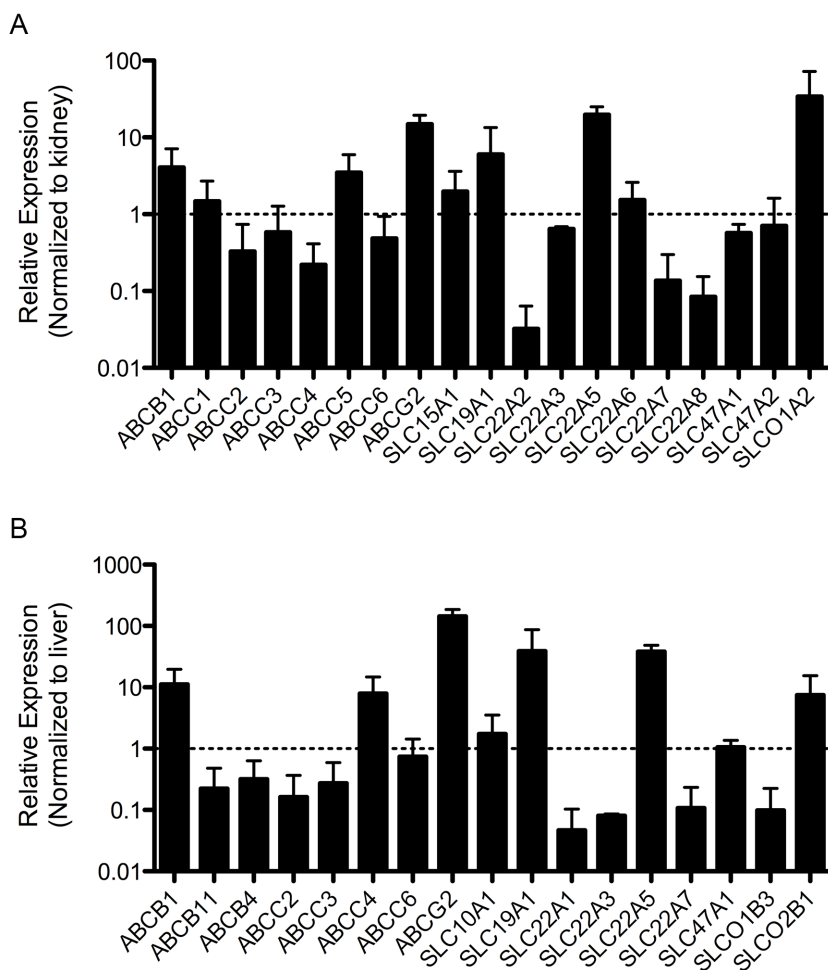


**Figure 2.4.** Comparative expression analysis of drug transporters in BMV, kidney and liver samples. Gene expression of SLC and ABC transporters with established roles in drug disposition in kidney (n=60) and liver (n=59) was determined by array-based RT-PCR and compared to BMV expression levels. BMV mRNA expression level of drug transporters normalized to average kidney (A) and liver (B) expression levels. Only genes detected across both BMV samples were included. Dotted lines represent the expression level in either kidney or liver. All values represent the mean  $\pm$  SD (n=2).

***Drug transporter expression in BMVs relative to kidney and liver.*** A well-known function of the BBB is to regulate CNS exposure to circulating xenobiotics, including many drugs by various mechanisms. Drug transporters have been well-characterized in playing important roles in the absorption, distribution, metabolism, and excretion (ADME) of drugs from the body through organs such as the kidney and liver [20]. To identify transporters that may support this critical BBB function, drug transporter expression was first normalized to average housekeeping gene levels within a given sample, followed by comparison of the normalized BMV values to the normalized kidney and liver values. *ABCB1*, *ABCC5*, *ABCG2*, *SLC22A5*, and *SLCO1A2* were expressed at higher levels (> 2-fold) in BMVs than in the kidney, while *ABCC1*, *ABCC3*, *ABCC6*, *SLC15A1*, *SLC19A1*, *SLC22A3*, *SLC22A6*, *SLC47A1*, and *SLC47A2* were expressed at similar levels (within 2-fold) between BMV and kidney samples (Figure 2.4A). *ABCB1*, *ABCC4*, *ABCG2*, *SLC19A1*, *SLC22A5*, and *SLCO2B1* were expressed at higher levels in BMVs than in the liver, while *ABCC6*, *SLC10A1*, and *SLC47A1* at similar levels between BMV and liver samples (Figure 2.4B). Even though some of these transporters are already known to interact with xenobiotics and/or are highly expressed at the BBB (i.e. *SLC22A5*, *SLCO2B1*, *ABCB1* and *ABCG2*), these results suggest that other drug transporters may also play a role in regulating xenobiotic penetration across the BBB. Moreover, two transporters known to play a role in both BBB and hepatic drug disposition, *ABCB1* and *ABCG2*, were expressed at approximately 10- and 150-fold higher levels, respectively in the BBB compared to the liver.

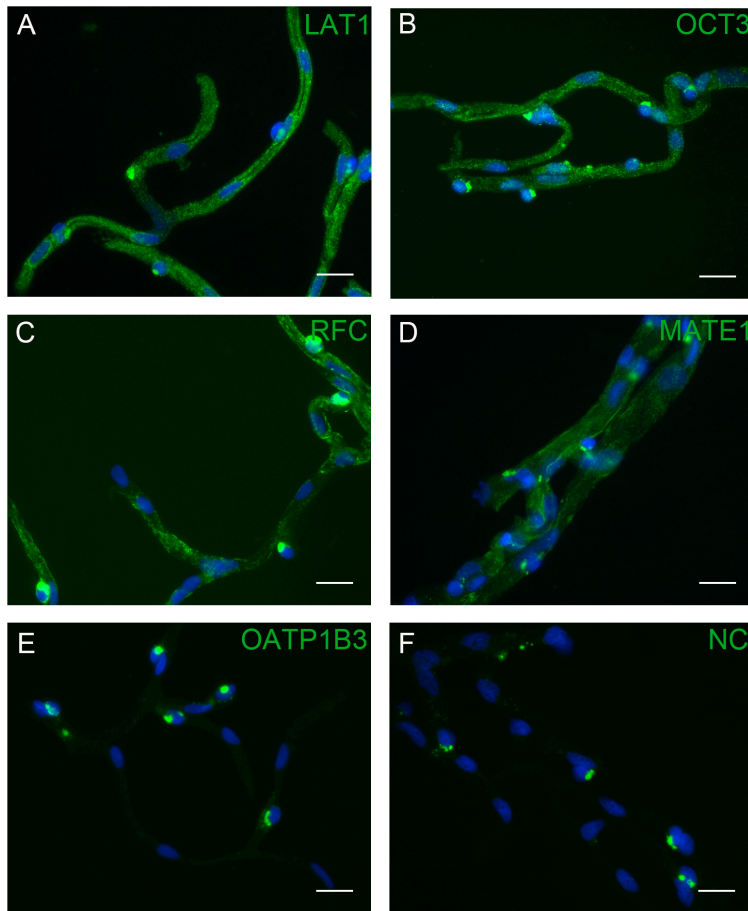


**Figure 2.5.** Protein expression of SLC transporters in BMVs. Immunofluorescence staining (green) determined the presence of LAT1 (A), OCT3 (B), RFC (C), and MATE1 (D), and the absence of OATP1B3 (E) in BMVs. OATP1B3 and LAT1 served as negative and positive controls, respectively. A negative control with primary antibody omitted is also shown in (F). Nuclei were stained with DAPI (blue), and scale bars are set to 20  $\mu\text{m}$  in all images.

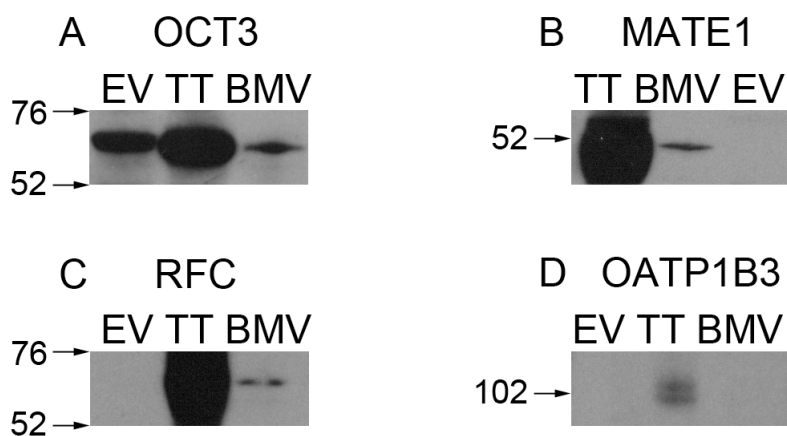


**Figure 2.6.** Confirmation of SLC transporter protein expression in BMVs and antibody specificity. Western blot analysis of BMVs detected the expression of OCT3 (A), MATE1 (B), and RFC (C). (D) OATP1B3 was included as a negative control and was not detected in BMVs. In all panels, antibody specificity was determined using HEK cells transfected with OCT3, MATE1, RFC, OATP1B3, or EV. All molecular weights indicated are in kDa. TT, transporter transfected cell lysate; EV, empty vector transfected cell lysate.

**Transporter protein expression in BMVs.** Protein expression of several transporters at the human BBB was further characterized by western blotting and IHC of isolated human BMVs. LAT1 (*SLC7A5*) was included as a positive control, and OATP1B3 (*SLCO1B3*) was included as a negative control since its mRNA expression level was near the limit of detection. LAT1, RFC, and OCT3 (*SLC22A3*) were detected in BMVs  $\leq 10 \mu\text{m}$  in diameter and produced average signal intensities 4.5 - 5.5-fold higher than negative control (Figure 2.5A-C). MATE1 (*SLC47A1*) was primarily detected in BMVs  $> 10 \mu\text{m}$  in diameter, and produced an average signal intensity approximately 3-fold greater than that of the negative control (Figure 2.5D). OATP1B3, however, was not detected in BMVs, and had average signal intensities within 2-fold of the negative control (Figure 4E). Western blot analysis confirmed the IHC results, and verified antibody specificity in HEK-EV and -transporter transfected cells (Figure 2.6). Taken together these results confirm LAT1 and RFC expression in the human BBB, and reveal the expression of OCT3 and MATE1 proteins in the human BBB.

**Table 2.2.** Genes expressed in human BMVs in comparison to housekeeping genes and paired cerebral cortex samples.

Gene	Relative Expression (% of House-keeping genes)	Relative Expression (Fold over cerebral cortex)
<i>ABCA10</i>	0.377	ND
<i>ABCA12</i>	0.127	0.518
<i>ABCA13</i>	0.281	0.927
<i>ABCA2</i>	6.59	2.07
<i>ABCA3</i>	0.772	1.00
<i>ABCA5</i>	1.11	1.46
<i>ABCA6</i>	0.482	2.65
<i>ABCA7</i>	0.191	1.67
<i>ABCA8</i>	0.224	0.729

ABCA9	1.077	3.12
ABCB1	13.1	10.4
ABCB10	0.821	1.99
ABCB11	0.132	0.447
ABCB4	0.195	1.19
ABCB6	3.87	2.96
ABCB7	0.509	2.57
ABCB8	0.201	1.88
ABCB9	0.209	ND
ABCC1	0.806	0.987
ABCC10	0.895	3.77
ABCC12	0.499	1.53
ABCC2	0.278	2.27
ABCC3	0.110	1.17
ABCC4	0.337	0.678
ABCC5	5.81	2.11
ABCC6	0.187	1.87
ABCC7	0.205	0.647
ABCC8	2.30	4.58
ABCC9	1.10	1.86
ABCD1	0.134	ND
ABCD2	0.481	0.856
ABCD3	5.14	1.36
ABCD4	0.257	0.939
ABCE1	0.549	1.22
ABCF1	2.00	1.26
ABCF2	0.984	1.56
ABCF3	0.867	3.99
ABCG1	1.62	0.773
ABCG2	4.15	8.96
ABCG4	0.693	1.18
ABCG5	0.186	1.05
ABCG8	0.515	3.17
SLC10A1	0.191	ND
SLC10A3	0.165	1.55
SLC10A4	0.510	1.34
SLC10A5	0.327	0.581
SLC10A6	0.192	1.46
SLC10A7	0.194	1.84
SLC11A2	0.322	0.600
SLC12A1	0.206	2.23

SLC12A2	0.519	1.63
SLC12A5	12.9	0.504
SLC12A6	0.909	1.09
SLC12A7	6.28	1.71
SLC13A3	0.179	1.65
SLC14A1	1.07	0.693
SLC15A1	0.115	1.27
SLC15A3	0.440	2.89
SLC15A4	0.837	0.985
SLC16A1	0.591	1.20
SLC16A10	0.243	0.662
SLC16A11	0.320	1.90
SLC16A13	0.0957	ND
SLC16A2	0.880	0.967
SLC16A4	0.298	ND
SLC16A6	0.357	1.93
SLC16A7	0.835	0.933
SLC16A8	0.323	2.86
SLC16A9	0.218	1.32
SLC17A2	0.256	1.54
SLC17A3	0.223	3.07
SLC17A4	0.301	ND
SLC17A5	0.478	0.906
SLC17A6	0.382	0.466
SLC17A7	28.3	1.06
SLC18A2	0.279	1.40
SLC19A1	0.642	ND
SLC19A2	0.293	0.696
SLC19A3	2.73	5.01
SLC1A1	2.63	0.834
SLC1A2	33.8	0.788
SLC1A3	0.663	1.21
SLC1A4	5.75	1.48
SLC1A6	0.172	2.15
SLC20A1	1.56	1.02
SLC20A2	5.86	1.06
SLC22A1	0.206	1.76
SLC22A10	0.357	1.46
SLC22A13	0.178	1.03
SLC22A15	0.788	1.30
SLC22A17	1.34	2.20



SLC22A18	0.280	1.04
SLC22A2	0.192	0.573
SLC22A23	0.495	2.23
SLC22A2 splice	0.113	0.724
SLC22A3	0.684	2.46
SLC22A5	1.20	1.51
SLC22A6	0.395	1.95
SLC22A7	0.146	1.22
SLC22A8	0.219	1.85
SLC22A9	1.94	1.38
SLC23A2	3.12	0.776
SLC24A1	0.183	1.16
SLC24A2	2.15	0.454
SLC24A3	0.334	0.489
SLC24A4	0.383	1.16
SLC24A6	0.191	1.55
SLC25A1	0.396	1.66
SLC25A10	0.164	1.40
SLC25A11	0.671	1.40
SLC25A12	2.22	0.816
SLC25A13	0.941	1.04
SLC25A14	0.271	1.10
SLC25A15	0.169	1.15
SLC25A16	0.491	1.12
SLC25A17	0.403	0.839
SLC25A18	1.57	1.41
SLC25A20	0.302	0.928
SLC25A22	4.22	0.667
SLC25A23	2.94	2.20
SLC25A24	0.298	2.68
SLC25A25	0.553	1.71
SLC25A27	1.10	0.476
SLC25A28	3.59	0.827
SLC25A29	0.149	1.48
SLC25A3	5.82	0.559
SLC25A30	0.754	1.45
SLC25A32	0.234	1.63
SLC25A36	3.01	1.55
SLC25A38	0.500	1.25
SLC25A39	0.759	2.93

SLC25A4	1.85	0.807
SLC25A41	0.249	ND
SLC25A42	0.207	1.50
SLC25A44	0.508	0.722
SLC25A5	3.88	0.627
SLC25A6	5.45	1.27
SLC25A9	0.180	1.43
SLC26A1	0.230	ND
SLC26A10	0.193	ND
SLC26A11	0.149	1.72
SLC26A2	0.968	5.11
SLC26A3	0.148	ND
SLC26A4	0.240	1.44
SLC26A6	0.382	3.69
SLC26A7	0.218	1.15
SLC26A8	0.210	0.902
SLC27A1	2.83	ND
SLC27A4	0.533	1.06
SLC27A6	0.168	1.43
SLC28A2	0.477	0.879
SLC28A3	0.117	ND
SLC29A1	0.419	2.34
SLC29A2	0.611	2.62
SLC29A3	0.272	1.47
SLC2A1	1.09	4.80
SLC2A2	0.162	1.06
SLC2A3	22.6	1.88
SLC2A4	0.149	ND
SLC2A5	0.356	1.04
SLC2A6	0.621	4.12
SLC2A8	0.455	0.901
SLC2A9	0.184	ND
SLC30A4	0.529	1.28
SLC30A7	0.279	1.30
SLC30A9	1.88	0.682
SLC31A1	1.86	1.39
SLC31A2	0.274	0.325
SLC32A1	0.339	0.589
SLC33A1	0.616	0.955
SLC35A1	2.42	1.51
SLC35A2	0.715	0.728

SLC35A3	0.252	2.36
SLC35A4	0.961	1.21
SLC35A5	0.330	1.04
SLC35B1	0.627	0.553
SLC35B2	0.268	0.622
SLC35B3	0.169	0.887
SLC35B4	0.615	0.540
SLC35C1	0.235	1.82
SLC35C2	0.277	0.990
SLC35D2	0.594	3.24
SLC35E1	1.24	0.538
SLC35E2	5.43	1.57
SLC35F1	0.902	0.346
SLC35F2	0.391	1.04
SLC35F3	0.105	ND
SLC35F5	4.03	1.51
SLC36A1	0.793	0.843
SLC36A4	0.613	0.745
SLC37A1	0.527	1.30
SLC37A3	0.177	1.31
SLC37A4	0.665	1.04
SLC38A1	1.20	0.453
SLC38A10	0.157	1.85
SLC38A11	1.90	10.5
SLC38A2	19.9	1.15
SLC38A3	6.39	2.30
SLC38A5	11.2	11.2
SLC38A6	0.173	ND
SLC38A7	0.223	2.45
SLC38A9	0.739	0.828
SLC39A1	0.751	1.86
SLC39A10	2.86	1.05
SLC39A12	0.285	0.444
SLC39A13	0.226	1.05
SLC39A14	0.333	0.738
SLC39A2	5.45	0.779
SLC39A3	1.28	1.00
SLC39A6	0.775	0.958
SLC39A7	0.933	2.97
SLC39A8	0.853	3.36
SLC39A9	0.248	0.942

SLC3A1	6.01	0.530
SLC3A2	3.66	1.31
SLC40A1	0.705	2.25
SLC41A1	0.714	1.21
SLC41A2	0.539	0.454
SLC41A3	0.342	0.383
SLC42A3	0.173	ND
SLC43A2	1.10	1.13
SLC43A3	0.414	1.78
SLC44A1	3.80	0.688
SLC44A2	7.07	1.17
SLC44A5	0.446	1.22
SLC45A1	0.186	1.19
SLC45A3	0.104	ND
SLC45A4	2.15	1.41
SLC46A2	0.192	ND
SLC46A3	0.517	0.996
SLC47A1	0.735	8.42
SLC47A2	0.205	2.06
SLC48A1	1.51	0.872
SLC4A10	13.3	0.767
SLC4A4	2.06	0.711
SLC4A5	0.178	2.21
SLC4A7	0.132	1.35
SLC4A8	0.580	0.391
SLC5A1	0.110	0.792
SLC5A10	0.194	2.48
SLC5A11	0.235	1.34
SLC5A4	0.779	1.68
SLC5A6	2.04	4.42
SLC6A1	1.93	2.48
SLC6A11	0.239	0.474
SLC6A12	2.61	12.0
SLC6A13	0.808	7.93
SLC6A15	0.817	0.394
SLC6A16	0.141	1.75
SLC6A17	2.48	0.665
SLC6A2	0.282	2.41
SLC6A20	0.251	2.05
SLC6A4	0.117	0.621
SLC6A7	1.44	0.756

SLC6A8	4.70	0.805
SLC7A1	4.80	2.72
SLC7A10	0.220	1.97
SLC7A11	1.54	1.16
SLC7A14	0.381	0.300
SLC7A2	0.518	3.10
SLC7A4	0.180	1.59
SLC7A5	6.91	13.4
SLC7A6	4.64	1.39
SLC7A7	0.656	2.32
SLC7A8	3.33	0.910
SLC7A9	0.272	1.27
SLC8A1	1.35	0.429
SLC8A2	1.66	0.599
SLC8A3	0.889	1.16
SLC9A1	0.893	0.773
SLC9A11	0.197	0.775
SLC9A2	0.676	1.11
SLC9A3R2	2.68	4.44
SLC9A5	0.322	ND
SLC9A6	1.76	0.412
SLC9A7	0.250	0.676
SLC9A8	0.287	1.98
SLC9A9	0.824	1.95
SLCO1A2	5.62	1.39
SLCO1B3	0.317	2.52
SLCO1C1	0.434	0.679
SLCO2A1	0.400	1.07
SLCO2B1	19.1	8.34
SLCO3A1	0.744	0.870
SLCO4A1	1.00	3.10
SLCO5A1	0.843	3.96

ND, not determined.

All values represent the mean of n=2 BMV samples.

### ***Expression and function of the reduced folate transporter, Rfc, in mouse***

**brain.** Functional implications of the mRNA expression profiling and IHC results were investigated by measuring the brain penetration of  $^3\text{H}$ -methotrexate in wild type male C57BL/6 mice. Methotrexate, a well-established substrate of human and mouse RFC [21, 22], was selected to probe RFC function at the BBB because its acute and chronic neurotoxicity [23, 24]. Before initiating pharmacokinetic studies, expression of the mouse ortholog, Rfc, in isolated mouse BMVs was confirmed by IHC (Figure 2.7A-B). Rfc was detected in mouse BMVs  $\leq 10\ \mu\text{m}$  in diameter and produced an average signal intensity approximately 4.5 fold that of negative control, similar to the signal intensity of RFC in human BMVs (see Figure 2.5C). These results indicate that the mouse is a suitable model for ascertaining the role of RFC in the BBB.

Mice have approximately 10-fold higher serum folate levels than humans [27]. Since endogenous circulating folates compete with  $^3\text{H}$ -methotrexate for uptake by Rfc, and to more closely simulate human serum folate levels, all mice were maintained on a folic acid deficient diet for two weeks prior to pharmacokinetic studies. A single i.v. dose of  $15\ \mu\text{g/kg}$   $^3\text{H}$ -methotrexate alone or concomitantly with either  $1.5\ \text{mg/kg}$  folinic acid, a reduced folate and Rfc substrate, or  $1.5\ \text{mg/kg}$  bromosulfophthalein, an Rfc inhibitor, was administered to the mice. Pharmacokinetic parameters were obtained by non-compartmental analysis (Table 2.3). Both folinic acid and bromosulfophthalein elevated the mean plasma concentrations of  $^3\text{H}$ -methotrexate at all time points (Figure 2.7C-D), and increased the area under the plasma concentration-time curve (AUC) three- and two-fold, respectively. Furthermore, both Rfc inhibitors reduced the volume of

distribution, indicating probable changes in tissue accumulation. Indeed, folinic acid and bromosulfophthalein significantly reduced the plasma normalized brain levels of  $^3\text{H}$ -methotrexate at 60 minutes by one third and one half of control levels, respectively (Figure 2.7E). Similar changes in  $^3\text{H}$ -methotrexate kidney accumulation were also observed (Table 2.3). These results indicate that a component of methotrexate uptake into the mouse brain occurs through a folinic acid- and bromosulfophthalein- sensitive, carrier-mediated process, such as transport by Rfc at the BBB.

**Table 2.3.** Pharmacokinetic parameters and kidney accumulation of [ $^3\text{H}$ ]-methotrexate (15  $\mu\text{g/kg}$ ) after i.v. administration alone, with folinic acid (1.5 mg/kg), or with bromosulfophthalein (1.5 mg/kg).

	Methotrexate	Methotrexate + Folinic Acid	Methotrexate + Bromosulfophthalein
AUC <sub>0-60</sub> (min*ng/mL)	242 $\pm$ 45.5	635 $\pm$ 196*	444 $\pm$ 112*
CL (mL/min*kg)	56.6 $\pm$ 9.13	22.9 $\pm$ 9.14*	29.0 $\pm$ 8.26*
Terminal t <sub>1/2</sub> (min)	19.2 $\pm$ 2.77	24.6 $\pm$ 4.04	24.0 $\pm$ 9.25
V <sub>ss</sub> (L/kg)	1.22 $\pm$ 0.271	0.697 $\pm$ 0.314*	0.889 $\pm$ 0.410
C <sub>0</sub> (ng/mL)	20.7 $\pm$ 6.46	39.4 $\pm$ 18.8	30.1 $\pm$ 10.0
Kidney/plasma (60 min)	165 $\pm$ 25.6	57.5 $\pm$ 20.0*	73.3 $\pm$ 16.9*

All pharmacokinetic values represent the mean  $\pm$  SD (n=4)

\*  $P < 0.05$  compared to methotrexate

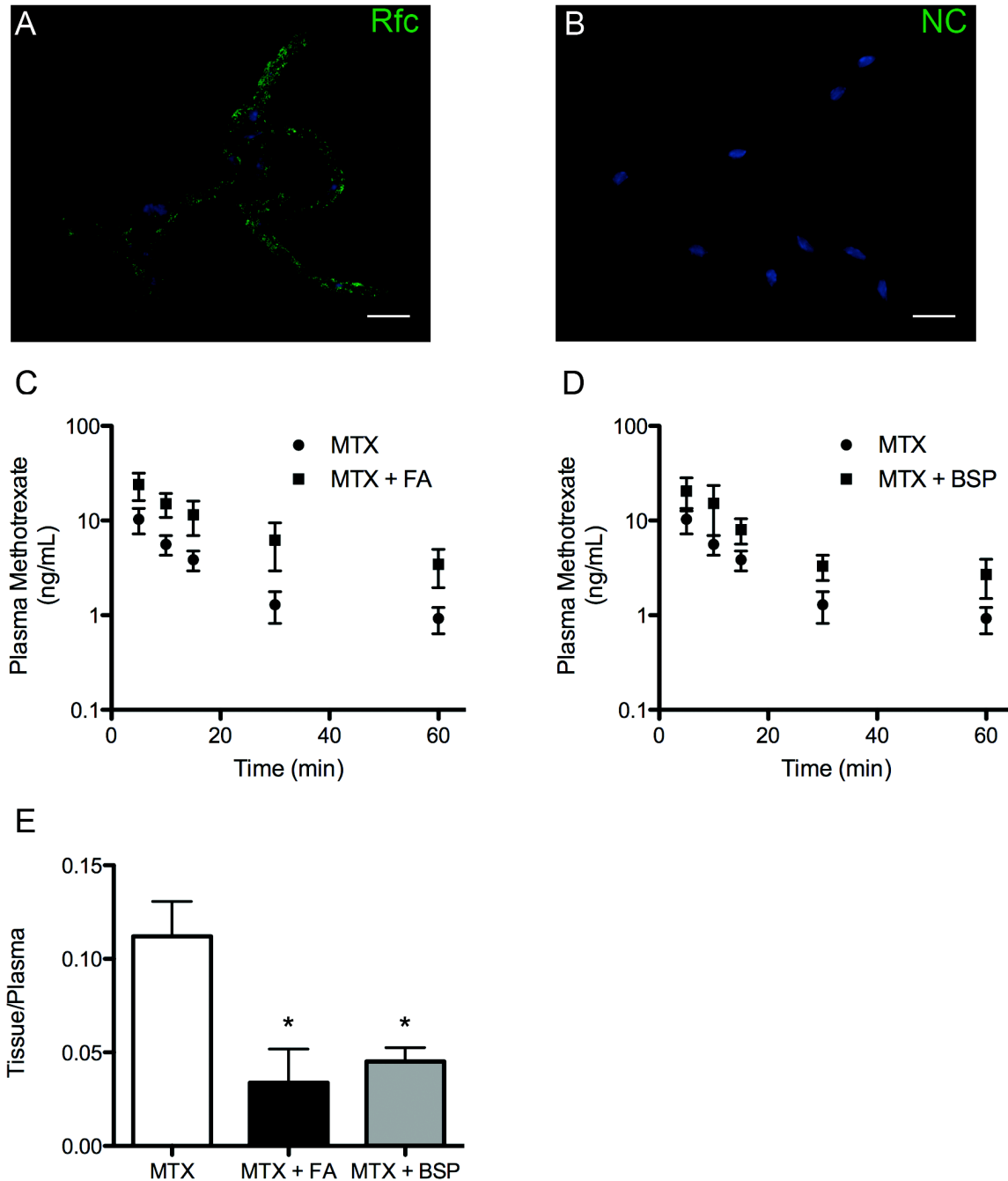


**Figure 2.7.** The role of the reduced folate carrier Rfc in methotrexate uptake into the mouse brain. (A) Immunofluorescence staining (green) revealed the presence of the reduced folate carrier (Rfc) in mouse BMVs. (B) Negative control (NC) with primary antibody omitted. Nuclei were stained with DAPI (blue), and scale bars are set to 20  $\mu$ m in all images.  $^3$ H-methotrexate plasma concentrations in wild type C57BL/6J mice



maintained on a folate deficient diet and dosed i.v. with  $^3\text{H}$ -methotrexate (15  $\mu\text{g/kg}$ ) alone, (C) with folinic acid (1.5 mg/kg), or (D) with bromosulfophthalein (1.5 mg/kg). Plasma concentrations were determined at 5, 10, 15, 30, and 60 minutes post dose. (E) Plasma normalized brain accumulation of  $^3\text{H}$ -methotrexate 60 min post dose in mice dosed with  $^3\text{H}$ -methotrexate alone, with folinic acid, or with bromosulfophthalein. All values represent the mean  $\pm$  SD (C-D) or SEM (E) (n=4). MTX, methotrexate; FA, folinic acid; BSP, bromosulfophthalein. \*  $P < 0.05$ .

## Discussion

We used a semi-unbiased, array-based expression profiling approach to identify SLC and ABC transporters expressed at the human BBB. Coupled with immunoassays, these results led to functional studies investigating how SLC transporters contribute to methotrexate uptake into the brain. Three key findings emerge from this study. First, there were a large number of SLC transporters with enriched expression in the human BBB. Second, SLC transporters previously unknown to be expressed at the BBB were identified. This finding expands the current knowledge of BBB function. Third, a comparative expression approach revealed that drug transporters with important roles in renal and hepatic drug disposition were expressed at similar or higher levels in the BBB.

***A large number of SLC transporters are enriched in the human BBB, including several previously unidentified transporters.*** Over the past two decades considerable information has been obtained about the role of ABC transporters in the BBB. In stark contrast, very little is known about SLC transporters in the BBB. In the current study, 65 SLC transporters were enriched or uniquely expressed in the human BBB (Figure 2.2; Table 2.2). These transporters interact with a diverse assortment of nutrients and help us better understand how the BBB supports CNS function. For example, sulfated proteoglycans are important components of the brain extracellular matrix that help to regulate neuronal growth, plasticity and regeneration [26]. Sulfates are charged inorganic molecules required for normal cell function that cannot diffuse across cell membranes [27], and would be highly unlikely to reach the brain independent of a carrier-mediated process. The previously unidentified *SLC26A1* and *SLC26A2* sulfate transporters [28] had highly enriched expression in BMVs (Figure 2.2),

suggesting that these two transporters may play a critical role in supplying the brain with sulfates required for proper proteoglycan synthesis.

Other previously unrecognized transporters that were identified include SLC6A13, SLC19A3, and SLC47A2. Their putative functional roles at the BBB are addressed in turn. The BBB plays a crucial role in removing the neurotransmitter  $\gamma$ -aminobutyric acid (GABA) from the brain interstitial fluid by effluxing it into the blood via the betaine/GABA transporter (BGT-1; *SLC6A12*) [29, 30]. We confirmed that SLC6A12 is expressed at high levels in the BBB, and also identified another GABA transporter, SLC6A13, with enriched expression in BMVs (Figure 2). It is possible that both transporters function in the elimination of excess GABA from the CNS. *SLC19A3* transports thiamine, and mutations in this transporter cause a biotin-responsive basal ganglia disease with bilateral necrosis in the caudate nucleus and putamen [31, 32]. Though the mutated transporter is well-recognized as being the cause of the disease, these studies establish that the transporter may also play a role in delivering its essential substrates to the CNS. *SLC47A2* encodes a multi-drug efflux pump, MATE2. It has largely been thought to be a kidney specific transporter with a central role in renal secretion of organic cations [33]. MATE2 together with the more abundantly expressed SLC47A1 (MATE1) may play a role in the entry or efflux of organic cations across the BBB and into the CNS. It will be interesting to learn whether SLC47A2, like SLC47A1, is expressed in larger microvessels (Figure 2.5D).

***Comparative expression studies suggest that xenobiotic transporters with important roles in liver and kidney drug disposition have important roles in the BBB.*** The BBB represents a major obstacle to delivering drugs into the CNS. Given

that CNS drugs continue to have a high failure rate [2], new approaches to delivering drugs across the BBB should be explored. To our knowledge, this is the first study comparing drug transporter expression in the BBB to other ADME organs. This analysis revealed numerous SLC drug transporters expressed in human BMVs at similar or higher mRNA levels than in the kidney and liver (Figure 2.4). Furthermore, SLC22A3 (OCT3) and MATE1 protein were also detected in BMVs (Figure 2.5). Many of these transporters, such as SLC22A3, SLC22A5 (OCTN2), SLC22A6 (OAT1), SLC47A1, and SLC47A2 often work in concert with each other and other transporters to eliminate drugs through the proximal tubule of the kidney and/or hepatocytes of the liver [33, 34]. These transporters may also work in concert at the BBB and provide a means to shuttle drugs into the CNS. These results will be useful in guiding functional studies aimed at elucidating how drugs cross the BBB (i.e. our studies with Rfc and methotrexate). For example, cationic opioid analgesics such as oxycodone cannot readily diffuse across the BBB to reach their opioid receptor targets. Animal models have provided evidence for transport of oxycodone across the BBB [37], and human brain endothelial cell lines indicate that this process is at least partially mediated by a proton-coupled organic cation antiporter [36]. MATE1 and MATE2 are proton-coupled organic cation antiporters that were detected in BMVs (Figure 2), and therefore may play a role in transporting oxycodone across the BBB.

***In vivo studies in mice suggest that the reduced folate carrier, Rfc (Slc19a1), mediates the uptake of methotrexate into the brain.*** RFC mRNA was expressed in human BMVs at similar levels as the kidney (Figure 2.4), where it has a well-established role in the renal secretion of methotrexate [37]. This process is similar

to how intrathecally administered methotrexate is taken up from the cerebrospinal fluid (CSF) by RFC in the choroid plexus and subsequently effluxed into the blood [38, 39]. Although methotrexate lacks many of the physicochemical properties that would favor passive permeation across the BBB and into CNS, several lines of evidence indicate that intravenously administered methotrexate does reach the CNS. First, high-dose methotrexate is part of first-line therapy for the treatment of primary CNS lymphoma, a rare type of primary brain tumor [40]. Second, methotrexate causes severe neurotoxic side effects such as seizures, dementia, and leukoencephalopathy when administered at high doses ( $\geq 1 \text{ g/m}^2$ ) [23]. Finally, in mice MTX has been detected in the CSF, and is cytotoxic to proliferating hippocampal cells when dosed intravenously [41, 42]. Despite this large body of evidence for entry of the drug into the brain, the mechanism of methotrexate uptake into the CNS has remained unclear.

Our expression profiling and IHC results (Figure's 2.2, 2.4, and 2.5) confirm previous reports of RFC expression at the human and mouse BBB [6, 43], indicating that it may contribute to methotrexate uptake into the CNS. Our pharmacokinetic studies indicate that methotrexate uptake into the mouse brain occurs through a bromosulfophthalein- and folinic acid-sensitive, carrier-mediated process (Figure 2.7). This process may occur at either or both the BBB and the blood-CSF barrier created by the choroid plexus. We propose that Rfc in the BBB contributes substantially to the brain uptake of methotrexate.

First, folate is primarily supplied to the brain in its reduced forms by a complex process that involves endocytic uptake from the blood at the choroid plexus by the

alpha folate receptor (FR $\alpha$ ), intracellular release from endosomes, and carrier-mediated transport into the CSF by RFC [9]. However, methotrexate has a much lower affinity than reduced folates do for FR $\alpha$ , making it highly unlikely that methotrexate will outcompete these endogenous ligands for FR $\alpha$  transport [39, 44]. Second, bromosulphophthalein has been shown to distinguish between transporter- and receptor-mediated cellular uptake of methotrexate [45, 46]. Our results indicate that a component of methotrexate uptake into the brain is bromosulphophthalein-sensitive, and therefore unlikely to be receptor-mediated (Figure 2.7E). Finally, only about 10% of methotrexate is converted to 7-hydroxy-methotrexate during first-pass metabolism in the liver [47]. Since methotrexate was given intravascularly, virtually all of the methotrexate measured in these studies represents the parent form of the drug. Although these observations are in line with Rfc-mediated transport of methotrexate across the BBB into the brain, further experiments to distinguish between Rfc in the choroid plexus versus BBB are needed to establish the relative contributions of the two processes.

In summary, our results suggest a broad role for SLC transporters in the BBB in terms of maintaining CNS homeostasis of small molecules including vitamins, amino acids, neurotransmitters and various other essential nutrients. Finding that a broad array of xenobiotic transporters are expressed in the BBB suggest that these transporters may be targeted to achieve the CNS delivery of pharmaceuticals needed for the treatment of neurodegenerative and other diseases that affect the CNS.

## References

1. Abbott NJ, Patabendige AA, Dolman DE, Yusof SR, Begley DJ. Structure and function of the blood-brain barrier. *Neurobiology of disease*. 2010;37(1):13-25.
2. Hurko O, Ryan JL. Translational research in central nervous system drug discovery. *NeuroRx*. 2005;2(4):671-82.
3. Clark DE. In silico prediction of blood-brain barrier permeation. *Drug Discov Today*. 2003;8(20):927-33.
4. Begley DJ. ABC transporters and the blood-brain barrier. *Curr Pharm Des*. 2004;10(12):1295-312.
5. Shawahna R, Uchida Y, Decleves X, Ohtsuki S, Yousif S, Dauchy S, et al. Transcriptomic and quantitative proteomic analysis of transporters and drug metabolizing enzymes in freshly isolated human brain microvessels. *Mol Pharm*. 2011;8(4):1332-41.
6. Uchida Y, Ohtsuki S, Katsukura Y, Ikeda C, Suzuki T, Kamiie J, et al. Quantitative targeted absolute proteomics of human blood-brain barrier transporters and receptors. *J Neurochem*. 2011;117(2):333-45.
7. Doran A, Obach RS, Smith BJ, Hosea NA, Becker S, Callegari E, et al. The impact of P-glycoprotein on the disposition of drugs targeted for indications of the central nervous system: evaluation using the MDR1A/1B knockout mouse model. *Drug Metab Dispos*. 2005;33(1):165-74.
8. Sasongko L, Link JM, Muzi M, Mankoff DA, Yang X, Collier AC, et al. Imaging P-glycoprotein transport activity at the human blood-brain barrier with positron emission tomography. *Clin Pharmacol Ther*. 2005;77(6):503-14.

9. Spector R. Nutrient transport systems in brain: 40 years of progress. *J Neurochem.* 2009;111(2):315-20.
10. Hammerstad JP, Pate BD, Hewitt KA, Chan GL, Ruth TJ, Calne DB. The transport of L-6-fluorodopa and its metabolites from blood to cerebrospinal fluid and brain. *Ann Neurol.* 1993;34(4):603-8.
11. Geier EG, Schlessinger, A., Fan, H., Gable, J. E., Irwin, J. J., Sali, A., Giacomini, K. M. Structure-based ligand discovery for the Large-neutral Amino Acid Transporter 1, LAT-1. *PNAS.* 2013.
12. Paproski RJ, Wuest M, Jans HS, Graham K, Gati WP, McQuarrie S, et al. Biodistribution and uptake of 3'-deoxy-3'-fluorothymidine in ENT1-knockout mice and in an ENT1-knockdown tumor model. *J Nucl Med.* 2010;51(9):1447-55.
13. Lepist EI, Damaraju VL, Zhang J, Gati WP, Yao SY, Smith KM, et al. Transport of A1 adenosine receptor agonist tecadenoson by human and mouse nucleoside transporters: evidence for blood-brain barrier transport by murine equilibrative nucleoside transporter 1 mENT1. *Drug Metab Dispos.* 2013;41(4):916-22.
14. Dahlin A, Geier E, Stocker SL, Cropp CD, Grigorenko E, Bloomer M, et al. Gene expression profiling of transporters in the solute carrier and ATP-binding cassette superfamilies in human eye substructures. *Mol Pharm.* 2013;10(2):650-63.
15. Dauchy S, Dutheil F, Weaver RJ, Chassoux F, Daumas-Duport C, Couraud PO, et al. ABC transporters, cytochromes P450 and their main transcription factors: expression at the human blood-brain barrier. *J Neurochem.* 2008;107(6):1518-28.
16. Pfaffl MW. A new mathematical model for relative quantification in real-time RT-PCR. *Nucleic Acids Res.* 2001;29(9):e45.



17. More SS, Itsara M, Yang X, Geier EG, Tadano MK, Seo Y, et al. Vorinostat increases expression of functional norepinephrine transporter in neuroblastoma in vitro and in vivo model systems. *Clin Cancer Res.* 2011;17(8):2339-49.
18. Roberts LM, Black DS, Raman C, Woodford K, Zhou M, Haggerty JE, et al. Subcellular localization of transporters along the rat blood-brain barrier and blood-cerebral-spinal fluid barrier by in vivo biotinylation. *Neuroscience.* 2008;155(2):423-38.
19. Schneider CA, Rasband WS, Eliceiri KW. NIH Image to ImageJ: 25 years of image analysis. *Nat Methods.* 2012;9(7):671-5.
20. Morrissey KM, Wen CC, Johns SJ, Zhang L, Huang SM, Giacomini KM. The UCSF-FDA TransPortal: a public drug transporter database. *Clin Pharmacol Ther.* 2012;92(5):545-6.
21. Roy K, Tolner B, Chiao JH, Sirotnak FM. A single amino acid difference within the folate transporter encoded by the murine RFC-1 gene selectively alters its interaction with folate analogues. Implications for intrinsic antifolate resistance and directional orientation of the transporter within the plasma membrane of tumor cells. *J Biol Chem.* 1998;273(5):2526-31.
22. Chiao JH, Yang CH, Roy K, Pain J, Sirotnak FM. Ligand-directed immunoaffinity purification and properties of the one-carbon, reduced folate transporter. Interspecies immuno-cross-reactivity and expression of the native transporter in murine and human tumor cells and their transport-altered variants. *J Biol Chem.* 1995;270(50):29698-704.
23. Froklage FE, Reijneveld JC, Heimans JJ. Central neurotoxicity in cancer chemotherapy: pharmacogenetic insights. *Pharmacogenomics.* 2011;12(3):379-95.

24. Sioka C, Kyritsis AP. Central and peripheral nervous system toxicity of common chemotherapeutic agents. *Cancer Chemother Pharmacol*. 2009;63(5):761-7.
25. Leamon CP, Reddy JA, Dorton R, Bloomfield A, Emsweller K, Parker N, et al. Impact of high and low folate diets on tissue folate receptor levels and antitumor responses toward folate-drug conjugates. *J Pharmacol Exp Ther*. 2008;327(3):918-25.
26. Kwok JC, Warren P, Fawcett JW. Chondroitin sulfate: a key molecule in the brain matrix. *Int J Biochem Cell Biol*. 2012;44(4):582-6.
27. Markovich D. Physiological roles and regulation of mammalian sulfate transporters. *Physiol Rev*. 2001;81(4):1499-533.
28. Alper SL, Sharma AK. The SLC26 gene family of anion transporters and channels. *Mol Aspects Med*. 2013;34(2-3):494-515.
29. Kakee A, Takanaga H, Terasaki T, Naito M, Tsuruo T, Sugiyama Y. Efflux of a suppressive neurotransmitter, GABA, across the blood-brain barrier. *J Neurochem*. 2001;79(1):110-8.
30. Takanaga H, Ohtsuki S, Hosoya K, Terasaki T. GAT2/BGT-1 as a system responsible for the transport of gamma-aminobutyric acid at the mouse blood-brain barrier. *J Cereb Blood Flow Metab*. 2001;21(10):1232-9.
31. Ozand PT, Gascon GG, Al Essa M, Joshi S, Al Jishi E, Bakheet S, et al. Biotin-responsive basal ganglia disease: a novel entity. *Brain*. 1998;121 ( Pt 7):1267-79.
32. Zeng WQ, Al-Yamani E, Acierno JS, Jr., Slaugenhaupt S, Gillis T, MacDonald ME, et al. Biotin-responsive basal ganglia disease maps to 2q36.3 and is due to mutations in SLC19A3. *Am J Hum Genet*. 2005;77(1):16-26.

33. Morrissey KM, Stocker SL, Wittwer MB, Xu L, Giacomini KM. Renal transporters in drug development. *Annu Rev Pharmacol Toxicol.* 2013;53:503-29.
34. Nies AT, Koepsell H, Damme K, Schwab M. Organic cation transporters (OCTs, MATEs), in vitro and in vivo evidence for the importance in drug therapy. *Handb Exp Pharmacol.* 2011(201):105-67.
35. Bostrom E, Simonsson US, Hammarlund-Udenaes M. In vivo blood-brain barrier transport of oxycodone in the rat: indications for active influx and implications for pharmacokinetics/pharmacodynamics. *Drug Metab Dispos.* 2006;34(9):1624-31.
36. Shimomura K, Okura T, Kato S, Couraud PO, Schermann JM, Terasaki T, et al. Functional expression of a proton-coupled organic cation (H<sup>+</sup>/OC) antiporter in human brain capillary endothelial cell line hCMEC/D3, a human blood-brain barrier model. *Fluids Barriers CNS.* 2013;10(1):8.
37. Nozaki Y, Kusuhara H, Endou H, Sugiyama Y. Quantitative evaluation of the drug-drug interactions between methotrexate and nonsteroidal anti-inflammatory drugs in the renal uptake process based on the contribution of organic anion transporters and reduced folate carrier. *J Pharmacol Exp Ther.* 2004;309(1):226-34.
38. Halwachs S, Lakoma C, Schafer I, Seibel P, Honscha W. The antiepileptic drugs phenobarbital and carbamazepine reduce transport of methotrexate in rat choroid plexus by down-regulation of the reduced folate carrier. *Mol Pharmacol.* 2011;80(4):621-9.
39. Spector R, Johanson CE. Vectorial ligand transport through mammalian choroid plexus. *Pharm Res.* 2010;27(10):2054-62.

40. Ricard D, Idbaih A, Ducray F, Lahutte M, Hoang-Xuan K, Delattre JY. Primary brain tumours in adults. *Lancet*. 2012;379(9830):1984-96.
41. Guo P, Wang X, Liu L, Belinsky MG, Kruh GD, Gallo JM. Determination of methotrexate and its major metabolite 7-hydroxymethotrexate in mouse plasma and brain tissue by liquid chromatography-tandem mass spectrometry. *J Pharm Biomed Anal*. 2007;43(5):1789-95.
42. Yang M, Kim JS, Kim J, Kim SH, Kim JC, Wang H, et al. Neurotoxicity of methotrexate to hippocampal cells in vivo and in vitro. *Biochem Pharmacol*. 2011;82(1):72-80.
43. Hinken M, Halwachs S, Kneuer C, Honscha W. Subcellular localization and distribution of the reduced folate carrier in normal rat tissues. *Eur J Histochem*. 2011;55(1):e3.
44. Westerhof GR, Schornagel JH, Kathmann I, Jackman AL, Rosowsky A, Forsch RA, et al. Carrier- and receptor-mediated transport of folate antagonists targeting folate-dependent enzymes: correlates of molecular-structure and biological activity. *Mol Pharmacol*. 1995;48(3):459-71.
45. Henderson GB, Strauss BP. Characteristics of a novel transport system for folate compounds in wild-type and methotrexate-resistant L1210 cells. *Cancer Res*. 1990;50(6):1709-14.
46. Henderson GB, Tsuji JM, Kumar HP. Mediated uptake of folate by a high-affinity binding protein in sublines of L1210 cells adapted to nanomolar concentrations of folate. *J Membr Biol*. 1988;101(3):247-58.

47. Tian H, Cronstein BN. Understanding the mechanisms of action of methotrexate: implications for the treatment of rheumatoid arthritis. Bull NYU Hosp Jt Dis. 2007;65(3):168-73.

## **CHAPTER 3**

### **Development of LAT1-targeted Cisplatin Analogs and a Lat1 Null Mouse**

#### **Introduction**

Most FDA-approved drugs with central nervous system (CNS) targets are thought to cross the BBB by diffusion. However, some drugs utilize solute carrier (SLC) influx transporters at the BBB to penetrate the CNS. The large-neutral amino acid transporter 1 (LAT1) is a heterodimeric nutrient transporter composed of SLC3A2 and SLC7A5 (4F2hc and 4F2lc), and is responsible for transporting branched chain and aromatic amino acids from the blood to the brain, while also transporting drugs, such as the anti-Parkinson's drug, L-3,4-dihydroxy-L-phenylalanine (levodopa), across the BBB [1, 2]. This directional transport is possible because LAT1 is expressed in both the blood- and brain-facing membranes of the BBB [3-5]. This expression pattern makes LAT1 an ideal target for drug delivery to the CNS. Moreover, several studies have illustrated that chemically modifying existing FDA-approved drugs to target LAT1 enhances their penetration across the BBB into the CNS [6, 7]. However, this strategy has not been applied to the poorly CNS permeable platinum-based chemotherapeutics, some of the most effective anti-cancer drugs available.

Platinum-based drugs function by covalently binding to cellular DNA to form DNA adducts that subsequently activate DNA-damage recognition/repair, cell-cycle arrest, and apoptotic signaling pathways [8]. Cisplatin and carboplatin-based therapies are indicated for the treatment of metastatic testicular and ovarian tumors, and advanced bladder cancer, but are also known to be effective in treating both primary lung and

breast tumors [9, 10]. Furthermore, platinum-based doublet therapy is considered the standard of care for treating lung cancer. Because currently available platinum analogs cannot cross the BBB, they are generally considered ineffective for the treatment of metastases to the brain or primary tumors of the CNS. However, if platinum-based chemotherapeutics could penetrate the CNS, they may be effective in treating CNS metastases, particularly those that frequently arise from primary lung and breast tumors. A small clinical study illustrated this idea by treating CNS metastases in patients diagnosed with a variety of primary cancers, including lung and ovarian cancer, with carboplatin in conjunction with osmotic disruption of the BBB. The authors of this study demonstrated a significant increase in median survival time for patients with brain metastases from lung, lymphoma, and ovarian carcinomas relative to previously reported median survival times under standard treatment regimens [11]. However, BBB disruption does not selectively allow carboplatin to cross the BBB, and leaves the CNS vulnerable to insult by circulating toxins. Targeting LAT1 to enhance the BBB penetration of platinum-based chemotherapeutics obviates the need for BBB disruption, and may provide a safer and more effective strategy for treating metastatic brain tumors.

Historically, new generation platinum compounds have been developed to reduce toxicity or resistance, but not to improve platinum delivery to specific organs, particularly to the CNS. The goal of research described in this chapter was two-fold: determine whether LAT1 could be targeted with platinum-based drugs, and generate a mouse model with reduced Lat1 function to investigate LAT1-specific drug uptake across the BBB. This goal was addressed with cell-based assays to characterize LAT1's interaction with synthetic cisplatin analogs, and the characterization of

genetically modified mice with pharmacokinetic studies to assess Lat1's contributions to drug uptake across the BBB *in vivo*.

## **Materials and Methods**

**Cell lines.** A human embryonic kidney cell line stably expressing the Tet repressor and stably transfected with plasmids expressing *SLC7A5* and *SLC3A2* under the control of tetracycline inducible promoter (HEK-LAT1) were obtained from Pfizer. Cells were maintained at 37°C and 5% CO<sub>2</sub> in DME H21 media containing 10% FBS, 2 mM L-glutamine, 100 units/ml penicillin, 100 µg/ml streptomycin, and 3 µg/ml blasticidin.

Two different clones (BH3 and CC3) of VGB6 mouse embryonic stem cells with an integrated bacterial artificial chromosome (BAC) vector expressing neomycin phosphotransferase instead of *Slc7a5* were obtained from the Knockout Mouse Project Repository (Figure 3.4; KOMP; University of California, Davis). Targeted VGB6 cells were karyotyped and maintained in knockout DMEM containing 15% knockout serum replacement, 2 mM L-glutamine, 100 units/ml penicillin, 100 µg/ml streptomycin, 1 mM sodium pyruvate, non-essential amino acids, 4 µg/ml insulin, and 0.04 U/ml leukemia inhibitory factor on mouse embryonic fibroblasts at 37°C and 5% CO<sub>2</sub> at the University of California, San Francisco ES Cell Targeting core until microinjection.

**RNA extraction and reverse transcriptase PCR.** Total RNA was extracted from non-induced and doxycycline induced HEK-LAT1 cells grown to 90% confluence in poly-D-lysine-coated 24-well plates (BD Falcon, Franklin Lakes, NJ) with the RNeasy Plus Micro Kit (Qiagen, Valencia, CA), according to the kit instructions. After isolation, RNA samples were stored at -80°C. One µg of total RNA was reverse transcribed using



the SuperScript VILO cDNA Synthesis Kit (Life Technologies, Grand Island, NY) according to the manufacturer's instructions. The resulting cDNA samples were diluted 10-fold and stored at -80°C.

**Real Time-PCR.** Five ng of template cDNA were mixed with one of the following TaqMan Gene Expression Assays (Life Technologies): GAPDH (Hs99999905\_m1), ACTB (Hs01060665\_m1), or SLC7A5 (Assay ID: Hs01001190\_m1). This mixture was then diluted with 2X TaqMan Fast Universal Master Mix (Life Technologies) to a final reaction volume of 10  $\mu$ L in 96-well reaction plates. Reaction plates were run on the Applied Biosystems 7900HT Fast Real-Time PCR System with the following profile: 95°C for 20 seconds followed by 40 cycles of 95°C for 3 seconds and 60°C for 30 seconds. The relative expression of SLC7A5 was calculated by the  $\Delta\Delta C_T$  comparative expression method [12].

**Western blot analysis.** Protein was extracted from BMVs, and transporter- and empty vector transfected human embryonic kidney cells by incubating with prechilled CellLytic Mcell lysis buffer (Sigma-Aldrich, St Louis, MO) containing a protease inhibitor cocktail for 20 min at 4°C. Homogenates were centrifuged for 10 min at 15,000 rpm at 4°C, and the protein concentration of the supernatant determined by BCA protein assay (Thermo Fisher Scientific, Rockford, IL) using the manufacturer's protocol. Up to 20  $\mu$ g of total protein was subjected to SDS-PAGE using a Tris-glycine 4-15% polyacrylamide gel (Bio-Rad, Hercules, CA), and then transferred onto a polyvinylidene difluoride membrane (Bio-Rad, Hercules, CA). Membranes were blocked in Protein-free T20 Blocking Buffer (Thermo Fisher Scientific, Rockford, IL) for 1 hr at room temperature, and then incubated with a primary antibody against Lat1 (Abbiotec, San Diego, CA) or a

$\beta$ -actin-HRP conjugated antibody (Santa Cruz Biotechnology, Santa Cruz, CA) diluted in blocking buffer overnight at 4°C. Membranes were then washed with Tris-buffered saline containing 0.1% tween 20 (TBST) at pH 7.4 6 times for 5 min prior to incubating with HRP-conjugated goat anti-rabbit IgG diluted in TBST for 1 hr at room temperature. Membranes were then washed 6 times for 5 min in TBST again, and developed with Pierce ECL Western Blotting Substrate (Thermo Fisher Scientific, Rockford, IL) using the manufacturer's protocol. All scanned membrane images were processed and quantified using ImageJ.

***LAT1-targeted platinum design and synthesis.*** Seven LAT1-targeted platinum analogs were designed to have LAT1 substrates covalently attached to either the leaving group or non-leaving group side of the platinum atom (Figure 3.1), and synthesized according to established protocols [13, 14]. In some cases, such as with 149, 187, and 207, analogs structurally similar to LAT1 substrates were covalently attached to the platinum atom due to feasibility of chemical synthesis. All analogs were synthesized and validated by nuclear magnetic resonance at the University of Minnesota by Dr. Swati More.

***Cellular uptake studies.*** Uptake studies were performed as described previously [15]. Briefly, HEK-LAT1 cells were seeded at a density of  $2 \times 10^5$  cells per well in poly-D-lysine-coated 24-well (BD Falcon) plates. After 24 hours, cells were exposed to growth medium either with 2 mM sodium butyrate and doxycycline for 24 hours to induce LAT1 expression or without these inducers as a control. Once cells reached 80-90% confluence, they were rinsed with pre-warmed, sodium-free choline buffer (140 mM choline chloride, 2 mM KCl, 1 mM  $MgCl_2$ , 1 mM  $CaCl_2$ , 1 M Tris), and then

incubated in 0.3 ml of pre-warmed choline buffer containing 1  $\mu$ M unlabeled gabapentin and 10 nM [ $^3$ H]-gabapentin (American Radiolabeled Chemicals, St. Louis, MO) for 3 minutes at 37°C. The reaction was terminated by washing cells twice with 1.0 ml of ice-cold choline buffer, followed by addition of 700  $\mu$ l lysis buffer (0.1% SDS v/v, 0.1 N NaOH). Intracellular radioactivity was determined by scintillation counting and normalized per well protein content as measured by BCA protein assay (Pierce, Rockford, IL).

Cellular platinum accumulation was determined as previously described [16]. Briefly, HEK-LAT1 cells were seeded and grown as described above for measuring [ $^3$ H]-gabapentin uptake, except with the addition of pre-warmed choline buffer containing 10  $\mu$ M cisplatin or LAT1-targeted platinum compound instead of gabapentin, and incubated for 2 hours at 37°C and 5% CO<sub>2</sub>. The reaction was terminated by washing cells twice with 1.0 ml of ice-cold choline buffer, followed by addition of 100  $\mu$ l of 70% nitric acid at 65°C for at least 2 hours to break down cells. Distilled water containing 10 ppb iridium (Sigma-Aldrich, St. Louis, MO) and 0.1% TritonX-100 was used to dilute the nitric acid to 7% (v/v). Platinum concentration was measured by inductively coupled plasma mass spectrometry (ICP-MS) at the Analytical Facility of the University of California, Santa Cruz. Cellular platinum concentration was normalized to total protein content that was determined from a 24-well plate of HEK-LAT1 cells treated identically as the uptake plate.

**Cell proliferation studies.** HEK-LAT1 cells were seeded at  $5 \times 10^3$  cells per well in poly-D-lysine-coated 96-well plates (BD Falcon), and on the following day cells were exposed to growth medium either with 2 mM sodium butyrate and doxycycline for

24 hours to induce LAT1 expression, or without these inducers as a control. After induction, cells were treated with fresh growth medium (no sodium butyrate or doxycycline) containing either drug (0.32 to 500  $\mu$ M) or vehicle (0.85% saline solution) for 72 hours. Cell density was measured 72 hours post-treatment using the CellTiter-Glo cell viability kit (Promega, Madison, WI) according to the manufacturer's instructions. Cell lysates were transferred to white opaque 96-well plates (Corning Life Sciences) and bioluminescence was measured on a Glomax luminometer (Promega). Cell viability was expressed as percent of vehicle treatment, and drug concentration-response curves were generated using GraphPad Prism version 5.0 (La Jolla, CA). These curves were analyzed using a curve fit for sigmoid dose-response, and the concentration at which cell growth was inhibited by 50% ( $GI_{50}$ ) was derived.

**Generation of transgenic mice.** Chimeric mice were generated at the Gladstone Transgenic Gene-targeting core (San Francisco, CA) by injecting both BH3 and CC3 clones into the blastocoel cavity of day 3.5 embryos from albino C57BL/6J- $tyr^{<c-2J}$  mice, and implanted into host female albino C57BL/6J- $tyr^{<c-2J}$  mice. Clones BH3 and CC3 produced 13 and 2 chimeras, respectively, which were mated to albino C57BL/6J- $tyr^{<c-2J}$  mice (Jackson Laboratory, Bar Harbor, ME) to determine germ line transmission of the Slc7a5-targeted construct and generate mice heterozygous for Lat1. Subsequent heterozygous mice were then mated to generate homozygous mutant mice.

**Animals.** All mice strains were housed under a 12-hour light/dark cycle with free access to water and standard chow (Harlan Laboratories, Indianapolis, IN). Wild type albino C57BL/6J- $tyr^{<c-2J}$  mice used for crossing to chimeric mice were obtained from the Jackson Laboratory (Bar Harbor, ME). All animals used in experiments were

between 8 to 10 weeks of age. All experiments in mice were approved by the Institutional Animal Care and Use Committee of University of California at San Francisco (protocol # AN089117-01B).

***Pharmacokinetic and tissue distribution studies.*** Male C57BL/6 wild type and Lat1 heterozygous mice were dosed with 200  $\mu\text{Ci/kg}$  [ $^3\text{H}$ ]-gabapentin (300 ng/kg) or [ $^3\text{H}$ ]-levodopa (2.2  $\mu\text{g/kg}$ ) (American Radiolabeled Chemicals) in saline via tail vein injection. Blood samples were collected at 5, 10, 15, 30, 60, 90, 120, and 240 min by tail bleeding into heparinized microhematocrit capillary tubes (Fisher Scientific, Pittsburgh, PA), and centrifuged for 5 min at 12,000 times g to obtain plasma. Mice were sacrificed 15 or 240 min after injection, perfused with 10 mL of ice cold PBS, and brain, testicle, lung, heart, skeletal muscle from the left hind flank, liver, and kidney tissues were collected immediately, and dissolved in Solvable (PerkinElmer, Waltham, MA) overnight at 50°C. The amount of [ $^3\text{H}$ ]-gabapentin or [ $^3\text{H}$ ]-levodopa in plasma and tissue samples was quantified by liquid scintillation counting using a Beckman LS 6500 scintillation counter (Brea, CA). Pharmacokinetic parameters were obtained by non-compartmental analysis using WinNonlin 6.3 (Pharsight Corporation, Mountain view, CA).

***Statistical analysis.*** Data were analyzed in GraphPad Prism version 5.0 by either Student's unpaired t-test, one-way ANOVA followed by Dunnett's multiple comparison test, two-way ANOVA followed by Bonferroni correction, or Chi-square test. Probability values lower than 0.05 were considered statistically significant.

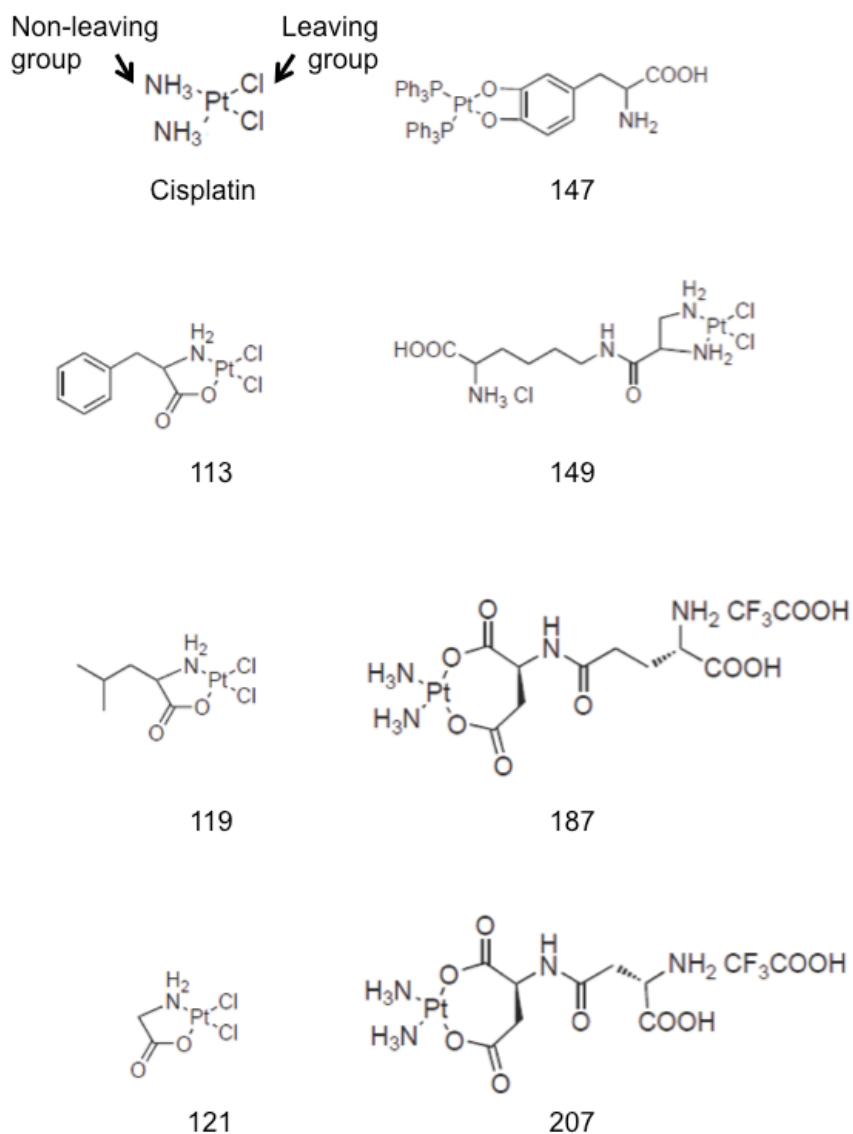


**Figure 3.1. Chemical structures of LAT1-targeted platinum compounds.** The structure of cisplatin is depicted in the top left, with the leaving and non-leaving group sides of the platinum atom labeled. LAT1-targeted platinum compounds were designed to have LAT1 substrates, or substrate analogs covalently attached to the leaving or non-leaving group side of the platinum atom. Numbers below the chemical structures are used to refer to each compound.

## Results

**Cellular accumulation of LAT1-targeted platinum analogs.** HEK-LAT1 cells induced to overexpress LAT1 by treatment with doxycycline had a 250-fold and 125-fold increase in SLC7A5 and SLC3A2 mRNA expression, respectively, relative non-induced cells (Figure 3.2a). Furthermore, the LAT1 drug substrate, gabapentin, accumulated to 10-fold higher levels in induced HEK-LAT1 cells relative to non-induced cells (Figure 3.2b). These results validate HEK-LAT1 cells as an *in vitro* model for measuring LAT1-mediated transport.

Seven LAT1-targeted platinum compounds were screened for transport by LAT1 in cellular uptake studies with HEK-LAT1 cells. Only compound 207 showed a modest (two-fold) increase in the rate of total platinum accumulation (Figure 3.3). However, the overall rate of accumulation for compound 207 was 15-fold lower than cisplatin in induced cells. All other compounds, including both negative controls, cisplatin and compound 121, demonstrated no change (approximately one-fold) in the rate of platinum accumulation in induced versus non-induced cells. Interestingly, compound 147 had a 15-fold higher rate of cellular accumulation than cisplatin in both induced and non-induced cells.

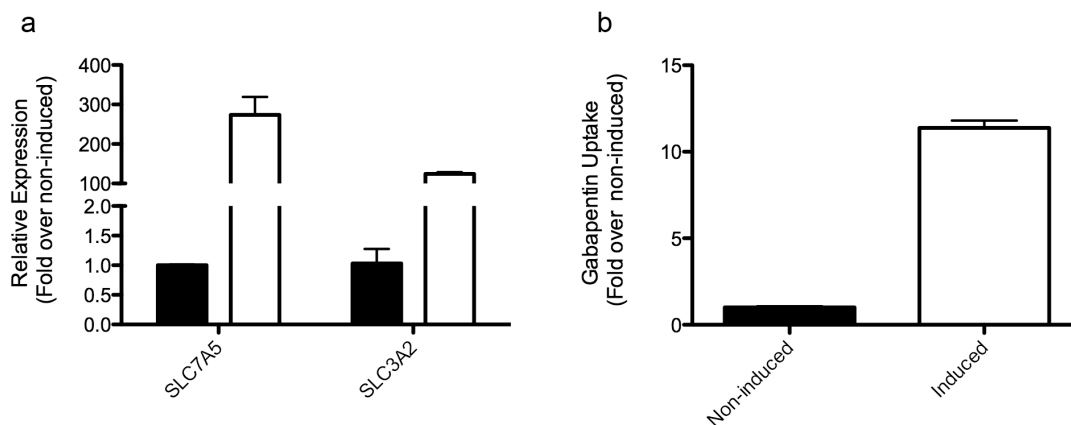


**Figure 3.2. Characterization of HEK-LAT1 cells.** (a) Real-time PCR quantification of SLC7A5 and SLC3A2 gene expression in cells induced to overexpress both genes by treatment with doxycycline (white bars) relative to non-induced cells (black bars). (b) Gabapentin (1  $\mu$ M unlabeled gabapentin and 10 nM [ $^3$ H]-gabapentin) accumulation in cells induced to overexpress both genes by treatment with doxycycline (white bars) relative to non-induced cells (black bars). All values represent the mean  $\pm$  SEM of 3 separate experiments.



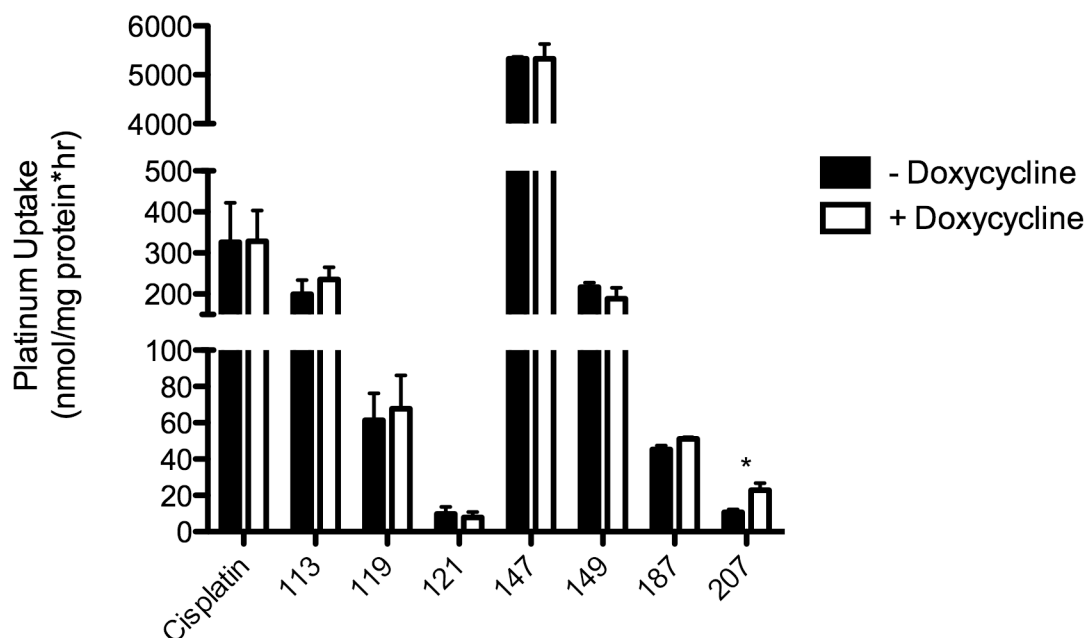


**Figure 3.3. Rate of platinum accumulation in HEK-LAT1 cells.** Cells either induced to overexpress LAT1 by treatment with doxycycline (white bars) or non-induced cells (black bars) were exposed to 10  $\mu$ M of each LAT1-targeted platinum compound or cisplatin for 2 hours at 37°C and 5% CO<sub>2</sub>. Intracellular platinum content was normalized to total protein and incubation time to obtain the rate of platinum accumulation. All values represent the mean  $\pm$  SEM of 2-3 separate experiments. \* $P$  < 0.05 by Student's t-test.

**Cytotoxicity of LAT1-targeted platinum compounds.** The cytotoxic potency of seven LAT1-targeted platinum compounds and cisplatin (negative control) was determined by measuring growth inhibition of induced versus non-induced HEK-LAT1 cells (Table 3.1). The  $GI_{50}$  values of compounds 147 and 207 (~5-10  $\mu$ M) were similar to cisplatin, while all other compounds were at least 10-fold less potent than cisplatin in non-induced cells. This is especially interesting considering there is up to a 300-fold difference in the cellular accumulation rates of all three compounds in induced cells (Figure 3.3). More importantly, after incubating cells with each compound for 72 hours, overexpression of LAT1 conferred resistance to compound 207 (resistance factor = 0.42), but had no effect on the potency of cisplatin or the other six LAT1-targeted platinum compounds (resistance factors ~ 1.00). However, this LAT1-dependent resistance was abrogated with shorter exposure times (resistance factors ~ 1.00; Table 3.1). These data partially agree with the cell accumulation results (Figure 3.3) in that both suggest compound 207 is a LAT1 substrate. However, while the cell accumulation results indicate that LAT1 mediates net uptake of compound 207 into cells over short incubation times (hours), the cytotoxicity data suggest that LAT1 mediates net efflux of compound 207 out of cells over long incubation times (days).

**Table 3.1. Cytotoxic potency of LAT1-targeted platinum compounds and cisplatin against HEK-LAT1 cells.**

<b>Compound</b>	<b>Time (hr)</b>	<b>- Doxycycline (<math>\mu\text{M}</math>)</b>	<b>+ Doxycycline (<math>\mu\text{M}</math>)</b>	<b>Resistance Factor<sup>a</sup></b>
113	72	104 $\pm$ 12.8	100 $\pm$ 5.04	1.04
119	72	ND	ND	ND
121	72	ND	ND	ND
147	72	5.83 $\pm$ 0.801	4.34 $\pm$ 0.911	1.34
149	72	117 $\pm$ 4.55	119 $\pm$ 14.1	0.983
187	72	ND	ND	ND
207*	72	9.35 $\pm$ 1.22	22.3 $\pm$ 4.02	0.419
207	24	15.1 $\pm$ 1.94	15.4 $\pm$ 3.14	0.981
207	2	86.2 $\pm$ 0.80	109 $\pm$ 11.1	0.790
Cisplatin	72	8.09 $\pm$ 1.76	9.08 $\pm$ 3.12	0.891
Cisplatin	24	34.2 $\pm$ 3.35	38.2 $\pm$ 2.18	0.895
Cisplatin	2	142 $\pm$ 9.25	129 $\pm$ 2.00	1.10

\*,  $P < 0.05$

a, *Resistance factor* is the ratio of - doxycycline: + doxycycline.

ND, Not determined because  $\text{GI}_{50}$  value was greater than 200  $\mu\text{M}$ .

All values represent the mean  $\text{GI}_{50} \pm \text{SEM}$  of 2-4 separate experiments.

**Generation of Lat1 deficient mice.** Targeted constitutive deletion of Lat1 from C57BL/6NTac-derived ES cells was accomplished with a BAC-based vector, and the confirmed Lat1 null (Lat1  $-/-$ ) cells were used to generate chimeric mice (see Materials and Methods; Figure 3.4). Out of 15 viable chimeric mice (14 male; 1 female), two clone BH3-derived chimeras had germline transmission of the Lat1 null allele and produced heterozygous offspring. Unfortunately, after genotyping over 60 offspring from 10 different heterozygous breeding pairs, no Lat1 null mice have been observed (Table 3.2). This result indicates that Lat1 likely plays an important role during embryonic development, and loss of Lat1 is embryonic lethal.

**Table 3.2. Observed versus expected genotypes of pups from heterozygous breeding pairs.**

Genotype	Observed*	Expected*
Wild Type	21	16
Heterozygous	42	31
Lat1 Null	0	16

\*,  $P < 0.0001$

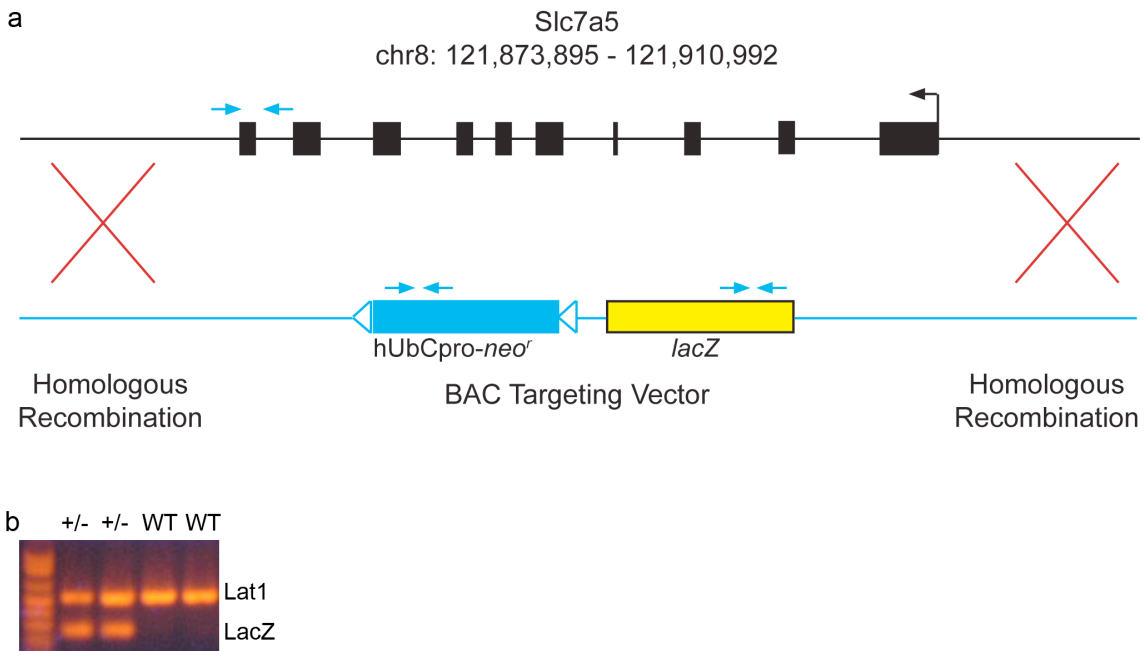


**Figure 3.4. Strategy for targeted deletion of Lat1 in C57BL/6NTac ES cells.** (a) A BAC-based vector containing the neomycin phosphotransferase (*neo'*) gene regulated by the human ubiquitin C promoter (hUbCprom) and  $\beta$ -galactosidase gene (*lacZ*) regulated by the endogenous Slc7a5 (Lat1) promoter was used to constitutively delete the Slc7a5 gene through homologous recombination. Triangles represent loxP sites, black boxes represent exons, the black arrow represents the start codon for Lat1, and blue arrows represent primer sites used to determine mice genotypes. (b) PCR products of ~550 and ~300 base pairs from reactions containing either the Lat1 or *lacZ* genotyping primers, respectively, and genomic DNA isolated from the tails of four mice.

**Characterization of heterozygous mice.** Since Lat1 null mice are not viable, heterozygous mice were characterized as an *in vivo* model for determining Lat1's contribution to drug disposition. Before pharmacokinetic studies began, general characteristics of heterozygous mice were determined. Heterozygous mice had no obvious anatomical or morphological abnormalities, and were indistinguishable from their wild type littermates. Furthermore, average body and organ weights of adult 8-week-old heterozygous and wild type littermates were similar (Table 3.3).

Lat1 mRNA and protein expression were also characterized to determine whether heterozygous mice are valuable for measuring Lat1 function *in vivo*. Lat1 mRNA expression was measured in tissues with high Lat1 expression levels, such as the brain, testes, spleen, and bone marrow [17, 18], and the kidney as a negative control tissue with low Lat1 expression (Figure 3.5a). In all tissues tested, Lat1 mRNA was reduced by greater than 50% in heterozygous mice relative to wild type littermates, including those with low levels of Lat1 such as the kidney. A polyclonal antibody against Lat1 was validated by Western blot of brain, testes, and kidney tissue extracts (Figure 3.5b). A single band ~52 kDa was observed in the brain and testes, but was absent from the kidneys when tissue extracts were separated under reducing conditions (UniProt predicted molecular weight ~55 kDa). However, no difference in Lat1 protein expression was observed in the brain and testes of heterozygous and wild type littermate mice. Since Lat1 and 4f2hc are linked by a disulfide bond and this heterodimer is the primary species expressed at the cell surface [18], brain lysates were analyzed under non-reducing conditions (Figure 3.5c). Expression of the Lat1-4f2hc

heterodimer was unchanged between heterozygous and wild type littermate mice. Thus, while Lat1 mRNA expression appears to be reduced in heterozygous mice relative to wild type littermates, it is unclear if Lat1 protein expression is also decreased in heterozygous mice.

Pharmacokinetic studies with established Lat1 drug substrates, gabapentin and levodopa, were used to determine if heterozygous mice have reduced Lat1 function. There were no differences between all pharmacokinetic variables in heterozygous versus wild type mice administered a 300 ng/kg (200  $\mu$ Ci/kg) intravascular bolus dose of [ $^3$ H]-gabapentin (Figure 3.6a; Table 3.4). Similar results were obtained in the tissue distribution studies for most tissues, with no differences observed in the gabapentin tissue/plasma of the testes, lung, heart, skeletal muscle, liver, and kidney between heterozygous and wild type mice 15 minutes after administration (Figure 3.6b). Interestingly, gabapentin brain accumulation in heterozygous mice was approximately 40% lower than in wild type mice (Figure 3.6c). Reduced Lat1 brain function in heterozygous mice was confirmed using another prototypical Lat1 drug substrate, levodopa, which had approximately 40% lower brain accumulation in heterozygous mice relative to wild type mice following an intravascular bolus dose of 2.2  $\mu$ g/kg (200  $\mu$ Ci/kg; Figure 3.6c). These results agree with the observed reductions in brain expression of Lat1 mRNA in heterozygous mice relative to wild type littermates, and suggest that Lat1 plays an important role in mediating drug uptake into the brain.

**Table 3.3. Body and organ weights of heterozygous and wild type mice.**

	<b>Heterozygous</b>	<b>Wild Type</b>	<b>Ratio</b>
Body Weight (g)	23.3 ± 1.69	24.0 ± 1.90	0.963
Brain (mg)	461 ± 26.7	476 ± 19.5	0.969
Testicle (mg)	77.1 ± 9.51	68.0 ± 8.37	1.13
Kidney (mg)	171 ± 19.5	168 ± 17.9	1.02
Heart (mg)	127 ± 17.0	130 ± 30.8	0.978
Lung (mg)	54.3 ± 14.0	54.0 ± 5.48	1.01

All values represent the mean ± SD of 7 heterozygous and 5 wild type 8-10 week old

male mice; Ratio = heterozygous : Wild type.

**Table 3.4. Pharmacokinetic parameters after intravascular administration of a 300 ng/kg bolus dose of [<sup>3</sup>H]-gabapentin to heterozygous and wild type mice.**

	<b>Heterozygous</b>	<b>Wild Type</b>	<b>Fold Change</b>
AUC <sub>0-240</sub> (min*ng/mL)	22.9 ± 3.23	20.3 ± 3.76	1.13
CL (mL/min*kg)	12.9 ± 1.81	14.3 ± 2.81	0.900
Terminal t <sub>1/2</sub> (min)	67.0 ± 3.28	78.7 ± 13.9	0.851
V <sub>ss</sub> (L/kg)	1.06 ± 0.0910	1.23 ± 0.231	0.862
C <sub>0</sub> (ng/mL)	464 ± 81.0	438 ± 107	1.06

All values represent the mean ± SD of n = 4 8-10 week old male mice per genotype;

Fold change = heterozygous : Wild type.



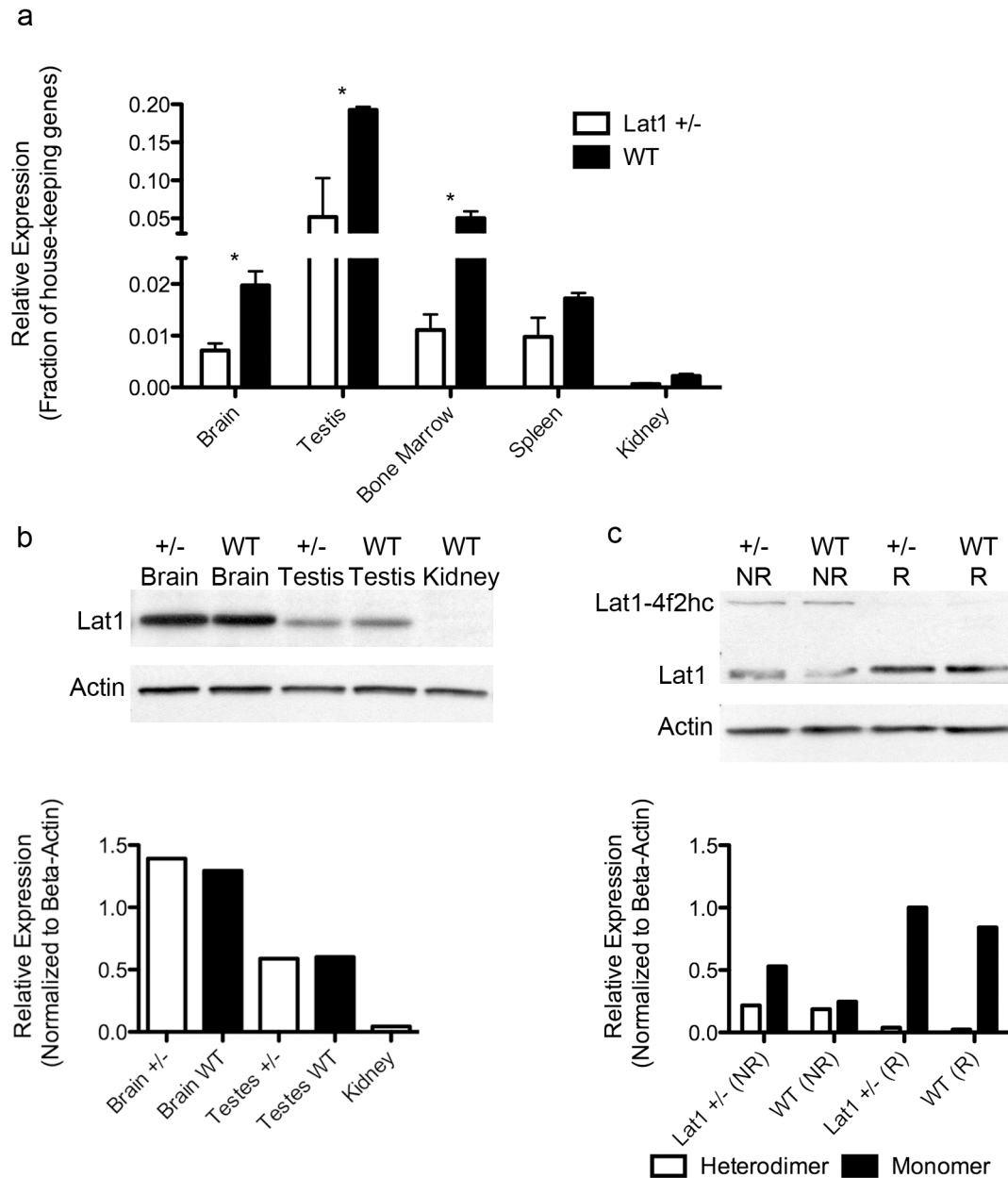


**Figure 3.5. Lat1 mRNA and protein expression in heterozygous and wild type littermate mice.** (a) Real-time PCR quantification of Lat1 mRNA expression in brain, testis, bone marrow, spleen, and kidney tissue lysates from heterozygous (white columns) and wild type (black columns) mice. Lat1 expression was normalized to the average expression levels of two housekeeping genes. Values represent the mean  $\pm$  SEM of  $n=3$  mice/genotype. (b-c) Western blot detection of Lat1 protein in whole brain

lysates from heterozygous and wild type mice. Lat1 (monomer) and Lat1-4f2hc (heterodimer) had approximate molecular weights of 52 and 95 kDa, respectively, and  $\beta$ -actin was used as a loading control. Semi-quantitative analysis of Western blots is depicted below each blot in (b) and (c). +/-, heterozygous mice. WT, wild type mice. NR, sample run under non-reducing conditions. R, sample run under reducing conditions with 2-Mercaptoethanol. All mice were 7-9-week-old males. \*,  $P < 0.05$ .

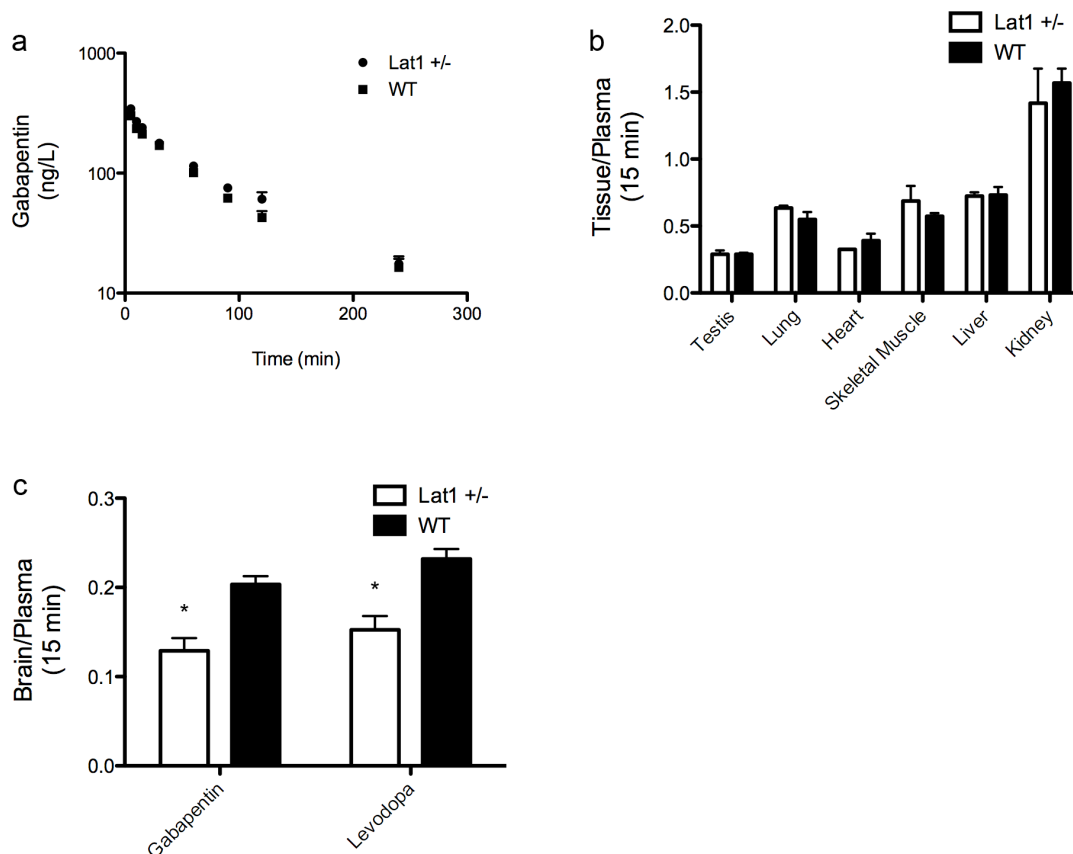


**Figure 3.6. Pharmacokinetics and tissue distribution of Lat1 drug substrates.** (a) Gabapentin plasma concentration-time curve, and (b) tissue distribution in heterozygous and wild type littermates following a 300 ng/kg (200  $\mu$ Ci/kg) intravascular bolus dose of [ $^3$ H]-gabapentin. Plasma concentration values at 5, 10, 15, 30, 60, 90, 120, and 240 minutes post dose are the mean  $\pm$  SD of n=4 mice per genotype. Tissue distribution values are the mean  $\pm$  SEM of n=3 heterozygous mice and n=3 wild type mice. (c) Brain uptake of [ $^3$ H]-gabapentin and [ $^3$ H]-levodopa (2.2  $\mu$ g/kg; 200  $\mu$ Ci/kg) in heterozygous and wild type littermates following an intravascular bolus dose. Values are the mean  $\pm$  SEM of n=3 mice per genotype. All mice were 7-9-week-old C57BL/6 males. \*,  $P < 0.05$ .

## Discussion

LAT1-targeted cisplatin derivatives were synthesized and screened for LAT1-dependent transport and cytotoxicity using cell-based uptake and proliferation assays. Furthermore, a transgenic mouse with reduced LAT1 function was generated as an *in vivo* model for determining LAT1-mediated drug penetration across the BBB. Three key findings emerge from these studies. First, LAT1 transports cytotoxic platinum-based drugs. Second, complete loss of Lat1 function is embryonic lethal. Third, heterozygous mice have reduced Lat1 function in the brain, despite no observable differences in Lat1 protein expression.

***LAT1 transports targeted platinum-based chemotherapeutics.*** LAT1 was first characterized by its ability to transport aromatic and branched-chain amino acids [19], and was later found to transport several drugs, such as gabapentin and levodopa [20]. This characteristic combined with being highly expressed in tumor and brain endothelial cells have made LAT1 an attractive drug target. Previous studies have demonstrated that modifying approved drugs to target LAT1 can increase drug uptake across the BBB [6, 7], and that both small molecule and antibody therapies targeting LAT1 may be effective treatments for a variety of cancers [21, 22]. In this study, one out of seven LAT1-targeted platinum compounds was identified as a weak LAT1 substrate (compound 207; Figure 3.3). The low success rate was likely due to the initial synthesis strategy, which prioritized feasibility of synthesis over optimizing compound structure. Furthermore, while the cell accumulation studies suggest LAT1 mediates net uptake of compound 207, the cytotoxicity studies suggest that LAT1 may be mediating net efflux of these drugs out of cells during longer exposure times (Table 3.1). These

results are in agreement with LAT1's facilitative, obligatory exchange mechanism of transport [23], since the direction of net transport may change as a substrate's concentration gradient across the plasma membrane changes over time. This is supported by the elimination of LAT1's protective effect at shorter exposure times.

Another interesting result was the lack of correlation between cellular platinum accumulation and cytotoxic potency. Cisplatin had a 13-fold higher rate of accumulation in induced HEK-LAT1 cells relative to compound 207 (Figure 3.3), yet compound 207 was equipotent to cisplatin over longer exposure times, and more potent over shorter exposure times (Table 3.1). Once inside the cell, platinum-based drugs can be sequestered in subcellular organelle and deactivated by reacting with metallothionein and glutathione [24], both of which prevent drug binding to genomic DNA. It is possible that compound 207 is less susceptible to these processes than cisplatin once inside the cell, and is therefore more free to bind genomic DNA. Another possibility is that compound 207 binds to genomic DNA more efficiently than cisplatin, thereby requiring lower intracellular drug concentrations to achieve a similar cytotoxic effects as cisplatin. However, additional studies are required to elucidate the mechanism underlying the differences in cisplatin and compound 207 cytotoxic potencies.

Despite some discrepancies in the cell accumulation and cytotoxicity data, these proof-of-concept studies indicate that LAT1 can transport cytotoxic, platinum-based compounds, and provide a foundation to develop improved LAT1-targeted platinum-based drugs.

***Constitutive genetic ablation of Lat1 is embryonic lethal.*** After genotyping over 60 F2 offspring, no Lat1 null mice have been observed (Table 3.2). Since this

result is highly unlikely to occur by chance alone, it is probable that Lat1 deletion is lethal during embryonic development. Furthermore, these results are in agreement with reports by transgenic mouse repositories that indicate mice homozygous for Lat1 deletion are not viable (Mutant Mouse Regional Resource Centers). Influx transporters are responsible for supplying cells with a wide variety of essential nutrients from dietary sources, and genetic ablation of these transport pathways can result in embryonic lethality. For example, folate is an essential B vitamin required during embryonic development, and deletion of *Slc19a1*, the reduced folate carrier, results in embryonic lethality [25]. Lat1-mediated transport is a major route by which cells are supplied with essential amino acids, such as phenylalanine and leucine [26]. Furthermore, essential amino acids play an important role in pre-implantation embryonic development by promoting normal blastocyst development [27]. Since LAT1 is expressed during pre-implantation embryonic development [28], it is possible that lack of LAT1 function leads to an inadequate supply of essential amino acids and disrupts proper blastocyst development. Studies are ongoing to determine at which stage of embryonic development loss of Lat1 function is lethal.

***Heterozygous mice have reduced brain uptake of Lat1 drug substrates.***

Previous studies have frequently suggested that LAT1 plays an important role in mediating drug uptake across the BBB [29-31]. However, all of these studies probed LAT1 function in the BBB with small molecule inhibitors (primarily amino acids) that are not necessarily specific to LAT1. In this study, genetically modified mice heterozygous for Lat1 were validated as a model for measuring Lat1-specific contributions to drug uptake across the BBB. Heterozygous mice had reduced Lat1 mRNA expression in

several tissues, including the brain (Figure 3.5). More importantly, the tissue accumulation of gabapentin and levodopa in heterozygotes was only reduced in the brain (Figure 3.6). Since LAT1 expression in the brain is almost exclusively in the BBB (Chapter 2, Figure 2.2a), these changes are likely due to reduced Lat1 function in the BBB. This expression pattern may explain how Lat1 alters the brain accumulation of gabapentin and levodopa, but other organs with high Lat1 expression, such as the testes, do not have altered accumulation. It is possible that in other organs with high Lat1 expression, no change in gabapentin or levodopa accumulation was observed because other transporters that interact with the drugs are also expressed. In contrast, in the BBB, Lat1 may be the primary transporter for these compounds. These results confirm previous studies of LAT1 function in the BBB, and validate Lat1 heterozygous mice as a model for measuring Lat1-mediated brain uptake.

Despite decreased Lat1 function and mRNA expression at the BBB, there were no observable changes in Lat1 protein in the brain or testes of heterozygous mice relative to wild type littermates (Figure 3.5). However, the observed functional changes were modest in magnitude, and suggest that any change in Lat1 protein expression would be small. The Western blotting technique used to measure Lat1 protein expression is semi-quantitative in nature, and may not be sensitive enough to detect the small, subtle changes in protein expected in these studies. More importantly, numerous studies attempting to correlate mRNA and protein levels in model organisms and humans have often observed a very poor correlation, including decreased mRNA expression, but no change in the protein expression of many different genes [32-35].

These discordant results are not completely unexpected, but need to be confirmed with further studies using more sensitive protein quantification methods, such as ELISA.

In summary, these studies suggest that platinum-based drugs can be modified to target LAT1, and establish a new strategy for developing anti-cancer platinum analogs. Finding that Lat1 null mice are not viable highlights the important roles essential nutrient transporters play during embryonic development. Finally, Lat1 heterozygous mice provide a new tool for determining Lat1-mediated brain uptake of drugs, and suggest influx transporters play an important role in regulating drug penetration across the BBB.

## References

1. Wang Y, Welty DF. The simultaneous estimation of the influx and efflux blood-brain barrier permeabilities of gabapentin using a microdialysis-pharmacokinetic approach. *Pharmaceutical research*. 1996;13(3):398-403.
2. Alexander GM, Schwartzman RJ, Grothusen JR, Gordon SW. Effect of plasma levels of large neutral amino acids and degree of parkinsonism on the blood-to-brain transport of levodopa in naive and MPTP parkinsonian monkeys. *Neurology*. 1994;44(8):1491-9.
3. Uchida Y, Ohtsuki S, Katsukura Y, Ikeda C, Suzuki T, Kamiie J, et al. Quantitative targeted absolute proteomics of human blood-brain barrier transporters and receptors. *J Neurochem*. 2011;117(2):333-45.
4. Roberts LM, Black DS, Raman C, Woodford K, Zhou M, Haggerty JE, et al. Subcellular localization of transporters along the rat blood-brain barrier and blood-cerebral-spinal fluid barrier by in vivo biotinylation. *Neuroscience*. 2008;155(2):423-38.



5. Sanchez del Pino MM, Peterson DR, Hawkins RA. Neutral amino acid transport characterization of isolated luminal and abluminal membranes of the blood-brain barrier. *J Biol Chem.* 1995;270(25):14913-8.
6. Killian DM, Hermeling S, Chikhale PJ. Targeting the cerebrovascular large neutral amino acid transporter (LAT1) isoform using a novel disulfide-based brain drug delivery system. *Drug delivery.* 2007;14(1):25-31.
7. Gynther M, Jalkanen A, Lehtonen M, Forsberg M, Laine K, Ropponen J, et al. Brain uptake of ketoprofen-lysine prodrug in rats. *International journal of pharmaceutics.* 2010;399(1-2):121-8.
8. Kelland L. The resurgence of platinum-based cancer chemotherapy. *Nat Rev Cancer.* 2007;7(8):573-84.
9. Goffin J, Lacchetti C, Ellis PM, Ung YC, Evans WK, Lung Cancer Disease Site Group of Cancer Care Ontario's Program in Evidence-Based C. First-line systemic chemotherapy in the treatment of advanced non-small cell lung cancer: a systematic review. *J Thorac Oncol.* 2010;5(2):260-74.
10. Doolittle ND, Peereboom DM, Christoforesidis GA, Hall WA, Palmieri D, Brock PR, et al. Delivery of chemotherapy and antibodies across the blood-brain barrier and the role of chemoprotection, in primary and metastatic brain tumors: report of the Eleventh Annual Blood-Brain Barrier Consortium meeting. *J Neurooncol.* 2007;81(1):81-91.
11. Fortin D, Gendron C, Boudrias M, Garant MP. Enhanced chemotherapy delivery by intraarterial infusion and blood-brain barrier disruption in the treatment of cerebral metastasis. *Cancer.* 2007;109(4):751-60.

12. Pfaffl MW. A new mathematical model for relative quantification in real-time RT-PCR. *Nucleic Acids Res.* 2001;29(9):e45.
13. Moradell S, Lorenzo J, Rovira A, van Zutphen S, Aviles FX, Moreno V, et al. Water-soluble platinum(II) complexes of diamine chelating ligands bearing amino-acid type substituents: the effect of the linked amino acid and the diamine chelate ring size on antitumor activity, and interactions with 5'-GMP and DNA. *J Inorg Biochem.* 2004;98(11):1933-46.
14. Watabe M, Kai M, Goto K, Ohmuro H, Furukawa S, Chikaraishi N, et al. Preparation of platinum(II) complexes with L-serine using KI. X-ray crystal structure, HPLC and <sup>195</sup>Pt NMR spectra. *J Inorg Biochem.* 2003;97(2):240-8.
15. Chen Y, Zhang S, Sorani M, Giacomini KM. Transport of paraquat by human organic cation transporters and multidrug and toxic compound extrusion family. *J Pharmacol Exp Ther.* 2007;322(2):695-700.
16. Zhang S, Lovejoy KS, Shima JE, Lagpacan LL, Shu Y, Lapuk A, et al. Organic cation transporters are determinants of oxaliplatin cytotoxicity. *Cancer Res.* 2006;66(17):8847-57.
17. Kanai Y, Segawa H, Miyamoto K, Uchino H, Takeda E, Endou H. Expression cloning and characterization of a transporter for large neutral amino acids activated by the heavy chain of 4F2 antigen (CD98). *The Journal of biological chemistry.* 1998;273(37):23629-32.
18. Nakamura E, Sato M, Yang H, Miyagawa F, Harasaki M, Tomita K, et al. 4F2 (CD98) heavy chain is associated covalently with an amino acid transporter and

controls intracellular trafficking and membrane topology of 4F2 heterodimer. J Biol Chem. 1999;274(5):3009-16.

19. Kanai Y, Segawa H, Miyamoto K, Uchino H, Takeda E, Endou H. Expression cloning and characterization of a transporter for large neutral amino acids activated by the heavy chain of 4F2 antigen (CD98). J Biol Chem. 1998;273(37):23629-32.

20. del Amo EM, Urtti A, Yliperttula M. Pharmacokinetic role of L-type amino acid transporters LAT1 and LAT2. Eur J Pharm Sci. 2008;35(3):161-74.

21. Oda K, Hosoda N, Endo H, Saito K, Tsujihara K, Yamamura M, et al. L-type amino acid transporter 1 inhibitors inhibit tumor cell growth. Cancer science. 2010;101(1):173-9.

22. Ohkawa M, Ohno Y, Masuko K, Takeuchi A, Suda K, Kubo A, et al. Oncogenicity of L-type amino-acid transporter 1 (LAT1) revealed by targeted gene disruption in chicken DT40 cells: LAT1 is a promising molecular target for human cancer therapy. Biochem Biophys Res Commun. 2011;406(4):649-55.

23. Verrey F, Closs EI, Wagner CA, Palacin M, Endou H, Kanai Y. CATs and HATs: the SLC7 family of amino acid transporters. Pflugers Archiv : European journal of physiology. 2004;447(5):532-42.

24. Hall MD, Okabe M, Shen DW, Liang XJ, Gottesman MM. The role of cellular accumulation in determining sensitivity to platinum-based chemotherapy. Annu Rev Pharmacol Toxicol. 2008;48:495-535.

25. Zhao R, Russell RG, Wang Y, Liu L, Gao F, Kneitz B, et al. Rescue of embryonic lethality in reduced folate carrier-deficient mice by maternal folic acid supplementation

reveals early neonatal failure of hematopoietic organs. *J Biol Chem.*

2001;276(13):10224-8.

26. Christensen HN. Role of amino acid transport and countertransport in nutrition and metabolism. *Physiol Rev.* 1990;70(1):43-77.

27. Van Winkle LJ. Amino acid transport regulation and early embryo development. *Biol Reprod.* 2001;64(1):1-12.

28. Chrostowski MK, McGonnigal BG, Stabila JP, Padbury JF. LAT-1 expression in pre- and post-implantation embryos and placenta. *Placenta.* 2009;30(3):270-6.

29. Nutt JG, Woodward WR, Hammerstad JP, Carter JH, Anderson JL. The "on-off" phenomenon in Parkinson's disease. Relation to levodopa absorption and transport. *N Engl J Med.* 1984;310(8):483-8.

30. Hammerstad JP, Pate BD, Hewitt KA, Chan GL, Ruth TJ, Calne DB. The transport of L-6-fluorodopa and its metabolites from blood to cerebrospinal fluid and brain. *Ann Neurol.* 1993;34(4):603-8.

31. Thurlow RJ, Brown JP, Gee NS, Hill DR, Woodruff GN. [3H]gabapentin may label a system-L-like neutral amino acid carrier in brain. *Eur J Pharmacol.* 1993;247(3):341-5.

32. Vogel C, Marcotte EM. Insights into the regulation of protein abundance from proteomic and transcriptomic analyses. *Nat Rev Genet.* 2012;13(4):227-32.

33. Tian Q, Stepaniants SB, Mao M, Weng L, Feetham MC, Doyle MJ, et al. Integrated genomic and proteomic analyses of gene expression in Mammalian cells. *Mol Cell Proteomics.* 2004;3(10):960-9.

34. Stark AM, Pfannenschmidt S, Tscheslog H, Maass N, Rosel F, Mehdorn HM, et al. Reduced mRNA and protein expression of BCL-2 versus decreased mRNA and

increased protein expression of BAX in breast cancer brain metastases: a real-time PCR and immunohistochemical evaluation. *Neurol Res.* 2006;28(8):787-93.

35. Lichtinghagen R, Musholt PB, Lein M, Romer A, Rudolph B, Kristiansen G, et al. Different mRNA and protein expression of matrix metalloproteinases 2 and 9 and tissue inhibitor of metalloproteinases 1 in benign and malignant prostate tissue. *Eur Urol.* 2002;42(4):398-406.

## CHAPTER 4

### Structure-based ligand discovery for the Large-neutral Amino Acid Transporter 1, LAT1

#### Introduction

***The large-neutral amino acid transporter (LAT1, SLC7A5).*** LAT1 is a sodium-independent exchanger found in the brain, testis, and placenta, where it mediates transport of large-neutral amino acids (e.g., tyrosine) and thyroid hormones (e.g., triiodothyronine (T3)) across the cell membrane [1]. More specifically, LAT1 is highly expressed in the blood- and brain-facing membranes of the Blood-Brain-Barrier (BBB) to supply the central nervous system (CNS) with essential nutrients and to help maintain the neural microenvironment [2]. LAT1 is also an important drug target because it transports several prescription drugs, such as the antiparkinsonian drug L-Dopa and the anticonvulsant gabapentin across the BBB, thereby enabling their pharmacologic effects [3, 4]. This function at the BBB has made LAT1 a target for drug delivery by modifying CNS impermeable drugs such that they become LAT1 substrates, and have enhanced BBB penetration [5, 6].

In addition, LAT1 expression levels are increased in many types of cancer, including non-small cell lung cancer and glioblastoma multiforme (GBM) [7, 8]. LAT1 expression increases as cancers progress, leading to higher expression levels in high-grade tumors and metastases [9]. In particular, LAT1 plays a key role in cancer-associated reprogrammed metabolic networks by supplying growing tumor cells with essential amino acids that are used as nutrients to build biomass and signaling

molecules to enhance proliferation by activating pro-growth pathways such as the mTOR pathway [10]. Furthermore, inhibiting LAT1 function reduces tumor cell proliferation, indicating that it may be a viable target for novel anticancer therapies [11-13]. A cancer drug targeting LAT1 can therefore be a LAT1 inhibitor that deprives the cancer cells of nutrients or a cytotoxic LAT1 substrate with an intracellular target (e.g., a metabolic enzyme).

***LAT1 structure.*** LAT1 is a large protein with 12 putative membrane-spanning helices [14]. To transport solutes across the membrane, LAT1 binds SLC3A2, a glycoprotein with a single membrane spanning helix that serves as a chaperone for LAT1 [14]. The atomic structure of human LAT1 is not known, but LAT1 exhibits significant sequence similarity to prokaryotic transporters such as members of the acid/polyamine/organocation transporter (APC) family, whose representative structures have been recently determined by X-ray crystallography [15-19]. Structures of the arginine:agmatine antiporter AdiC from *E. coli* [15, 17, 18] and *Salmonella enterica* [20] in different conformations reveal an internal two-fold pseudo-symmetry, similar to the structures of the sodium and chloride dependent leucine transporter, LeuT [19, 21]. These data, combined with structures of additional related transporters [22] and Molecular Dynamics (MD) simulations [23], suggest a common transport mechanism among the LAT1 homologs and LeuT, where the role of sodium in LeuT is proposed to be mimicked by a proton in some APC transporters [23]. Thus, LAT1 probably also transports ligands across the cell membrane *via* the ‘alternating access’ transport mechanism [22, 24, 25].

In this study, we take an integrated computational and experimental approach to characterize novel LAT1 ligands. We construct structural models of LAT1 based on structures of homologous APC family transporters from prokaryotic organisms, and then perform virtual ligand screening of metabolite and prescription drug libraries against these models to predict small molecule ligands. The top scoring hits are tested experimentally for LAT1 inhibition and transport using *cis*-inhibition experiments and *trans*-stimulation assays, respectively. Furthermore, we characterize the effect of select validated ligands on cell proliferation. Finally, we describe the pharmacological implications of our results, including how the intended and unintended effects of the discovered ligands may be mediated by LAT1 transport across the BBB as well as their potential use as chemical tools to characterize the role of LAT1 in cancer.

## Materials and Methods

**Template selection.** To identify potential templates for modeling LAT1, we used fold-recognition and modeling servers HHpred [26] and I-Tasser [27], as well as analyzed the LAT1 entries in the database of comparative protein structure models ModBase [28] and the Transporter Classification Database (TCDB) [29]. These computational tools revealed that LAT1 exhibits significant sequence similarity to protein structures in the APC (Amino acid-Polyamine-organoCation) superfamily of the Orientations of Proteins in Membranes (OPM) database [30]. To select the optimal template for structure-based ligand discovery, we used the following considerations: (i) sequence similarity to LAT1, (ii) structure quality, and (iii) conformation, including



whether it is ligand-bound or not, and whether the structure is in an occluded, inward-facing, or outward-facing conformation.

**Comparative model construction.** LAT1 was modeled using MODELLER-10v8 based on the X-ray structure of the arginine/agmatine transporter AdiC from *E. coli* in the outward-occluded arginine-bound conformation (PDB identifier 3L1L) [17]. We also modeled LAT1 based on the structure of the amino acid, polyamine, and organo-cation transporter ApcT from *M. jannaschii* in an inward-*apo* conformation (PDB id 3GI9) [16]. We relied on a previously published alignment [15] as well as alignments obtained from the Promals3D server [31], where gaps were present primarily, but not only, in the predicted extracellular loops and were manually refined (Figure 4.1). For each template structure and alignment, 100 models were generated using the standard ‘automodel’ routine of MODELLER-10v8 [32]. The initial models were assessed using Z-DOPE, a normalized atomic distance-dependent statistical potential based on known protein structures [33]. For selected LAT1 models, the binding site was refined by repacking the sidechains on a fixed backbone using Scwrl4 [34]. The final models for virtual screening were selected based on their ability to discriminate known ligands from decoy compounds using “enrichment curves” derived from ligand docking calculations [35-37]. These final models were also evaluated based on residue hydrophobicity [38] and evolutionary conservation profiles (Figure 4.2) [39].

**Residue conservation and hydrophobicity analysis.** Evolutionary conservation was calculated using the ConSurf server (<http://consurf.tau.ac.il/>) [39]. For the LAT1 model, we used the default parameters. The conservation values for the AdiC structure were not complete using a variety of similarity cutoffs and databases, probably

because prokaryotic proteins in this family are highly divergent in sequence [19]. Thus, for the AdiC structure, we used the cutoff on sequence identity of 20%, the cutoff on the E-value of 0.1, and the UniProt database. The computed conservation values were mapped onto the LAT1 model and the template structure using Chimera [40], using the scripts provided by the ConSurf server. The hydrophobicity profile was computed using Chimera, relying on the Kyte-Doolittle hydrophobicity scale [38].

The conservation and hydrophobicity profiles are generally similar in the LAT1 model and the AdiC structure, further confirming the model. The minor differences in the hydrophobicity profiles of LAT1 and AdiC can be partially explained by the differences in their binding partners. For example, LAT1 binds the single transmembrane protein SLC3A2, while AdiC is not known to be involved in a similar interaction. Finally, hydrophobic and non-conserved positions are usually predicted to face the estimated location of the lipid membrane, while conserved and hydrophilic residues are modeled in the core, where they may be involved in helix-helix interactions and ligand recognition [41, 42]. In contrast, the conservation profile on the surface of the experimentally determined AdiC structure does not give such a clear signal, possibly because it is involved in protein-protein interactions.

***Selection of molecules for experimental testing.*** The top 500 highest-ranking hits in each of the four computational screens (*ie*, two datasets against two models) were analyzed manually. In particular, we examined similarities of the docking poses of these ligands to those in the predicted complexes of LAT1 with known ligands. Additionally, we discarded top ranked hits for several reasons [36, 43, 44]: 1) likely false positives related to the limitation of the docking programs, including docking poses with

high internal energies or stranded polar groups, 2) compounds that are not purchasable or too expensive, 3) compounds that are not novel, as we tried to balance between chemically novel molecules and those that are pharmacologically interesting but might not exhibit novel chemistry.

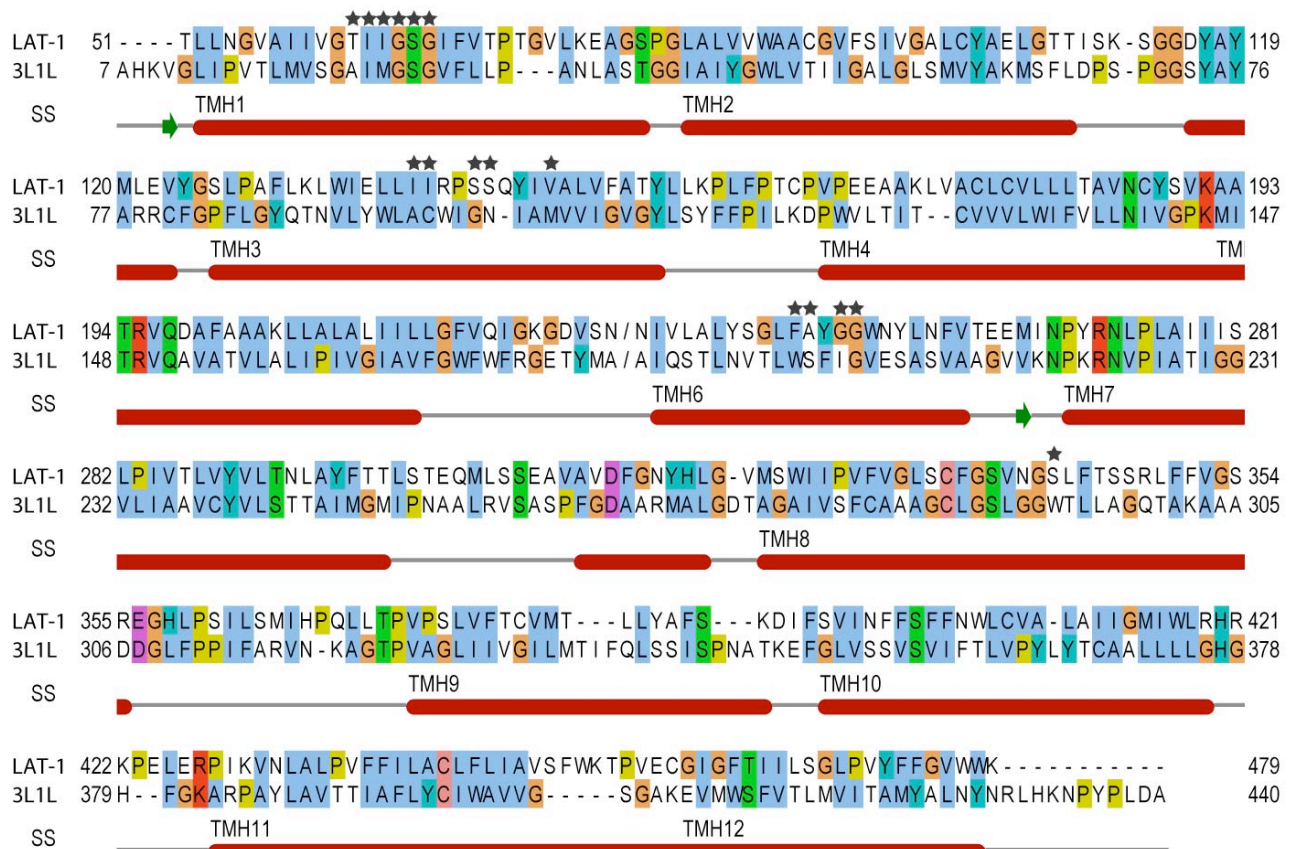


**Figure 4.1. LAT1-AdiC alignment.** The sequence alignment was visualized using Jalview [45]. The aligned residues are colored based on their type using the “Clustlx” color scheme. The template structure (PDB code 3L1L) helical and strand segments are indicated with red rectangles and green arrows, respectively. The transmembrane helices (TMH) of 3L1L were defined using the PPM server [46]; the remainder of the secondary structure segments (SS) were defined by the DSSP program [47]. The residues that are important for LAT1 ligand binding according to our model are highlighted with grey stars. The LAT1 loop that was excluded from modeling is marked with ‘/’.

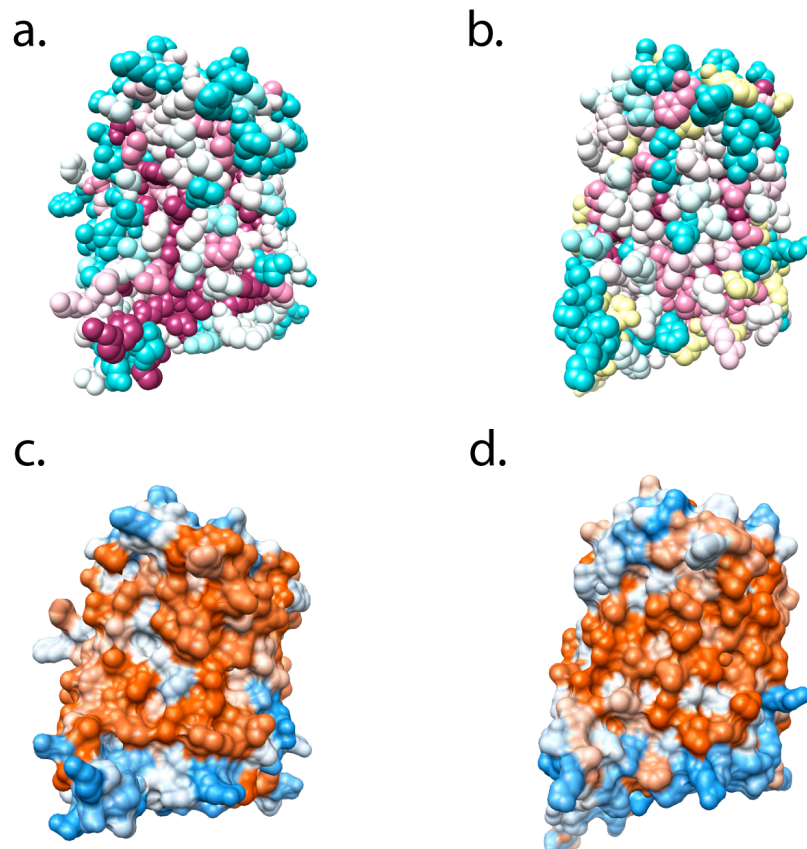


**Figure 4.2. Conservation and hydrophobicity profiles for the LAT1 model and the AdiC structure.** Side-views of the LAT1 model and the AdiC structure. Evolutionary conservation grades (from 1-9) are mapped onto the surface of the LAT1 model (**a**) and the AdiC structure (**b**); the residue positions are colored in cyan for most variable, to white, and to maroon for most conserved; unassigned positions are colored yellow. Hydrophobicity values are mapped onto the surface of the LAT1 model (**c**) and the AdiC structure (**d**); the residues are colored in blue for the most hydrophilic, to white, and to orange for the most hydrophobic.

**Virtual screening and ligand docking.** Virtual screening against the LAT1 models was performed using a semi-automatic docking procedure [37], relying on DOCK 3.5.54 [48]. The docking poses of the database molecules were ranked by DOCK score, which is a sum of van der Waals, Poisson–Boltzmann finite-difference electrostatics, and ligand desolvation penalty terms. Poses of the 500 highest-ranked compounds from each one of the docking screens were inspected by eye to prioritize compounds for experimental testing [35, 36].

**Chemical similarity calculations.** The chemical novelty of the top hits was first evaluated using Instant JChem 5.7.0, 2011, ChemAxon (<http://www.chemaxon.com>). Specifically, we calculated the chemical dissimilarity measure ‘JCDissimilarityCFTanimoto’ among the top small molecule hits and the 44 known LAT1 ligands from the databases ChEMBL [49] and UniProt [50], as well as from the literature [1]; predicted ligands with values higher than 0.7 were classified as chemically novel.

**Cell lines.** Stably transfected human embryonic kidney 293 cells were created by transfecting pcDNA5/FRT (Invitrogen) vector containing the full-length human LAT1 cDNA (HEK-LAT1) and the empty vector (HEK-EV) using Lipofectamine 2000 (Invitrogen) per the manufacturer’s instructions. Transfected cells were maintained in DMEM-H21 containing 10% FBS, 100 units/mL penicillin, 100 µg/mL streptomycin, and 200 µg/mL hygromycin B at 37 °C and 5% CO<sub>2</sub>. Stable LAT1 knock down cells were created by infecting 2 x 10<sup>5</sup> T98G GBM cells with lentivirus produced by the UCSF Lentiviral RNAi core [51] carrying a pSicoR vector expressing green fluorescent protein (GFP) and either an anti-LAT1 shRNA (T98G-KD; Table 4.1) or empty vector (T98G-EV) at a multiplicity of infection equal to 10. One week post-infection GFP<sup>+</sup> cells were

isolated using fluorescence-activated cell sorting (FACS) analysis by the Laboratory for Cell Analysis at the UCSF Comprehensive Cancer Center. GFP<sup>+</sup> T98G-KD and T98G-EV cells were validated for LAT1 RNA and functional knock down as described below. T98G, T98G-KD, and T98G-EV cells were maintained in DMEM-H21 containing 10% FBS, 100 units/mL penicillin, and 100 µg/mL streptomycin at 37°C and 5% CO<sub>2</sub>.

**Table 4.1 Anti-LAT-1 shRNA sequences.**

<b>Cell Line<sup>a</sup></b>	<b>Position<sup>b</sup></b>	<b>Sequence<sup>c</sup></b>
T98G-KD1	3861	GAAAGTAGCTGCTAGTGAA
T98G-KD2	4294	GCTAACGTCTTACTAATTT
T98G-KD3	4512	GTTAATGGCTAACCTGTTA

a, *Cell line* indicates the name given to T98G glioblastoma cells stably expressing a given shRNA construct.

b, *Position* indicates the first base pair within the human SLC7A5 mRNA sequence each shRNA targets.

c, *Sequence* of each construct targeting LAT-1 mRNA.

***Inhibition of [<sup>3</sup>H]-Gabapentin uptake.*** Uptake studies were performed as described previously [52]. Briefly, HEK-LAT1 cells were seeded at a density of  $2 \times 10^5$  cells per well in poly-D-lysine-coated 24-well (BD Falcon) plates and were grown to 80-90% confluence. Cells were rinsed with pre-warmed, sodium-free choline buffer (140 mM choline chloride, 2 mM KCl, 1 mM  $MgCl_2$ , 1 mM  $CaCl_2$ , 1 M Tris), and then incubated in 0.3 ml of pre-warmed choline buffer containing 1  $\mu$ M unlabeled gabapentin and 10 nM [<sup>3</sup>H]-gabapentin (American Radiolabeled Chemicals) for 3 minutes at 37°C in the presence of 10 and 100  $\mu$ M test compound (Sigma-Aldrich). The reaction was terminated by washing cells twice with 1.0 ml of ice-cold choline buffer, followed by addition of 700  $\mu$ l lysis buffer (0.1% SDS v/v, 0.1 N NaOH). Intracellular radioactivity was determined by scintillation counting and normalized per well protein content as measured by BCA protein assay (Pierce). Concentration-dependent inhibition was measured under the same conditions as for the single-point measurements. Cells were incubated with 0.5, 1, 10.0, 50.0, 100.0, and 200.0  $\mu$ M 3,5 diiodo-L-tyrosine or 10.0, 50.0, 100.0, 400.0, 800.0, and 1,600.0  $\mu$ M acivicin. The concentration at which 50% of [<sup>3</sup>H]-gabapentin accumulation is inhibited ( $IC_{50}$ ) was computed by fitting the data using GraphPad Prism version 5.0.

***Trans-stimulation of [<sup>3</sup>H]-L-Leucine efflux.*** Trans-stimulation studies were performed by monitoring intracellular L-leucine efflux from HEK-LAT1 cells stimulated by extracellular addition of known or putative LAT1 substrates. HEK-LAT1 cells were seeded under the same conditions described for inhibition experiments. Cells were rinsed with pre-warmed choline buffer, and then preloaded with [<sup>3</sup>H]-L-Leucine (Perkin Elmer) by incubating cells in 0.3 ml of pre-warmed choline buffer containing 1  $\mu$ M



unlabeled and 10 nM radiolabeled substrate for 5 minutes at 37°C. Uptake was terminated by washing cells twice with 1.0 ml of ice-cold choline buffer, and [<sup>3</sup>H]-L-Leucine efflux was then induced by addition of 1 mM test compound (Sigma-Aldrich) in pre-warmed choline buffer for 1 minute at 37°C. Trans-stimulation was terminated by washing cells twice with 1.0 ml of ice-cold choline buffer, followed by addition of 700 µl lysis buffer (0.1% SDS v/v, 0.1 N NaOH). Intracellular radioactivity was determined as described above.

**Cell proliferation assay.** T98G-KD and T98G-EV cells were seeded at  $2.5 \times 10^3$  cells per well in 96-well plates (Corning Life Sciences), and on the following day cells were exposed to growth medium containing either drug or vehicle (0.85% saline solution) for 48 hours. Cell density was measured on the treatment day and 48 hours post-treatment using the CellTiter-Glo cell viability kit (Promega) according to the manufacturer's instructions. Cell lysates were transferred to white opaque 96-well plates (Corning Life Sciences) and bioluminescence was measured on a Glomax luminometer (Promega). Proliferation of each cell line after 48 hours was first normalized to the density measured on treatment day (0 hours), followed by normalization of drug to vehicle treatment.

**LAT1 mRNA expression.** LAT1 expression was measured as described previously [53]. Briefly, total RNA was isolated from cells plated in 6-well plates (Corning Life Sciences) with Qiagen's RNeasy RNA Isolation Kit per the manufacturer's protocol, and stored at -80°C until use. Reverse transcriptase PCR was done on 2 µg of total RNA using the Invitrogen SuperScript VILO cDNA Synthesis Kit per the manufacturer's

protocol to create a cDNA library. The resulting cDNA was used as template for qRT-PCR using TaqMan Gene Expression Assays for human LAT1 (Assay ID: Hs01001190\_m1) and human GAPDH (Assay ID: Hs99999905\_m1). qRT-PCR reactions were carried out in 96-well reaction plates in a volume of 10  $\mu$ L using the TaqMan Fast Universal Master Mix (Applied Biosystems). Reactions were run on the Applied Biosystems 7500 Fast Real-Time PCR System with the following profile: 95°C for 20 seconds followed by 40 cycles of 95°C for 3 seconds and 60°C for 30 seconds. The relative expression of each mRNA was calculated by the comparative  $\Delta\Delta C_t$  method.

***LAT1 kinetic studies.*** The kinetics of L-leucine uptake in HEK-LAT1 cells were determined as described previously [52]. Briefly, varying amounts of unlabeled L-leucine were added to the uptake solutions to give increasing total ( $[^3\text{H}]$  plus unlabeled L-leucine) substrate concentrations, ranging from 1 to 300  $\mu\text{M}$  at 37°C. Nonspecific cell-associated radioactivity was determined by measuring substrate uptake at 4°C at each substrate concentration, and these values were then subtracted from the results at 37°C in LAT1-transfected cells to give the final kinetic data. The  $K_m$  and  $V_{\max}$  values were obtained by fitting the Michaelis-Menten equation  $V = V_{\max} \times [S]/(K_m + [S])$  using GraphPad Prism version 5.0, where  $V$  refers to the rate of substrate transport,  $V_{\max}$  refers to the maximum rate of substrate transport,  $[S]$  refers to the concentration of substrate, and  $K_m$  is defined as the concentration of substrate at the half-maximal transport rate.

***Statistical analysis.*** Data were analyzed by either one-way ANOVA followed by Dunnett's multiple comparison test, or two-way ANOVA followed by Bonferroni

correction for multiple testing. Probability values lower than 0.05 were considered statistically significant.

## Results

***LAT1 predicted structure and ligand binding.*** LAT1 was modeled based on the X-ray structure of the arginine/agmatine transporter AdiC from *E. coli* in the outward-occluded arginine-bound conformation [17] and the structure of the amino acid, polyamine, and organo-cation transporter ApcT from *Methanococcus jannaschii* in an inward-*apo* conformation [16] (Figure 4.1) (Materials and Methods) . The final LAT1 model contains the whole transmembrane domain of the protein (i.e., the 12 transmembrane helices), including the residues constituting the predicted ligand binding site. Comparative models were first scored using Z-DOPE, a normalized atomic distance-dependent statistical potential based on known protein structures [33]. The Z-DOPE scores of the top models were -0.3, suggesting that 60% of its C $\alpha$  atoms are within 3.5 Å of their correct positions [54] (Table 4.2). Each model was also evaluated based on its ability to discriminate between known ligands and likely non-binders (“decoys”), using “enrichment curves” derived from ligand docking calculations [35]. The logAUC score for the final refined LAT1 model was 31.9 (Table 4.2), suggesting that it is suitable for predicting ligands for experimental testing [35, 37, 55].

**Table 4.2. Assessment of the LAT-1 models**

<b>Occluded conformation</b>		
<b>Model<sup>a</sup></b>	<b>Z-DOPE<sup>b</sup></b>	<b>logAUC<sup>c</sup></b>
Template Structure	-1.23	10.1
Initial model	-0.3	21.5
Model 1	-0.23	31.3
Model 2	-0.12	31.9

a, *Model* marks the model assessed by the two scores; *Template structure* is ApcT[17];

*Initial model* represents the top scoring model computed by MODELLER[27].

*Model 1* and *Model 2* are the final models used for virtual screening.

b, *Z-DOPE* is a normalized atomic distance-dependent statistical potential based on known protein structures [28]. Per-residue Z-DOPE score of the initial model was also compared to that of the template structure (not shown).

c, *logAUC* is the area under the enrichment curve[30]. An enrichment curve is obtained by plotting the percentage of actual ligands found (y-axis) within the top ranked subset of all database compounds (x-axis on logarithmic scale).

The model of LAT1 interacting with phenylalanine indicates that the majority of the key polar interactions between LAT1 and the carboxyl and amino group of the amino acid ligands are conserved between LAT1 and the AdiC template structure (Figure 4.3a and Figure 4.1). For example, the backbone polar groups of LAT1 residues T62, I63, I64, S66, G67, F252, A253, and G255 are predicted to form polar interactions with phenylalanine (Figure 4.3). These residues correspond to A22, I23, M24, S26, G27, W202, S203, and I205 of AdiC that make similar interactions with the carboxyl and amino groups of its ligand arginine [17]. Because the carboxyl and amino groups are conserved among all other known LAT1 ligands, such as thyroxine and gabapentin (Figure 4.3b), we hypothesize that they make similar interactions with LAT1.

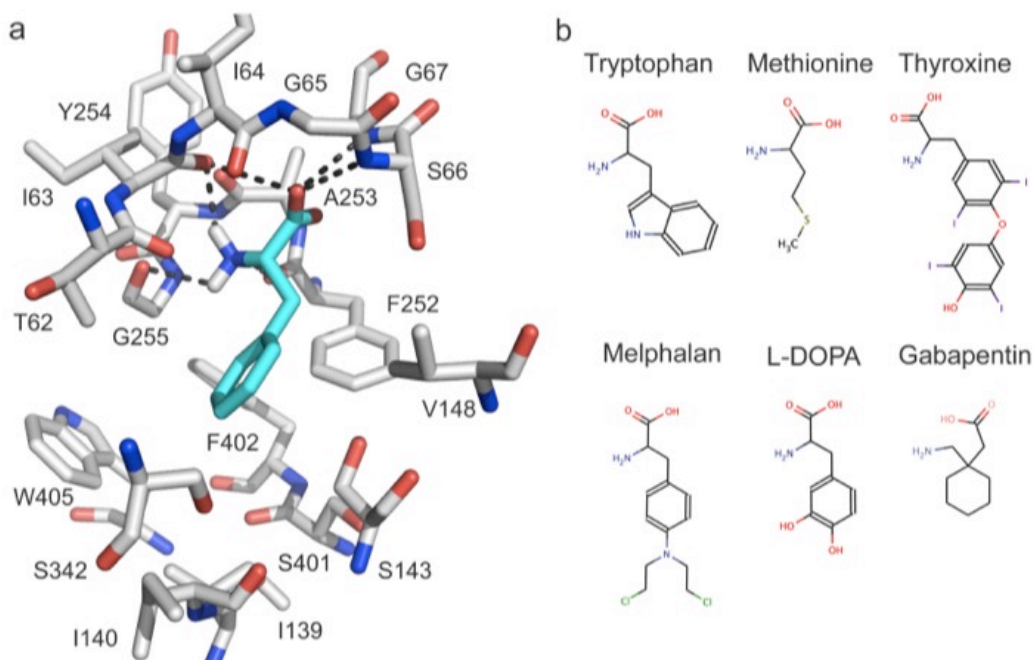


**Figure 4.3. Predicted LAT1 structure and ligand binding mode.** (a) Predicted structure of the LAT1 – phenylalanine complex. LAT1 (grey) and phenylalanine (cyan) are shown as stick models; oxygen, nitrogen, and hydrogen atoms are depicted in red, blue, and white, respectively; key hydrogen bonds between phenylalanine and LAT1 (involving residues Thr62, Ile63, Ile64, Ser66, Gly67, Phe252, Ala253, and Gly255) are shown as dotted grey lines. (b) Structures of representative LAT1 substrates. Known LAT1 substrates, including metabolites (Tryptophan, Methionine, and Thyroxine) and prescription drugs (Melphalan, L-DOPA, and Gabapentin) are shown using MarvinView 5.4.1.1 (<http://www.chemaxon.com/>).

Conversely, differences in the ligand preferences of LAT1 and AdiC may be explained by two major differences in the binding sites of the LAT1 model and the AdiC structure (Figure 4.4). First, several residues with hydrophobic side chains (i.e., I139, V148, F252, and F402, W405) are located in the LAT1 binding site, likely contributing to increased ligand binding affinity of hydrophobic amino acids to LAT1 *via* van der Waals interactions and the hydrophobic effect (e.g., the tryptophan indole ring). Some of these hydrophobic residues are replaced by non-hydrophobic residues in LAT1 homologs, including the template structure AdiC and other SLC7 members. For instance, the aromatic residue W405 in LAT1 corresponds to the polar T361 in AdiC. Second, several binding site residues in AdiC are replaced by residues with smaller side chains in LAT1, creating a larger volume in LAT1's binding site that can accommodate larger amino acids. For instance, M104, I205, and W293 in AdiC correspond to the smaller V148, G255, and S342 in LAT1 (Figure 4.3a and Figure 4.4).

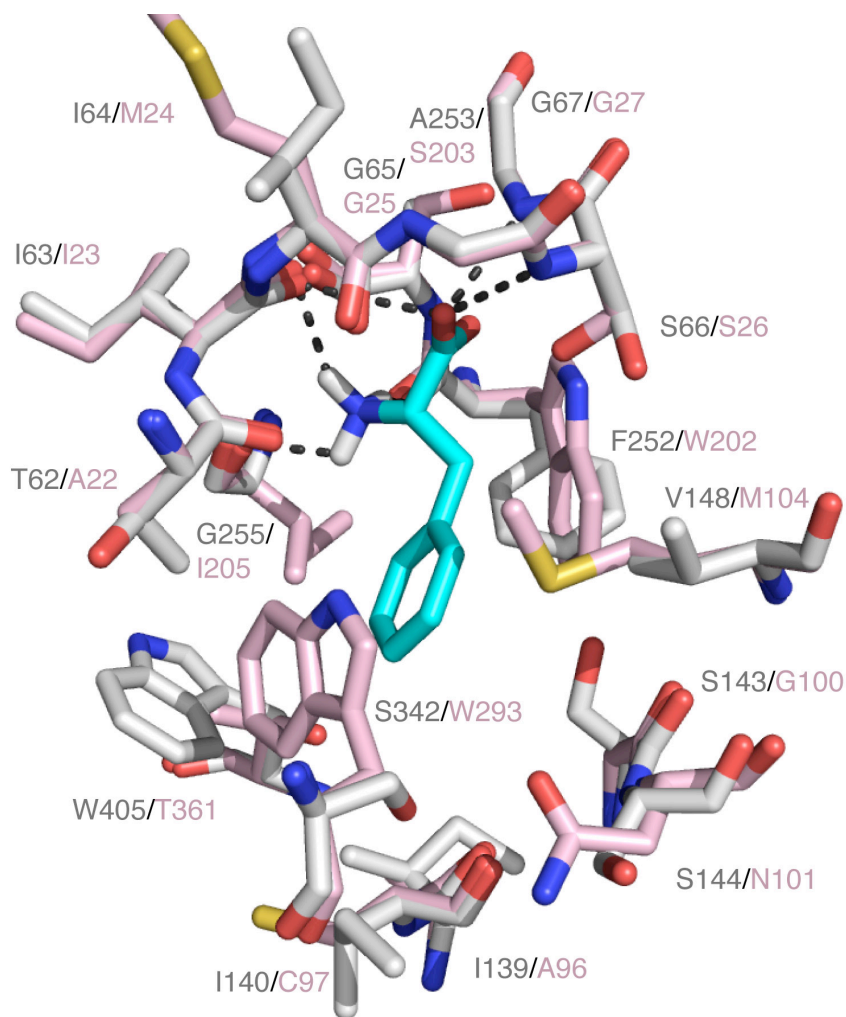


**Figure 4.4. Binding sites of LAT1 and AdiC.** LAT1 model (light grey) is superposed on the X-ray structure of AdiC (pink). All other protein atoms are illustrated by sticks; oxygen, nitrogen, and sulfur atoms are colored in red, purple, and yellow, respectively. Phenylalanine, a substrate of LAT1, is depicted in cyan sticks and its predicted hydrogen bonds with LAT1 (involving residues T62, I63, I64, S66, G67, F252, A253, and G255) are shown as dotted grey lines.

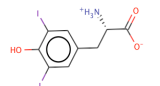
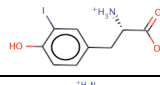
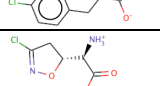
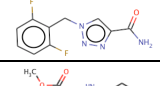
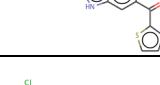
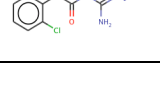
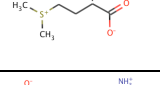
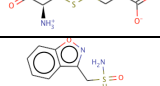
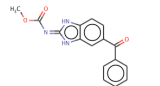
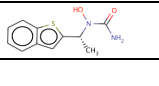
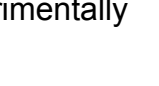



**Virtual screening of drugs and metabolites.** We computationally screened filtered libraries of 6,436 and 12,730 small molecules from the KEGG DRUG and KEGG LIGAND COMPOUND databases [35], respectively, against two LAT1 models (Figure 4.5). Some of the top-scoring hits were shown previously to be LAT1 ligands, increasing our confidence in the binding site model. For example, the known substrate L-Trp was ranked #50 in the docking screen of KEGG LIGAND COMPOUND. The 200 (3.1%) KEGG DRUG and 500 (3.9%) KEGG COMPOUND top-scoring hits against our top two models were analyzed manually. A compound was selected for experimental testing based on three criteria: (i) similarity between its docking pose and those of known ligands in complex with LAT1 [35]; (ii) the chemical novelty of its scaffold, especially if it occurred frequently among the top scoring compounds; and (iii) its pharmacological effect [35].

**Experimental validation of predicted ligands.** A LAT1 overexpressing cell line was generated by stably transfecting HEK cells with human LAT1 cDNA. HEK-LAT1 cells expressed 20-fold higher levels of LAT1 mRNA relative to HEK-EV cells, and demonstrated LAT1-specific uptake of the established system L substrates, gabapentin and L-leucine (Figure 4.6a-d). Twelve of the top-scoring molecules were selected for experimental testing by *cis*-inhibition assay (Table 4.3; Figure 4.5). Each molecule was tested as a LAT1 ligand by determining its ability to inhibit transport of a known LAT1 substrate, gabapentin in HEK-LAT1 cells at concentrations of 10  $\mu$ M and 100  $\mu$ M (Figure 4.7). The known LAT1 inhibitor, 2-aminobicyclo-(2, 2, 1)-heptane-2-carboxylic acid (BCH), was also included as a positive control. At 100  $\mu$ M, inhibition of intracellular gabapentin accumulation ranged from 88% (3,5-diiodo-L-tyrosine) to less than 10%

(cystine, mebendazole, and nocadezole), with the metabolites 3,5-diiodo-L-tyrosine and 3-iodo-L-tyrosine, as well as the tryptophan hydroxylase inhibitor fenclonine and the anticancer agent acivicin, demonstrating significant inhibition of gabapentin and L-leucine transport (Figure 4.6e and 4.7a). Acivicin also obtained a dissimilarity score of 0.74 using the JCDissimilarityCFTanimoto score, which calculates dissimilarities among molecules based on chemical fingerprints, indicating that it is a chemically novel LAT1 ligand (Table 4.3).

**Table 4.3. Small molecules tested in uptake kinetic assays.**

<b>Docking screen</b>			
<b>Name<sup>a</sup></b>	<b>Function<sup>b</sup></b>	<b>Dissimilarity<sup>c</sup></b>	<b>Sketch<sup>d</sup></b>
<b>3,5-L-Diiodotyrosine</b>	Tyrosine metabolism; thyroid hormone deficiency treatment; radioactive agent	0.26	
<b>3-Iodo-L-tyrosine</b>	Tyrosine metabolism; radioactive agent	0.23	
<b>Fenclonine</b>	Serotonin inhibitor	0.18	
<b>Acivicin</b>	Antineoplastic	0.74	
Rufinamide	Antiepileptic	0.79	
Nocodazole	Antineoplastic	0.74	
Guanfacine; Estulic	Antihypertensive; treatment of attention deficit hyperactivity disorder	0.70	
Cabagin U (Vitamin U)	Gastrointestinal agent	0.13	
Cystine	Anti-inflammatory	0.66	
Zonisamide	Anticonvulsant	0.83	
Mebendazole	Interferes with carbohydrate metabolism and inhibits polymerization of microtubules	0.69	
Zileuton	Anti-inflammatory	0.73	

a, *Name* is the generic or chemical name of the molecule; names of experimentally confirmed hits are marked in bold font.

b, *Function* specifies the pharmacological function of the drug or the physiological function of the metabolite, as applicable.

c, *Dissimilarity* is calculated relying on the Chemaxon fingerprints

(<http://www.chemaxon.com>). Dissimilarity values of > 0.7 suggest that the

molecule is chemically different from all known LAT-1 ligands.

d, *Sketch* provides the 2D sketch of the molecule.

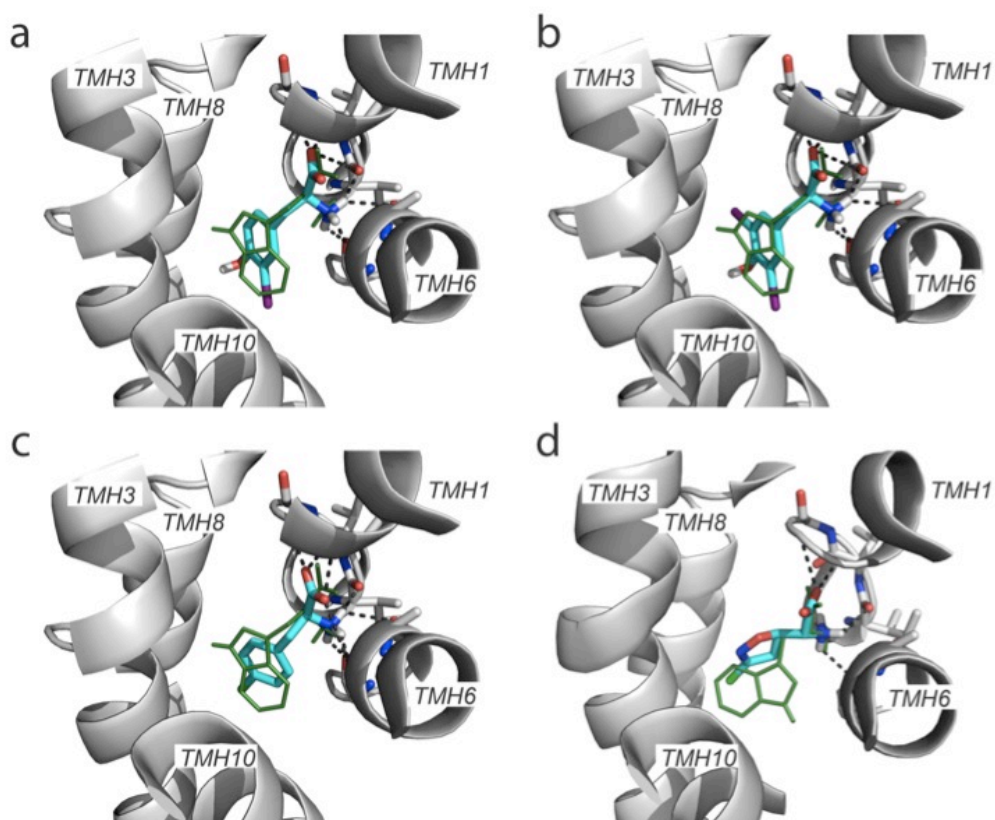


**Figure 4.5. Predicted binding modes for LAT1 ligands.** Predicted binding modes of the known substrate tryptophan (green lines) and four ligands discovered in the docking screen (a-d). Residues making polar interactions with the ligand are illustrated with sticks; carbon atoms are colored in white, nitrogen atoms in blue, and oxygen atoms in red; hydrogen bonds are represented by dotted grey lines. The predicted pose of a known LAT1 ligand, tryptophan, is shown with green lines. The compounds depicted are 3-iodo-L-tyrosine (a), 3,5-diiodo-L-tyrosine (b), fenclonine (c), and acivicin (d). Halogen atoms in the discovered ligands are colored in purple (iodine) and green (chlorine).

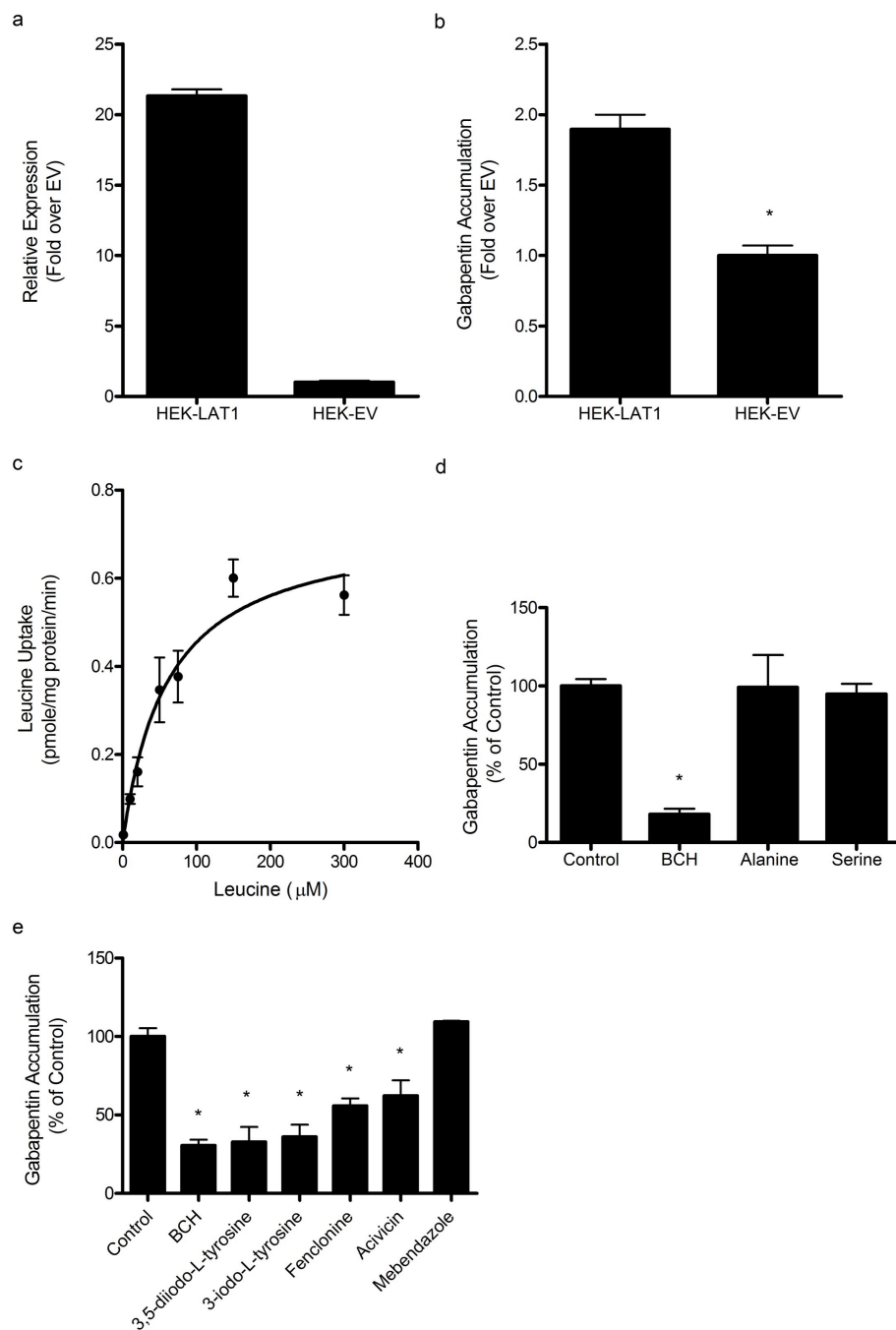


**Figure 4.6. Validation of LAT1 function in HEK-LAT1 cells.** (a) Overexpression of LAT1 in transfected HEK-LAT1 cells relative to EV cells. (b) Validation of LAT1 function in LAT1 transfected cells. Gabapentin (1 μM unlabeled and 10 nM radiolabeled) uptake in HEK-LAT1 cells was ~2-fold higher than in EV cells. (c) Kinetics of L-leucine uptake

in HEK-LAT1 cells. L-leucine uptake was measured at 1, 10, 20, 50, 75, 150, and 300  $\mu\text{M}$  and the curve was fit to the Michaelis-Menten equation to obtain a  $K_m$  value of  $60.6 \pm 13.1 \mu\text{M}$ . (d) Distinguishing LAT1 from LAT-2 uptake of gabapentin in HEK-LAT1 cells by *cis*-inhibition with L-alanine. Cells were co-incubated with gabapentin and either 1 mM BCH (LAT1 and LAT-2 inhibitor), L-alanine (LAT-2 inhibitor), or L-serine (negative control). BCH reduced intracellular gabapentin accumulation by ~83%, while L-alanine and L-serine were not able to inhibit intracellular gabapentin accumulation. (e) Predicted LAT1 ligands were validated by *cis*-inhibition of L-leucine uptake in HEK-LAT1 cells. Cells were co-incubated with L-leucine (1  $\mu\text{M}$  unlabeled and 10 nM radiolabeled) and predicted ligands at 100  $\mu\text{M}$  concentration. BCH is included as a positive control. Each point is the mean of 2-3 separate experiments; error bars represent SEM. Statistical analysis by one-way ANOVA and Dunnett's multiple comparison test in (d) and (e), and two-tailed unpaired t-test in (b); the \* symbol indicates  $P < 0.05$ .

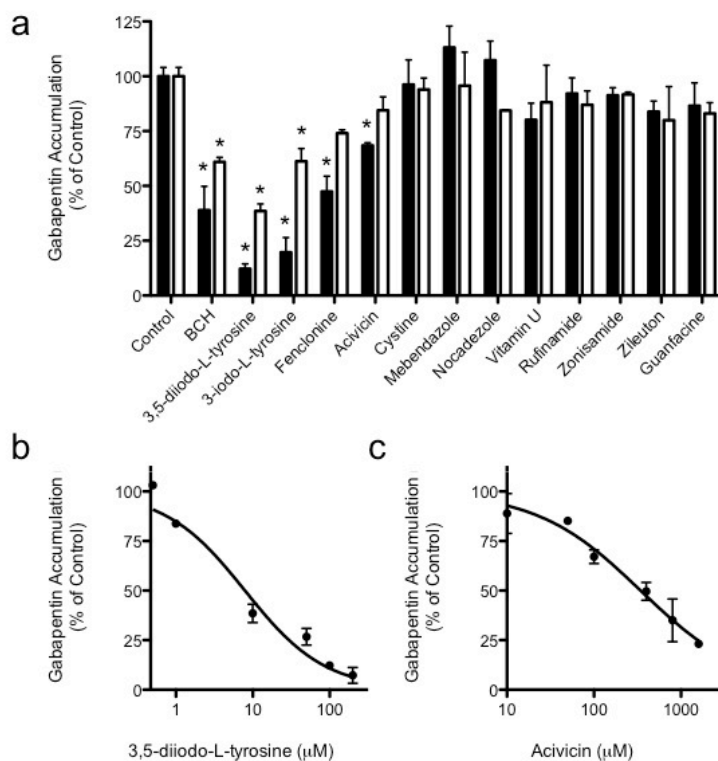


**Figure 4.7. Experimental validation of predicted LAT1 ligands.** Predicted LAT1 ligands were validated by *cis*-inhibition of gabapentin uptake and *trans*-stimulation from HEK-LAT1 cells (a-c). (a) Cells were co-incubated with twelve predicted ligands and a positive control (BCH) at either 100 μM (black columns) or 10 μM (white columns) concentrations and gabapentin (1 μM unlabeled and 10 nM radiolabeled). Each column depicts the mean of 2-4 separate experiments; error bars represent the SEM. (b) and (c) Dose-dependent inhibition of gabapentin (1 μM unlabeled with 10 nM radiolabeled) accumulation by 3,5-diiodo-L-tyrosine ( $IC_{50} = 7.9 \mu M$ ) and acivicin ( $IC_{50} = 340 \mu M$ ), respectively. Each point is the mean of 2-3 separate experiments; error bars represent the SEM. Statistical analysis in (a) by one-way ANOVA and Dunnett's multiple comparison test; the \* symbol indicates  $P < 0.05$ .



The potencies of selected active ligands were further established by determining the IC<sub>50</sub> values for inhibiting gabapentin accumulation in the HEK-LAT1 cells. IC<sub>50</sub> values ranged from 7.9  $\mu$ M (3,5-diiodo-L-tyrosine; Figure 4.7b) to 340  $\mu$ M (acivicin; Figure 4.7c). At 10  $\mu$ M, inhibition of gabapentin accumulation ranged from 61% (3,5-diiodo-L-tyrosine) to less than 10%, with 3,5-diiodo-L-tyrosine and 3-iodo-L-tyrosine significantly inhibiting gabapentin transport (Figure 4.7a). Interestingly, 3,5-diiodo-L-tyrosine is a stronger inhibitor than the positive control BCH. In summary, one-third (four out of twelve) of the top-scoring molecules selected for experimental testing are LAT1 ligands capable of inhibiting gabapentin transport in HEK-LAT1 cells.

**Identification of LAT1 substrates.** The four molecules found to significantly inhibit gabapentin accumulation in the HEK-LAT1 cells were further analyzed as putative substrates by *trans*-stimulation assay. This assay takes advantage of LAT1's obligatory exchange mechanism of transport by exchanging intracellular L-Leucine from pre-loaded HEK-LAT1 cells with an extracellular molecule only if it is a LAT1 substrate. Three known LAT1 substrates served as positive controls and were able to induce L-leucine efflux from the HEK-LAT1 cells, including L-leucine (43%), gabapentin (36%), and BCH (30%) (Figure 4.8a). In contrast, glycine was used as a negative control because it is known not to be a LAT1 substrate, and did not induce any L-leucine efflux. Two of the four inhibitors confirmed in our *cis*-inhibition assay also induced L-leucine efflux. Acivicin and fenclonine induced L-leucine efflux by 27% and 29%, respectively, indicating that they are transported by LAT1. These results indicate that the drug-like molecules acivicin and fenclonine, which both have pharmacodynamic effects in the CNS, are likely LAT1 substrates. Surprisingly, both of the more potent LAT1 inhibitors,

the metabolites 3,5-diiodo-L-tyrosine and 3-iodo-L-tyrosine were only able to induce 7.9% and 5.4% L-leucine efflux, respectively, suggesting that they are inhibitors that only bind to, but are not transported by LAT1. Finally, guanfacine and rufinamide were also studied, and both did not induce significant L-leucine efflux.

***Inhibition of LAT1-dependent cell proliferation.*** LAT1 is highly expressed in various cancer cells, providing them with nutrients and signaling molecules for growth. Thus, a drug targeting LAT1 in cancer can be an inhibitor that deprives the cancer cells from nutrients or a cytotoxic substrate with an intracellular target. We therefore investigated the anti-proliferative effects of select validated LAT1 ligands including the LAT1 substrate acivicin and the inhibitor 3-iodo-L-tyrosine, by cell proliferation assay in the high LAT1 expressing GBM cell line, T98G [8]. The LAT1 specific effects of each ligand on cell growth were determined in control cells (T98G-EV) and cells with LAT1 expression (Figure 4.9a) and function (Figure 4.9b) knocked down (T98G-KD). The anticancer drug acivicin was a more potent growth inhibitor of T98G-EV (75% growth reduction) than T98G-KD (51% growth reduction) (Figure 4.8b). Similarly, 3-iodo-L-tyrosine had a more potent effect on T98G-EV cells, reducing their growth by 27% while having no effect on T98G-KD (Figure 4.8b, right). These results suggest that both 3-iodo-L-tyrosine and acivicin are capable of inhibiting cancer cell proliferation in a LAT1 dependent manner *via* two alternative mechanisms, including nutrient deprivation and cytotoxicity, respectively.

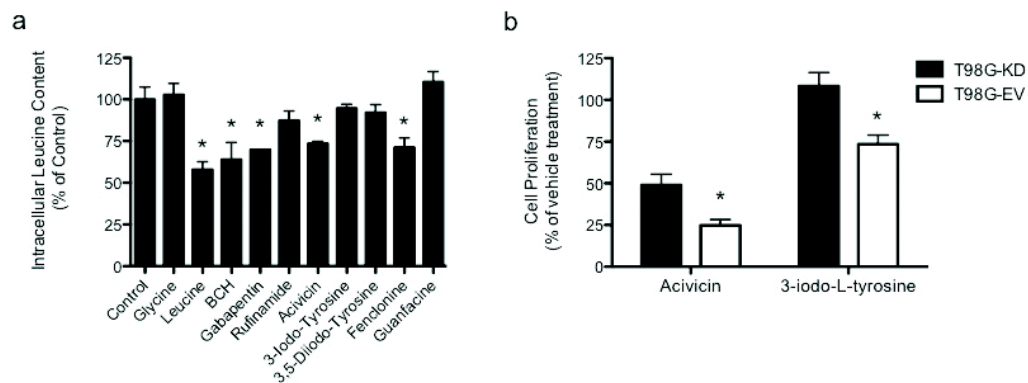


**Figure 4.8. Substrate determination and cytotoxicity characterization of predicted ligands.** Predicted LAT1 ligands validated in *cis*-inhibition assays were subjected to substrate determination by trans-stimulation of L-leucine efflux (1  $\mu$ M unlabeled and 10 nM radiolabeled). (a) Cells were pre-loaded with L-leucine. Efflux was induced by subsequent addition of each test compound at a concentration of 1 mM. Gabapentin, L-leucine, and BCH were included as positive controls, while glycine and guanfacine were included as negative controls. (b) The cytotoxic effects of acivicin (100  $\mu$ M) and 3-iodo-L-tyrosine (1 mM) against T98G glioblastoma cells stably expressing an shRNA against LAT1 (T98G-KD; black columns) or EV (T98G-EV; white columns) are depicted. Cell proliferation for both cell lines and treatment conditions are normalized to cell density at treatment day 0, and then to the vehicle control treatment at 48 hours. In both panels, each column represents the mean of 3-4 separate experiments, and error bars represent the SEM. Statistical analysis in (a) by one-way ANOVA and Dunnett's multiple comparison test, and (b) by two-way ANOVA and Bonferroni correction for multiple testing; the \* symbol indicates  $P < 0.05$ .

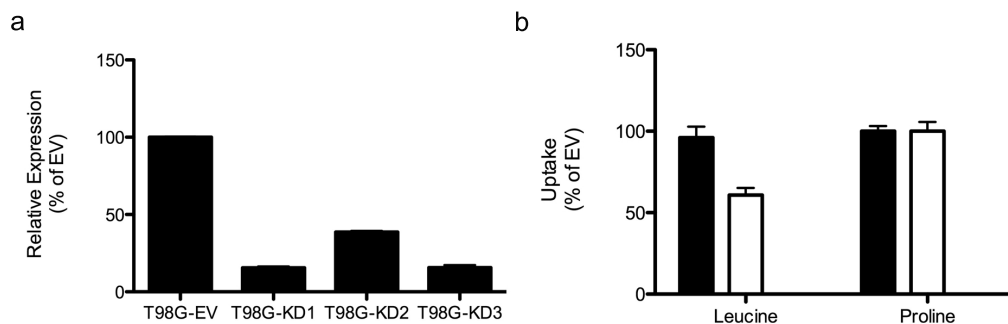


**Figure 4.9. Validation of LAT1 knock-down in T98G glioblastoma cells.** (a)

Reduced LAT1 mRNA in T98G cells expressing 3 different anti-LAT1 shRNA's. T98G-KD1 and T98G-KD3 both showed ~85% reduction in LAT1 mRNA. (b) Functional validation of LAT1 knockdown was determined by measuring cellular L-leucine and L-proline (1  $\mu$ M unlabeled and 10 nM radiolabeled) accumulation in T98G-KD1 (T98G-KD in main text; white columns) and T98G-EV (black columns) cells under the conditions described in Materials and Methods (uptake incubation time was 1 min). T98G-KD cells accumulated ~40% less L-leucine, a prototypical LAT1 substrate, than T98G-EV cells, while both cell lines accumulated similar amounts of the non-LAT1 substrate L-proline.

## Discussion

Three key findings emerge from our study. First, two drug-like molecules that interact with different proteins in the CNS are also substrates of LAT1. This finding may explain the mechanism by which these drugs penetrate the BBB to reach their targets in the CNS. It also provides a starting point for optimizing the two drugs for better BBB permeability. Second, two of the discovered LAT1 ligands, including one inhibitor and one substrate, inhibit proliferation of cancer cells. This result indicates that LAT1 can be targeted for cancer therapy *via* different mechanisms and reveals novel chemical tools for further characterizing the role of LAT1 in cancer. Third, the identified LAT1 ligands achieve their pharmacological effect (positive or negative) on the CNS or cancer by interacting with multiple targets. This finding suggests that effective therapy can be obtained by applying modeling and docking approaches to whole “systems”, including pathways and networks. We take each of the three key findings in turn.

***LAT1-mediated BBB drug permeability.*** Passive diffusion has long been thought of as the primary mechanism by which most drugs cross the BBB to permeate the CNS [56]. The contribution of carrier-mediated transport to this process is assumed to be minimal, even though different classes of membrane transporters have been shown to restrict and/or facilitate access of drugs, nutrients, and toxins to the CNS [57-59]. LAT1 is one such influx transporter known to transport nutrients and xenobiotics across the BBB. In this study, we identified two novel LAT1 substrates, including acivicin and fenclonine, which may also cross the BBB *via* LAT1-mediated transport. Both were found to be likely LAT1 substrates in *trans*-stimulation studies (Figure 4.7), and both are known to have pharmacodynamic effects in the CNS. Even though

previous studies have used *trans*-stimulation to establish whether or not a specific transporter can transport different compounds [60-62], this assay provides indirect evidence that a compound may be a substrate for a specific transporter. Nevertheless, acivicin was assessed in a clinical trial for treating various solid tumors that did not involve the CNS, but failed due to CNS-related toxic side effects (e.g., lethargy and confusion) [63]. Furthermore, these side effects were reversed when acivicin was concomitantly administered with a mixture of amino acids including the prototypical LAT1 substrate, L-leucine. These observations highly implicate LAT1 in mediating acivicin's CNS permeability in humans. The second molecule, fenclonine, is an irreversible tryptophan hydroxylase inhibitor used to deplete CNS serotonin levels in animal models of human disease [64]. Taken together with our results, LAT1 likely mediates the effects in the CNS by transporting fenclonine across the BBB. Therefore, influx transporters such as LAT1 may be important mediators of drug efficacy and toxicity in the CNS, and have a greater contribution to drug penetration across the BBB than previously thought.

***Targeting LAT1 for cancer therapy.*** Changes in cell metabolism are strongly associated with cancer. Membrane transporters have been shown to play a key role in such reprogrammed metabolic networks by providing nutrients to transforming cells. For example, the glucose transporter (GLUT1, *SLC2A1*) is upregulated in various cancers to provide glucose as a carbon source to accommodate an increased rate of anabolic cellular reactions and to maintain a microecosystem favorable for cancer cells [65]. Moreover, LAT1 imports essential amino acids that serve as nutrients and pro-proliferative signaling molecules by exporting glutamine brought into cancer cells *via* the

glutamine transporter, ASCT2 [10]. Thus, therapeutics targeting LAT1 can be (i) an inhibitor that selectively blocks transport by LAT1 and / or ASCT2, depriving the cancer cell of nutrients required for proliferation, or (ii) a cytotoxic substrate that is delivered into the cell *via* LAT1 and / or ASCT2 to act on an intracellular target. LAT1 ligands that act *via* each of these mechanisms were discovered in our screen (Figures 4.5, 4.7, and 4.9; Table 4.3).

First, 3-iodo-L-tyrosine is a thyroid hormone derivative typically used to treat hormone deficiencies and as a radioactive agent. Here, *cis*-inhibition and cell proliferation experiments identified 3-iodo-L-tyrosine as a potent LAT1 inhibitor (Figure 4.7a) that reduces proliferation of T98G glioblastoma cells (Figure 4.9b), possibly by starving these cells of nutrients supplied by LAT1. Our results suggest that aside from its putative anticancer applications, 3-iodo-L-tyrosine may also be useful as a diagnostic imaging agent to identify tumors and other disease states associated with LAT1 upregulation [66].

Second, acivicin is a cytotoxic agent with antitumor activity that targets glutamine-dependent amidotransferases in the biosynthesis of purines and pyrimidines [67]. *Trans*-stimulation and cell proliferation experiments indicate that acivicin is likely a LAT1 substrate (Figure 4.7), suggesting that LAT1 can be targeted for acivicin delivery into tumor cells. Interestingly, acivicin failed in various clinical trials (e.g., for advanced solid malignancies) due to CNS-related toxic side effects [63] or insufficient efficacy [68]. Thus, targeting LAT1 in a tumor with a drug that is a LAT1 substrate may not be a rational therapeutic strategy since LAT1 would also facilitate entry of the drug into the

CNS. However, design of other cytotoxic substrates of LAT1, which are not associated with deleterious CNS effects, may represent a viable drug development strategy for cancer. Although cell proliferation experiments indicate that multiple transporters may mediate acivicin accumulation in cells, the significant difference in sensitivity to acivicin between T98G-KD and –EV cells clearly indicates a LAT1-specific effect on cell proliferation, most likely by mediating acivicin uptake.

***Targeting biological ‘systems’ using a combined structural pharmacology approach.*** While polypharmacology can be exploited to improve the treatment of various nervous system disorders and cancers, it may also lead to toxicity. Virtual screening against the LAT1 model identifies ligands that likely achieve their pharmacological effect by interacting with multiple proteins. Current efforts to design reagents, including drugs or chemical tools, for treating complex diseases include optimizing binding affinities of one or more molecules against more than one target. Recent advances in comparative modeling and molecular docking for ligand discovery, coupled with the determination of a number of membrane protein structures, including transporters, enables us to target multiple components of a single pathway (e.g., mTOR) or organ (e.g., the BBB) using structure-based ligand discovery. Importantly, some of these newly determined structures represent different protein conformations, allowing *in silico* screens of small molecules against comparative models of different conformations to suggest chemically distinct ligands. For example, a structure-based approach predicted that molecules binding to a model for the outward-facing conformation of the GABA transporter 2 (GAT-2) were chemically distinct from those predicted to bind an occluded model [69]. Thus, as more structures of LAT1 homologs



are discovered, our results can be refined to identify novel LAT1 ligands for effective therapy and the study of CNS diseases and cancer.

In summary, we constructed structural models for LAT1 based on atomic structures of distantly related prokaryotic homologs. Two small organic molecule libraries containing endogenous metabolites and prescription drugs were then virtually screened against these models. Select top-ranked docking hits were tested experimentally, and four novel LAT1 ligands were identified: 3,5-diiodo-L-tyrosine, 3-iodo-L-tyrosine, fenclonine, and acivicin. Furthermore, acivicin and 3-iodo-L-tyrosine were found to have LAT1-mediated antiproliferative effects in a GBM cancer cell line. These findings provide new chemical tools to elucidate the role of membrane transporters as potential drug targets and in mediating tissue permeability to small organic molecules. Future studies should further elucidate the mechanism by which these novel ligands interact with LAT1.

## References

1. Kanai Y, *et al.* (1998) Expression cloning and characterization of a transporter for large neutral amino acids activated by the heavy chain of 4F2 antigen (CD98).. *The Journal of biological chemistry* 273(37):23629-23632.
2. Roberts LM, *et al.* (2008) Subcellular localization of transporters along the rat blood-brain barrier and blood-cerebral-spinal fluid barrier by in vivo biotinylation.. *Neuroscience* 155(2):423-438.
3. Alexander GM, Schwartzman RJ, Grothusen JR, & Gordon SW (1994) Effect of plasma levels of large neutral amino acids and degree of parkinsonism on the

- blood-to-brain transport of levodopa in naive and MPTP parkinsonian monkeys.. *Neurology* 44(8):1491-1499.
4. Wang Y & Welty DF (1996) The simultaneous estimation of the influx and efflux blood-brain barrier permeabilities of gabapentin using a microdialysis-pharmacokinetic approach.. *Pharm Res* 13(3):398-403.
  5. Killian DM, Hermeling S, & Chikhale PJ (2007) Targeting the cerebrovascular large neutral amino acid transporter (LAT1) isoform using a novel disulfide-based brain drug delivery system.. *Drug Deliv* 14(1):25-31.
  6. Gynther M, *et al.* (2010) Brain uptake of ketoprofen-lysine prodrug in rats.. *Int J Pharm* 399(1-2):121-128.
  7. Kaira K, *et al.* (2008) Prognostic significance of L-type amino acid transporter 1 expression in resectable stage I-III nonsmall cell lung cancer.. *Br J Cancer* 98(4):742-748.
  8. Kobayashi K, *et al.* (2008) Enhanced tumor growth elicited by L-type amino acid transporter 1 in human malignant glioma cells.. *Neurosurgery* 62(2):493-503; discussion 503-494.
  9. Kaira K, *et al.* (2008) L-type amino acid transporter 1 and CD98 expression in primary and metastatic sites of human neoplasms.. *Cancer Sci* 99(12):2380-2386.
  10. Nicklin P, *et al.* (2009) Bidirectional transport of amino acids regulates mTOR and autophagy.. *Cell* 136(3):521-534.
  11. Oda K, *et al.* (2010) L-type amino acid transporter 1 inhibitors inhibit tumor cell growth.. *Cancer Sci* 101(1):173-179.

12. Ohkawa M, *et al.* (2011) Oncogenicity of L-type amino-acid transporter 1 (LAT1) revealed by targeted gene disruption in chicken DT40 cells: LAT1 is a promising molecular target for human cancer therapy.. *Biochem Biophys Res Commun* 406(4):649-655.
13. Shennan DB & Thomson J (2008) Inhibition of system L (LAT1/CD98hc) reduces the growth of cultured human breast cancer cells.. *Oncol Rep* 20(4):885-889.
14. Verrey F, *et al.* (2004) CATs and HATs: the SLC7 family of amino acid transporters.. *Pflugers Arch* 447(5):532-542.
15. Gao X, *et al.* (2009) Structure and mechanism of an amino acid antiporter. *Science* 324(5934):1565-1568.
16. Shaffer PL, Goehring A, Shankaranarayanan A, & Gouaux E (2009) Structure and mechanism of a na<sup>+</sup>-independent amino Acid transporter. *Science* 325(5943):1010-1014.
17. Gao X, *et al.* (2010) Mechanism of substrate recognition and transport by an amino acid antiporter.. *Nature* 463(7282):828-832.
18. Kowalczyk L, *et al.* (2011) Molecular basis of substrate-induced permeation by an amino acid antiporter.. *Proc Natl Acad Sci U S A* 108(10):3935-3940.
19. Schlessinger A, *et al.* (2010) Comparison of human solute carriers. *Protein science : a publication of the Protein Society* 19(3):412-428.
20. Fang Y, *et al.* (2009) Structure of a prokaryotic virtual proton pump at 3.2 Å resolution. *Nature* 460(7258):1040-1043.

21. Yamashita A, Singh SK, Kawate T, Jin Y, & Gouaux E (2005) Crystal structure of a bacterial homologue of Na<sup>+</sup>/Cl<sup>-</sup>-dependent neurotransmitter transporters. *Nature* 437(7056):215-223.
22. Forrest LR, Kramer R, & Ziegler C (2011) The structural basis of secondary active transport mechanisms.. *Biochimica et biophysica acta* 1807(2):167-188.
23. Shi L & Weinstein H (2010) Conformational rearrangements to the intracellular open states of the LeuT and ApcT transporters are modulated by common mechanisms.. *Biophys J* 99(12):L103-105.
24. Jardetzky O (1966) Simple allosteric model for membrane pumps. *Nature* 211(5052):969-970.
25. Guan L & Kaback HR (2006) Lessons from lactose permease. *Annu Rev Biophys Biomol Struct* 35:67-91.
26. Shen MY & Sali A (2006) Statistical potential for assessment and prediction of protein structures. *Protein Sci* 15(11):2507-2524.
27. Eramian D, Eswar N, Shen MY, & Sali A (2008) How well can the accuracy of comparative protein structure models be predicted? *Protein Sci* 17(11):1881-1893.
28. Schlessinger A, *et al.* (2011) Structure-based discovery of prescription drugs that interact with the norepinephrine transporter, NET.. *Proc Natl Acad Sci U S A* 108(38):15810-15815.
29. Huang N, Shoichet BK, & Irwin JJ (2006) Benchmarking sets for molecular docking. *J Med Chem* 49(23):6789-6801.

30. Fan H, *et al.* (2009) Molecular docking screens using comparative models of proteins. *J Chem Inf Model* 49(11):2512-2527.
31. Mensch J, Oyarzabal J, Mackie C, & Augustijns P (2009) In vivo, in vitro and in silico methods for small molecule transfer across the BBB.. *J Pharm Sci* 98(12):4429-4468.
32. Smith BJ, *et al.* (2001) P-glycoprotein efflux at the blood-brain barrier mediates differences in brain disposition and pharmacodynamics between two structurally related neurokinin-1 receptor antagonists.. *The Journal of pharmacology and experimental therapeutics* 298(3):1252-1259.
33. Park S & Sinko PJ (2005) The blood-brain barrier sodium-dependent multivitamin transporter: a molecular functional in vitro-in situ correlation.. *Drug Metab Dispos* 33(10):1547-1554.
34. Abbott NJ, Patabendige AA, Dolman DE, Yusof SR, & Begley DJ (2010) Structure and function of the blood-brain barrier.. *Neurobiol Dis* 37(1):13-25.
35. Yamamoto A, Akanuma S, Tachikawa M, & Hosoya K (2010) Involvement of LAT1 and LAT2 in the high- and low-affinity transport of L-leucine in human retinal pigment epithelial cells (ARPE-19 cells).. *J Pharm Sci* 99(5):2475-2482.
36. Zhang L, Schaner ME, & Giacomini KM (1998) Functional characterization of an organic cation transporter (hOCT1) in a transiently transfected human cell line (HeLa).. *The Journal of pharmacology and experimental therapeutics* 286(1):354-361.

37. Meier C, Ristic Z, Klauser S, & Verrey F (2002) Activation of system L heterodimeric amino acid exchangers by intracellular substrates.. *Embo J* 21(4):580-589.
38. Hidalgo M, *et al.* (1998) A Phase I and pharmacological study of the glutamine antagonist acivicin with the amino acid solution aminosyn in patients with advanced solid malignancies.. *Clin Cancer Res* 4(11):2763-2770.
39. Delaville C, Navailles S, & Benazzouz A (2012) Effects of noradrenaline and serotonin depletions on the neuronal activity of globus pallidus and substantia nigra pars reticulata in experimental parkinsonism.. *Neuroscience* 202:424-433.
40. Kroemer G & Pouyssegur J (2008) Tumor cell metabolism: cancer's Achilles' heel.. *Cancer Cell* 13(6):472-482.
41. Lahoutte T, *et al.* (2003) Comparative biodistribution of iodinated amino acids in rats: selection of the optimal analog for oncologic imaging outside the brain.. *J Nucl Med* 44(9):1489-1494.
42. O'Dwyer PJ, Alonso MT, & Leyland-Jones B (1984) Acivicin: a new glutamine antagonist in clinical trials.. *J Clin Oncol* 2(9):1064-1071.
43. Bonomi P, Finkelstein D, & Chang A (1994) Phase II trial of acivicin versus etoposide-cisplatin in non-small cell lung cancer. An Eastern Cooperative Oncology Group study.. *Am J Clin Oncol* 17(3):215-217.
44. Schlessinger A, *et al.* (2012) High selectivity of the gamma-Aminobutyric acid (GABA) transporter 2 (GAT-2, SLC6A13) revealed by structure-based approach.. *The Journal of biological chemistry* .

45. Pei J, Kim BH, & Grishin NV (2008) PROMALS3D: a tool for multiple protein sequence and structure alignments.. *Nucleic acids research* 36(7):2295-2300.
46. Sali A & Blundell TL (1993) Comparative protein modelling by satisfaction of spatial restraints. *J Mol Biol* 234(3):779-815.
47. Krivov GG, Shapovalov MV, & Dunbrack RL, Jr. (2009) Improved prediction of protein side-chain conformations with SCWRL4. *Proteins*.
48. Carlsson J, *et al.* (2011) Ligand discovery from a dopamine D3 receptor homology model and crystal structure.. *Nature chemical biology* 7(11):769-778.
49. Kyte J & Doolittle RF (1982) A simple method for displaying the hydropathic character of a protein.. *Journal of molecular biology* 157(1):105-132.
50. Ashkenazy H, Erez E, Martz E, Pupko T, & Ben-Tal N (2010) ConSurf 2010: calculating evolutionary conservation in sequence and structure of proteins and nucleic acids.. *Nucleic acids research* 38(Web Server issue):W529-533.
51. Mysinger MM & Shoichet BK (2010) Rapid context-dependent ligand desolvation in molecular docking. *Journal of chemical information and modeling* 50(9):1561-1573.
52. Overington J (2009) ChEMBL. An interview with John Overington, team leader, chemogenomics at the European Bioinformatics Institute Outstation of the European Molecular Biology Laboratory (EMBL-EBI). Interview by Wendy A. Warr. *J Comput Aided Mol Des* 23(4):195-198.
53. Anonymous (2010) The Universal Protein Resource (UniProt) in 2010.. *Nucleic acids research* 38(Database issue):D142-148.
54. Wang X & McManus M (2009) Lentivirus production.. *J Vis Exp* (32).

55. Chen Y, Zhang S, Sorani M, & Giacomini KM (2007) Transport of paraquat by human organic cation transporters and multidrug and toxic compound extrusion family. *J Pharmacol Exp Ther* 322(2):695-700.
1. Kanai Y, Segawa H, Miyamoto K, Uchino H, Takeda E, Endou H. Expression cloning and characterization of a transporter for large neutral amino acids activated by the heavy chain of 4F2 antigen (CD98). *The Journal of biological chemistry*. 1998;273(37):23629-32.
2. Roberts LM, Black DS, Raman C, Woodford K, Zhou M, Haggerty JE, et al. Subcellular localization of transporters along the rat blood-brain barrier and blood-cerebral-spinal fluid barrier by in vivo biotinylation. *Neuroscience*. 2008;155(2):423-38.
3. Alexander GM, Schwartzman RJ, Grothusen JR, Gordon SW. Effect of plasma levels of large neutral amino acids and degree of parkinsonism on the blood-to-brain transport of levodopa in naive and MPTP parkinsonian monkeys. *Neurology*. 1994;44(8):1491-9.
4. Wang Y, Welty DF. The simultaneous estimation of the influx and efflux blood-brain barrier permeabilities of gabapentin using a microdialysis-pharmacokinetic approach. *Pharmaceutical research*. 1996;13(3):398-403.
5. Killian DM, Hermeling S, Chikhale PJ. Targeting the cerebrovascular large neutral amino acid transporter (LAT1) isoform using a novel disulfide-based brain drug delivery system. *Drug delivery*. 2007;14(1):25-31.
6. Gynther M, Jalkanen A, Lehtonen M, Forsberg M, Laine K, Ropponen J, et al. Brain uptake of ketoprofen-lysine prodrug in rats. *International journal of pharmaceutics*. 2010;399(1-2):121-8.



7. Kaira K, Oriuchi N, Imai H, Shimizu K, Yanagitani N, Sunaga N, et al. Prognostic significance of L-type amino acid transporter 1 expression in resectable stage I-III nonsmall cell lung cancer. *British journal of cancer*. 2008;98(4):742-8. PMID: 2259171.
8. Kobayashi K, Ohnishi A, Promsuk J, Shimizu S, Kanai Y, Shiokawa Y, et al. Enhanced tumor growth elicited by L-type amino acid transporter 1 in human malignant glioma cells. *Neurosurgery*. 2008;62(2):493-503; discussion -4.
9. Kaira K, Oriuchi N, Imai H, Shimizu K, Yanagitani N, Sunaga N, et al. L-type amino acid transporter 1 and CD98 expression in primary and metastatic sites of human neoplasms. *Cancer science*. 2008;99(12):2380-6.
10. Nicklin P, Bergman P, Zhang B, Triantafellow E, Wang H, Nyfeler B, et al. Bidirectional transport of amino acids regulates mTOR and autophagy. *Cell*. 2009;136(3):521-34.
11. Oda K, Hosoda N, Endo H, Saito K, Tsujihara K, Yamamura M, et al. L-type amino acid transporter 1 inhibitors inhibit tumor cell growth. *Cancer science*. 2010;101(1):173-9.
12. Ohkawa M, Ohno Y, Masuko K, Takeuchi A, Suda K, Kubo A, et al. Oncogenicity of L-type amino-acid transporter 1 (LAT1) revealed by targeted gene disruption in chicken DT40 cells: LAT1 is a promising molecular target for human cancer therapy. *Biochemical and biophysical research communications*. 2011;406(4):649-55.
13. Shennan DB, Thomson J. Inhibition of system L (LAT1/CD98hc) reduces the growth of cultured human breast cancer cells. *Oncology reports*. 2008;20(4):885-9.

14. Verrey F, Closs EI, Wagner CA, Palacin M, Endou H, Kanai Y. CATs and HATs: the SLC7 family of amino acid transporters. *Pflügers Archiv : European journal of physiology*. 2004;447(5):532-42.
15. Gao X, Lu F, Zhou L, Dang S, Sun L, Li X, et al. Structure and mechanism of an amino acid antiporter. *Science*. 2009;324(5934):1565-8.
16. Shaffer PL, Goehring A, Shankaranarayanan A, Gouaux E. Structure and mechanism of a  $\text{Na}^+$ -independent amino Acid transporter. *Science*. 2009;325(5943):1010-4.
17. Gao X, Zhou L, Jiao X, Lu F, Yan C, Zeng X, et al. Mechanism of substrate recognition and transport by an amino acid antiporter. *Nature*. 2010;463(7282):828-32.
18. Kowalczyk L, Ratera M, Paladino A, Bartoccioni P, Errasti-Murugarren E, Valencia E, et al. Molecular basis of substrate-induced permeation by an amino acid antiporter. *Proceedings of the National Academy of Sciences of the United States of America*. 2011;108(10):3935-40. PMID: 3054010.
19. Schlessinger A, Matsson P, Shima JE, Pieper U, Yee SW, Kelly L, et al. Comparison of human solute carriers. *Protein science : a publication of the Protein Society*. 2010;19(3):412-28. PMID: 2866268.
20. Fang Y, Jayaram H, Shane T, Kolmakova-Partensky L, Wu F, Williams C, et al. Structure of a prokaryotic virtual proton pump at 3.2 Å resolution. *Nature*. 2009;460(7258):1040-3.
21. Yamashita A, Singh SK, Kawate T, Jin Y, Gouaux E. Crystal structure of a bacterial homologue of  $\text{Na}^+/\text{Cl}^-$ -dependent neurotransmitter transporters. *Nature*. 2005;437(7056):215-23.

22. Forrest LR, Kramer R, Ziegler C. The structural basis of secondary active transport mechanisms. *Biochimica et biophysica acta*. 2011;1807(2):167-88.
23. Shi L, Weinstein H. Conformational rearrangements to the intracellular open states of the LeuT and ApcT transporters are modulated by common mechanisms. *Biophysical journal*. 2010;99(12):L103-5. PMID: 3000488.
24. Jardetzky O. Simple allosteric model for membrane pumps. *Nature*. 1966;211(5052):969-70.
25. Guan L, Kaback HR. Lessons from lactose permease. *Annu Rev Biophys Biomol Struct*. 2006;35:67-91.
26. Soding J, Biegert A, Lupas AN. The HHpred interactive server for protein homology detection and structure prediction. *Nucleic acids research*. 2005;33(Web Server issue):W244-8. PMID: 1160169.
27. Zhang Y. I-TASSER server for protein 3D structure prediction. *BMC bioinformatics*. 2008;9:40. PMID: 2245901.
28. Pieper U, Webb BM, Barkan DT, Schneidman-Duhovny D, Schlessinger A, Braberg H, et al. ModBase, a database of annotated comparative protein structure models, and associated resources. *Nucleic acids research*. 2011;39(Database issue):D465-74. PMID: 3013688.
29. Saier MH, Jr., Yen MR, Noto K, Tamang DG, Elkan C. The Transporter Classification Database: recent advances. *Nucleic Acids Res*. 2009;37(Database issue):D274-8.
30. Lomize MA, Lomize AL, Pogozheva ID, Mosberg HI. OPM: orientations of proteins in membranes database. *Bioinformatics*. 2006;22(5):623-5.

31. Pei J, Kim BH, Grishin NV. PROMALS3D: a tool for multiple protein sequence and structure alignments. *Nucleic acids research*. 2008;36(7):2295-300. PMCID: 2367709.
32. Sali A, Blundell TL. Comparative protein modelling by satisfaction of spatial restraints. *J Mol Biol*. 1993;234(3):779-815.
33. Shen MY, Sali A. Statistical potential for assessment and prediction of protein structures. *Protein Sci*. 2006;15(11):2507-24.
34. Krivov GG, Shapovalov MV, Dunbrack RL, Jr. Improved prediction of protein side-chain conformations with SCWRL4. *Proteins*. 2009.
35. Schlessinger A, Geier E, Fan H, Irwin JJ, Shoichet BK, Giacomini KM, et al. Structure-based discovery of prescription drugs that interact with the norepinephrine transporter, NET. *Proceedings of the National Academy of Sciences of the United States of America*. 2011;108(38):15810-5. PMCID: 3179104.
36. Carlsson J, Coleman RG, Setola V, Irwin JJ, Fan H, Schlessinger A, et al. Ligand discovery from a dopamine D3 receptor homology model and crystal structure. *Nature chemical biology*. 2011;7(11):769-78. PMCID: 3197762.
37. Huang N, Shoichet BK, Irwin JJ. Benchmarking sets for molecular docking. *J Med Chem*. 2006;49(23):6789-801.
38. Kyte J, Doolittle RF. A simple method for displaying the hydropathic character of a protein. *Journal of molecular biology*. 1982;157(1):105-32.
39. Ashkenazy H, Erez E, Martz E, Pupko T, Ben-Tal N. ConSurf 2010: calculating evolutionary conservation in sequence and structure of proteins and nucleic acids. *Nucleic acids research*. 2010;38(Web Server issue):W529-33. PMCID: 2896094.

40. Pettersen EF, Goddard TD, Huang CC, Couch GS, Greenblatt DM, Meng EC, et al. UCSF Chimera--a visualization system for exploratory research and analysis. *J Comput Chem.* 2004;25(13):1605-12.
41. Illergard K, Kauko A, Elofsson A. Why are polar residues within the membrane core evolutionary conserved? *Proteins.* 2011;79(1):79-91.
42. Fleishman SJ, Ben-Tal N. Progress in structure prediction of alpha-helical membrane proteins. *Current opinion in structural biology.* 2006;16(4):496-504.
43. Kuntz ID. Structure-based strategies for drug design and discovery. *Science.* 1992;257(5073):1078-82.
44. Shoichet BK. Virtual screening of chemical libraries. *Nature.* 2004;432(7019):862-5.
45. Clamp M, Cuff J, Searle SM, Barton GJ. The Jalview Java alignment editor. *Bioinformatics.* 2004;20(3):426-7.
46. Lomize MA, Pogozheva ID, Joo H, Mosberg HI, Lomize AL. OPM database and PPM web server: resources for positioning of proteins in membranes. *Nucleic acids research.* 2012;40(Database issue):D370-6. PMID: 3245162.
47. Kabsch W, Sander C. Dictionary of protein secondary structure: pattern recognition of hydrogen-bonded and geometrical features. *Biopolymers.* 1983;22(12):2577-637.
48. Mysinger MM, Shoichet BK. Rapid context-dependent ligand desolvation in molecular docking. *Journal of chemical information and modeling.* 2010;50(9):1561-73.
49. Overington J. ChEMBL. An interview with John Overington, team leader, chemogenomics at the European Bioinformatics Institute Outstation of the European

Molecular Biology Laboratory (EMBL-EBI). Interview by Wendy A. Warr. *Journal of computer-aided molecular design*. 2009;23(4):195-8.

50. The Universal Protein Resource (UniProt) in 2010. *Nucleic acids research*. 2010;38(Database issue):D142-8. PMID: 2808944.

51. Wang X, McManus M. Lentivirus production. *Journal of visualized experiments : JoVE*. 2009(32). PMID: 2865973.

52. Chen Y, Zhang S, Sorani M, Giacomini KM. Transport of paraquat by human organic cation transporters and multidrug and toxic compound extrusion family. *J Pharmacol Exp Ther*. 2007;322(2):695-700.

53. More SS, Itsara M, Yang X, Geier EG, Tadano MK, Seo Y, et al. Vorinostat increases expression of functional norepinephrine transporter in neuroblastoma in vitro and in vivo model systems. *Clinical cancer research : an official journal of the American Association for Cancer Research*. 2011;17(8):2339-49. PMID: 3247296.

54. Eramian D, Eswar N, Shen MY, Sali A. How well can the accuracy of comparative protein structure models be predicted? *Protein Sci*. 2008;17(11):1881-93.

55. Fan H, Irwin JJ, Webb BM, Klebe G, Shoichet BK, Sali A. Molecular docking screens using comparative models of proteins. *J Chem Inf Model*. 2009;49(11):2512-27. PMID: 2790034.

56. Mensch J, Oyarzabal J, Mackie C, Augustijns P. In vivo, in vitro and in silico methods for small molecule transfer across the BBB. *Journal of pharmaceutical sciences*. 2009;98(12):4429-68.

57. Smith BJ, Doran AC, McLean S, Tingley FD, 3rd, O'Neill BT, Kajiji SM. P-glycoprotein efflux at the blood-brain barrier mediates differences in brain disposition

and pharmacodynamics between two structurally related neurokinin-1 receptor antagonists. *The Journal of pharmacology and experimental therapeutics*. 2001;298(3):1252-9.

58. Park S, Sinko PJ. The blood-brain barrier sodium-dependent multivitamin transporter: a molecular functional in vitro-in situ correlation. *Drug metabolism and disposition: the biological fate of chemicals*. 2005;33(10):1547-54.

59. Abbott NJ, Patabendige AA, Dolman DE, Yusof SR, Begley DJ. Structure and function of the blood-brain barrier. *Neurobiology of disease*. 2010;37(1):13-25.

60. Yamamoto A, Akanuma S, Tachikawa M, Hosoya K. Involvement of LAT1 and LAT2 in the high- and low-affinity transport of L-leucine in human retinal pigment epithelial cells (ARPE-19 cells). *Journal of pharmaceutical sciences*. 2010;99(5):2475-82.

61. Zhang L, Schaner ME, Giacomini KM. Functional characterization of an organic cation transporter (hOCT1) in a transiently transfected human cell line (HeLa). *The Journal of pharmacology and experimental therapeutics*. 1998;286(1):354-61.

62. Meier C, Ristic Z, Klauser S, Verrey F. Activation of system L heterodimeric amino acid exchangers by intracellular substrates. *The EMBO journal*. 2002;21(4):580-9. PMID: 125871.

63. Hidalgo M, Rodriguez G, Kuhn JG, Brown T, Weiss G, MacGovren JP, et al. A Phase I and pharmacological study of the glutamine antagonist acivicin with the amino acid solution aminosyn in patients with advanced solid malignancies. *Clinical cancer research : an official journal of the American Association for Cancer Research*. 1998;4(11):2763-70.

64. Delaville C, Navailles S, Benazzouz A. Effects of noradrenaline and serotonin depletions on the neuronal activity of globus pallidus and substantia nigra pars reticulata in experimental parkinsonism. *Neuroscience*. 2012;202:424-33.
65. Kroemer G, Pouyssegur J. Tumor cell metabolism: cancer's Achilles' heel. *Cancer Cell*. 2008;13(6):472-82.
66. Lahoutte T, Mertens J, Caveliers V, Franken PR, Everaert H, Bossuyt A. Comparative biodistribution of iodinated amino acids in rats: selection of the optimal analog for oncologic imaging outside the brain. *Journal of nuclear medicine : official publication, Society of Nuclear Medicine*. 2003;44(9):1489-94.
67. O'Dwyer PJ, Alonso MT, Leyland-Jones B. Acivicin: a new glutamine antagonist in clinical trials. *Journal of clinical oncology : official journal of the American Society of Clinical Oncology*. 1984;2(9):1064-71.
68. Bonomi P, Finkelstein D, Chang A. Phase II trial of acivicin versus etoposide-cisplatin in non-small cell lung cancer. An Eastern Cooperative Oncology Group study. *American journal of clinical oncology*. 1994;17(3):215-7.
69. Schlessinger A, Wittwer MB, Dahlin A, Khuri N, Bonomi M, Fan H, et al. High selectivity of the gamma-Aminobutyric acid (GABA) transporter 2 (GAT-2, SLC6A13) revealed by structure-based approach. *The Journal of biological chemistry*. 2012.



## **CHAPTER 5**

### **Summary and Conclusions**

Over recent years, much progress has been made in discerning the roles of membrane transporters in many important biological processes. Furthermore, an increasing emphasis has been placed on investigating how solute carrier (SLC) and ATP-binding cassette (ABC) transporters determine the absorption, distribution, and elimination of many endogenous and exogenous compounds. As a part of this effort, numerous studies have explored transporter expression levels and cellular localization in many tissues throughout the body, especially those involved in drug disposition, and how these expression patterns influence tissue permeability to drugs [1-9]. For example, the multidrug resistance protein 1 (MDR1) is expressed in the blood-facing membrane of the blood-brain barrier (BBB), where it has a well-established role in preventing drug uptake into the brain [10] [11, 12]. However, no previous studies have attempted to identify the full complement of transporters, especially SLC influx transporters, in the human BBB in spite of its pharmacological importance.

The BBB maintains the neural microenvironment through the unique properties of the endothelial cells forming the central nervous system (CNS) vasculature [13, 14]. Since most of these properties prevent free exchange between the blood and brain, small molecule penetration through the BBB is generally restricted to two routes: transcellular passive diffusion for small, lipophilic molecules and carrier-mediated transport for hydrophilic molecules. These carriers are primarily SLC influx transporters,

many of which also mediate drug uptake into the CNS. This suggests that SLC influx transporters can be targeted to facilitate drug penetration across the BBB, especially for drugs that lack the physicochemical properties to passively diffuse into the CNS.

Since passive permeability is generally assumed to be the most important mechanism by which molecules translocate from the blood to the CNS, the current paradigm for increasing the CNS permeability of a systemically administered small molecule drug is to increase its lipophilicity by chemical modification to allow for more efficient passive diffusion across the BBB [15]. Other approaches that are yet to be proven clinically efficacious and safe include disruption of the BBB to create “leaks” in the barrier, and co-administration of an efflux transporter inhibitor with a drug that is a substrate of the same efflux transporter at the BBB [12, 16]. These latter approaches may subject the CNS to insult from circulating toxins, and disrupt the CNS microenvironment necessary for proper neural function. The overall goal of this research was to identify SLC influx transporters expressed at the human BBB, and determine how solute carrier (SLC) influx transporters can be exploited to deliver low CNS permeable platinum drugs across the BBB. Below is a chapter-by-chapter summary of the key findings and the challenges that remain to be addressed in future studies.

## **Chapter 2**

The neuroprotective function of the BBB presents a major challenge for CNS drug delivery. Previous studies characterizing membrane transporters that support this critical function in the BBB have typically used non-human tissue sources and focused on how ABC transporters limit drug penetration across the BBB [17-19]. Consequently,

SLC influx transporters that contribute to drug uptake across the BBB have been largely overlooked, especially in humans. The focus of chapter 2 was to identify and characterize SLC influx transporters expressed at the human BBB that may be targeted to deliver drugs into the CNS. Expression of 359 SLC and 49 ABC transporters in human cerebral cortex and isolated brain microvessels (BMV) was characterized. Analysis of SLC transporters identified uncharacterized BBB transporters (e.g. SLC6A13, SLC19A3 and SLC47A2), and found several xenobiotic transporters (e.g. SLCO1A2, SLCO2B1 and SLC47A1) expressed at similar or higher mRNA levels in BMVs relative to the liver or kidney. Immunohistochemistry identified the reduced folate carrier (RFC), MATE1, and OCT3 protein in BMVs. In mice, methotrexate uptake into the brain was sensitive to Rfc inhibitors, indicating that Rfc at least partially mediates the CNS permeability of methotrexate. Collectively, these findings have implications for the contribution of SLC transporters to BBB function and drug targeting to the CNS.

### **Chapter 3**

In chapter 2, the large-neutral amino acid transporter, LAT1 (*SLC7A5*), was found to be the most highly enriched influx transporter expressed in the human BBB. Since previous studies have established that LAT1 mediates drug uptake across the BBB, and enhances the brain uptake of targeted low CNS permeability drug analogs [20-24], LAT1 represents an ideal transporter to target with modified derivatives of cisplatin. Chapter 3 had two goals: demonstrate that LAT1-targeted cisplatin analogs are LAT1 substrates *in vitro*, and generate a mouse model with reduced Lat1 function to investigate LAT1-specific drug uptake across the BBB. After designing and synthesizing seven LAT1-targeted platinum compounds, uptake studies in LAT1-

overexpressing cells identified one as a weak LAT1 substrate (compound 207). Cytotoxicity assays in the same cell line indicated that compound 207 is equipotent to cisplatin over longer exposure times, and even more potent than cisplatin over shorter exposure times. To establish an *in vivo* model of LAT1-mediated brain uptake, the *Slc7a5* gene was deleted in mice. Unfortunately, homozygous deletion of Lat1 appears to be embryonic lethal. While Lat1 heterozygous mice were phenotypically similar to wild type littermates, these mice had reduced Lat1 mRNA expression in the brain, testes, spleen, bone marrow, and kidney, and reduced brain accumulation of two Lat1 drug substrates. These results indicate that LAT1 is capable of transporting cytotoxic platinum-based compounds, and create a foundation for developing more refined LAT1-targeted platinum drugs. Furthermore, Lat1 heterozygous mice will serve as an *in vivo* model for determining Lat1-mediated brain uptake of drugs and other small molecule substrates.

## **Chapter 4**

Even though chapter 3 established that LAT1 can transporter platinum-based drugs, only one targeted platinum compound was found to be a weak LAT1 substrate, indicating a need to design and synthesize additional LAT1-targeted platinum compounds. Furthermore, no previous studies have attempted to characterize the endogenous, xenobiotic, and drug ligand profile of LAT1 with an unbiased screen, thereby limiting our knowledge of the chemical space capable of interacting with LAT1. The goal of chapter 4 was to identify and characterize novel LAT1 ligands that could be used to design novel LAT1-targeted platinum compounds. *In silico* and *in vitro* approaches combining comparative modeling, virtual screening, and cell-based

experimental validation identified four LAT1 ligands. These results may rationalize the enhanced brain permeability of several drugs, including the anticancer agent acivicin. Aside from the BBB, LAT1 also plays an important role in cancer development. In this context, two putative LAT1 ligands were found to inhibit proliferation of a cancer cell line by different LAT1-specific mechanisms. Taken together, these results provide new chemical tools for characterizing the role of LAT1 in cancer metabolism and drug uptake across the BBB. Importantly, they also identified new chemical structures that will be useful in designing refined LAT1-targeted platinum compounds.

### **Challenges and Future Directions**

The research presented here has expanded the current knowledge of SLC transporters expressed at the human BBB, and how influx transporters contribute to the brain uptake of drugs. Nevertheless, in these studies only one BBB influx drug transporter was functionally characterized in mice, and almost no functional data exist for the majority of the other influx transporters identified in the BBB. Future studies investigating the subcellular localization of these transporters at the BBB (blood- or brain-facing membrane expression), and determining if they are functionally relevant to xenobiotic uptake across the BBB, particularly in humans, will be extremely informative.

These studies also indicate that LAT1 can transport cytotoxic platinum-based drugs, and confirm the importance of LAT1 in mediating drug uptake across the BBB. Even though these results support the idea that LAT1 may be able to increase the CNS permeability of platinum-based drugs, future studies are required to determine if platinum analogs have LAT1-specific enhanced BBB penetration relative to cisplatin. New chemical tools identified in these studies will greatly aid future efforts to design

additional LAT1-targeted platinum compounds. Once improved LAT1-targeted platinum compounds have been generated and validated *in vitro*, studies using genetic and xenograft models of primary and metastatic CNS tumors will be required to determine the efficacy of targeting influx transporters such as LAT1 to deliver drugs across the BBB for treating CNS diseases.

## References

1. Holland IB. ABC transporters, mechanisms and biology: an overview. *Essays Biochem.* 2011;50(1):1-17.
2. Hagenbuch B. Molecular properties of hepatic uptake systems for bile acids and organic anions. *J Membr Biol.* 1997;160(1):1-8.
3. Hagenbuch B, Gao B, Meier PJ. Transport of xenobiotics across the blood-brain barrier. *News Physiol Sci.* 2002;17:231-4.
4. Hagenbuch B. Drug uptake systems in liver and kidney: a historic perspective. *Clin Pharmacol Ther.* 2010;87(1):39-47. PMID: 2819296.
5. Koepsell H. Organic cation transporters in intestine, kidney, liver, and brain. *Annu Rev Physiol.* 1998;60:243-66.
6. Nigam SK, Bush KT, Bhatnagar V. Drug and toxicant handling by the OAT organic anion transporters in the kidney and other tissues. *Nat Clin Pract Nephrol.* 2007;3(8):443-8.
7. Schinkel AH, Jonker JW. Mammalian drug efflux transporters of the ATP binding cassette (ABC) family: an overview. *Adv Drug Deliv Rev.* 2003;55(1):3-29.

8. Sweet DH, Bush KT, Nigam SK. The organic anion transporter family: from physiology to ontogeny and the clinic. *Am J Physiol Renal Physiol*. 2001;281(2):F197-205.
9. You G. The role of organic ion transporters in drug disposition: an update. *Curr Drug Metab*. 2004;5(1):55-62.
10. International Transporter C, Giacomini KM, Huang SM, Tweedie DJ, Benet LZ, Brouwer KL, et al. Membrane transporters in drug development. *Nat Rev Drug Discov*. 2010;9(3):215-36.
11. Thiebaut F, Tsuruo T, Hamada H, Gottesman MM, Pastan I, Willingham MC. Immunohistochemical localization in normal tissues of different epitopes in the multidrug transport protein P170: evidence for localization in brain capillaries and crossreactivity of one antibody with a muscle protein. *J Histochem Cytochem*. 1989;37(2):159-64.
12. Kalvass JC, Polli JW, Bourdet DL, Feng B, Huang SM, Liu X, et al. Why Clinical Modulation of Efflux Transport at the Human Blood-Brain Barrier Is Unlikely: The ITC Evidence-Based Position. *Clin Pharmacol Ther*. 2013;94(1):80-94.
13. Abbott NJ, Patabendige AA, Dolman DE, Yusof SR, Begley DJ. Structure and function of the blood-brain barrier. *Neurobiology of disease*. 2010;37(1):13-25.
14. Hurko O, Ryan JL. Translational research in central nervous system drug discovery. *NeuroRx*. 2005;2(4):671-82.
15. Mensch J, Oyarzabal J, Mackie C, Augustijns P. In vivo, in vitro and in silico methods for small molecule transfer across the BBB. *Journal of pharmaceutical sciences*. 2009;98(12):4429-68.

16. Fortin D, Gendron C, Boudrias M, Garant MP. Enhanced chemotherapy delivery by intraarterial infusion and blood-brain barrier disruption in the treatment of cerebral metastasis. *Cancer*. 2007;109(4):751-60.
17. Uchida Y, Ohtsuki S, Katsukura Y, Ikeda C, Suzuki T, Kamiie J, et al. Quantitative targeted absolute proteomics of human blood-brain barrier transporters and receptors. *J Neurochem*. 2011;117(2):333-45.
18. Daneman R, Zhou L, Agalliu D, Cahoy JD, Kaushal A, Barres BA. The mouse blood-brain barrier transcriptome: a new resource for understanding the development and function of brain endothelial cells. *PLoS One*. 2010;5(10):e13741.
19. Warren MS, Zerangue N, Woodford K, Roberts LM, Tate EH, Feng B, et al. Comparative gene expression profiles of ABC transporters in brain microvessel endothelial cells and brain in five species including human. *Pharmacol Res*. 2009;59(6):404-13.
20. Nutt JG, Woodward WR. Levodopa pharmacokinetics and pharmacodynamics in fluctuating parkinsonian patients. *Neurology*. 1986;36(6):739-44.
21. Nutt JG, Woodward WR, Hammerstad JP, Carter JH, Anderson JL. The "on-off" phenomenon in Parkinson's disease. Relation to levodopa absorption and transport. *N Engl J Med*. 1984;310(8):483-8.
22. Hammerstad JP, Pate BD, Hewitt KA, Chan GL, Ruth TJ, Calne DB. The transport of L-6-fluorodopa and its metabolites from blood to cerebrospinal fluid and brain. *Ann Neurol*. 1993;34(4):603-8.



23. Killian DM, Hermeling S, Chikhale PJ. Targeting the cerebrovascular large neutral amino acid transporter (LAT1) isoform using a novel disulfide-based brain drug delivery system. *Drug delivery*. 2007;14(1):25-31.
24. Gynther M, Jalkanen A, Lehtonen M, Forsberg M, Laine K, Ropponen J, et al. Brain uptake of ketoprofen-lysine prodrug in rats. *International journal of pharmaceutics*. 2010;399(1-2):121-8.

**Publishing Agreement**

*It is the policy of the University to encourage the distribution of all theses, dissertations, and manuscripts. Copies of all UCSF theses, dissertations, and manuscripts will be routed to the library via the Graduate Division. The library will make all theses, dissertations, and manuscripts accessible to the public and will preserve these to the best of their abilities, in perpetuity.*

**Please sign the following statement:**

*I hereby grant permission to the Graduate Division of the University of California, San Francisco to release copies of my thesis, dissertation, or manuscript to the Campus Library to provide access and preservation, in whole or in part, in perpetuity.*



Author Signature

10/28/13

Date